



City Research Online

City, University of London Institutional Repository

Citation: Mukherjee, S. N. (1983). Nonlinear response of embedded structures under transient dynamic load. (Unpublished Doctoral thesis, The City University)

This is the accepted version of the paper.

This version of the publication may differ from the final published version.

Permanent repository link: <https://openaccess.city.ac.uk/id/eprint/35363/>

Link to published version:

Copyright: City Research Online aims to make research outputs of City, University of London available to a wider audience. Copyright and Moral Rights remain with the author(s) and/or copyright holders. URLs from City Research Online may be freely distributed and linked to.

Reuse: Copies of full items can be used for personal research or study, educational, or not-for-profit purposes without prior permission or charge. Provided that the authors, title and full bibliographic details are credited, a hyperlink and/or URL is given for the original metadata page and the content is not changed in any way.

THE CITY UNIVERSITY LIBRARY
81, JOHN STREET, LONDON, E.C.1.

CITY UNIVERSITY LIBRARY



3 8008 02046 8665

D4 8602/84

MUKHERJEE

P. 23 (vol. 1)

as pp X-2 to X-1 (vol. 2) missing

(we cannot ascertain the nature of this error as author cannot be contacted)

24/8/84

TO MY WIFE AND TO MY MOTHER

NONLINEAR RESPONSE OF EMBEDDED STRUCTURES
UNDER TRANSIENT DYNAMIC LOAD

Somendra Nath Mukherjee

PH. D

The City University
Northampton Square
LONDON EC1V 0HB

Department of Mechanical Engineering

ACKNOWLEDGEMENT

The author gratefully acknowledges the kind permission given by Brown, Boveri & Company Limited, Baden, Switzerland, to publish and reproduce illustrations, diagrams and computer printouts for this thesis.

DECLARATION

The University Librarian is granted the powers of discretion to allow the thesis to be copied in whole or in part without further reference to the author.

Table of Contents

<u>Subject</u>	<u>Section</u>	<u>Page</u>
Literature Study	1	6
Introduction	2	10
Historical Development	3	15
Continuum Mechanics	4	18
Formulation of Basic Equation	5	29
Method of Temporal Inegration	6	32
Temporal Integration of Assembled Finite Elements	7	42
Modal Equivalence of Superstructure	8	53
Method of Preventing Unwanted Reflection	9	62
Comparison of Finite element solution with closed form solution	10	77
Comparison between elastic and inelastic finite element and closed form solution	11	88
Modelling of Soil - Structure System		104
Case Study and Discussions	12	107
Appendix A		135
Appendix B		146
Appendix C		154

Tables

<u>Number</u>	<u>Contents</u>	<u>Page</u>
3.1	Program evaluation	17
4.1	Finite Element Matrices	27
12.1-12.5	Tabulated results of analysis corresponding to Section 12	117, 121, 123, 126, 128

ABSTRACT

A comprehensive literature study is devoted to Chapter 1. Starting from the linear analysis approach, the study points out the steady progress and development of numerical methods adopted by several authors, in the domain on nonlinear static and dynamic analysis. With regard to the nonlinear dynamic interaction between the superstructure and supporting soil mechanism, it is observed that research in this field is very sparse and inadequate, therefore the underlying motivation to dwell in this very interesting and complex field of research and investigation becomes obvious.

Chapter 2 contains the introduction to the problem concerned, and outlines the basic assumption, analytical procedure, and the limitations of the method applied in the solution technique. In a subsection of this chapter, an introduction to the general purpose nonlinear analysis is given. It is pointed out that certain design problems, particularly the design of nuclear power plants, the realization and reliable testing of the full scale structure, are almost prohibitive as far as cost is concerned, and in addition to this, is the problem of reliable monitoring and processing of response signals, during testing. Appropriate analytical procedures, if available, will therefore reduce the testing significantly and a better understanding of the structural behavior can be attained. Therefore it is pointed out here that a consistent continuum mechanics formulation and effective finite element discretization is the most important aspect of non-linear analysis. The other aspect is the use of proper material models to account for the nonlinear behavior of material which should adequately represent the actual material under field conditions.

In the third chapter, a historical development of non-linear analysis of static and dynamic problems is presented, which goes back as far as 1960. Since then, numerous papers have been published, using these methods, as proposed by the earlier authors who actually founded the basic concept of non-linear analysis. Continuous researches are going on in this field, to understand many problems, contrary to many notions we inherit from classical mechanics. As Professor Oden [12] pointed out, "No structure or machine ever built behaved linearly. All deformation need not be small, nor need they be reversible. Few materials are truly elastic, and fewer are linear."

In Chapter 4, the concept of continuum mechanics is explained, in the light of virtual work principle, and in the subsection, the appropriate finite element discretization of the continuum is given for the matrix calculation. In this subsection, basically the essential tools involved in nonlinear analysis are systematically discussed.

Formulation of the governing equation of motion for the structure and soil subgrade system due to support motion is explained in Chapter 5. The support motion is caused by time varying ground acceleration which characterizes the earthquake load.

In Chapter 6, some salient points of temporal integration operator are illustrated. Understanding of the basic principle of temporal integration in one dimensional problems is the key to more complex problems dealing with finite element applications.

Chapter 7 is devoted to temporal integration of the assembled finite elements. To avoid large integration error, which causes the calculated solution to "drift away" from the exact solution, as a consequence of linearization, equilibrium iteration is introduced [18], [23], to assure convergence to the solution within acceptable limits.

In chapter 8, a refined modelling technique using principle modes of vibration is discussed.

Travelling P and S waves in the finite element grid are reflected back from the fixed boundary. This can cause serious perturbations in the displacement and stress output in the vicinity of the structure. In chapter 9, a simple but effective way of approach used in this study to suppress the unwanted reflection is explained.

In chapter 10 a comparative study was made between the closed form solution and finite element solution of soil-structure interaction problem. The theoretical formulation is based on one dimensional wave propagation in an elastic medium.

In chapter 11 the stress profiles obtained by finite element method of one dimensional wave propagation in elastic, and inelastic medium are compared with the exact solution. This was done mainly to show the convergence of the finite element solution to the exact solution using modified NONSAP program in vol. 2.

In chapter 12 a case study is presented, and results are analyzed to gain an insight in the domain of non-linear soil-structure interaction. It is also pointed out the need for further research, and experiment in this highly complicated field on engineering, where the civil and mechanical engineers with their concerted effort can achieve an acceptable, economical and meaningful solution to this problem.

In appendix A failure behaviour of soil is discussed. Some experimental data obtained by Swarz (33) in bi and triaxial tests of soil were used to determine the Yield function and Yield criteria of soil.

In appendix B proposed experimental study of non-linear soil-structure interaction is suggested.

In appendix C, a comparative study between the elastic half space solution and solution of the equivalent finite element model of the elastic half space was made. The response spectrum obtained from the both analyses show fairly good agreement between the two methods.

In vol. 2 of the thesis the modified version of NONSAP program is presented. The program organization, the flow chart and the use of high speed storage of nodal and element data and the stiffness matrix are explained in block diagram.

The subroutine VELCOR, which is used in conjunction with the NONSAP is presented separately. This will enable the reader to follow the programming technique and ideas behind the program. A flow chart is provided so that the readers have a clear understanding of the program algorithm.

SUMMARY

Within the last 15 years, rapid developement in the solution of non-linear static and dynamic problems have taken place. Coupled geometric and material problems are not uncommon in practical Engineering problems. Exact solutions to these problems are almost non-existent.

Exact continuum mechanics formulation and finite element approximation coupled with stable numerical technique appear to be the best method of solution to these complex problems.

In this thesis, it is shown how a non-linear dynamic response of a deeply embedded structure under transient load such as earthquake can be analysed using finite element technique based on exact continuum mechanics formulation.

1. Literature study

Previous work

The previous work which contributes directly to this present study may be divided into three categories:

The first category deals with the analysis of several kinds of structures subjected to earthquake loading. These studies are carried out employing varieties of analytical techniques, and help to find out what is important in the analysis of response of soil and structure under earthquake load. Housner [1] has shown that behavior of buildings during earthquake depends on the size and distance of the epicenter of the earthquake, period and damping of the structure. The analysis of the structural response can be performed by means of Housner's response spectra. The analyses are based on lumped-mass and stiffness models of structures, whose bases are subjected to motions measured in basements of actual buildings during earthquake. In this way, the effect of interaction on the base motion of the structure is known, and thus allows the upper stories to be analysed.

In case the basement response to earthquake loading to surrounding soil is not known, the second approach is to apply known earthquake records to the base of the building, which implies that the foundation medium is rigid. This has been done by several authors for buildings and for earth banks and dams [1, 2]. These reports are useful for theoretical insight into motions of buildings and stress levels in soil structures. Now the question arises from these analyses is whether to take the flexibility of the foundation medium into account or not. If yes, would it change the results significantly? Parmalee [3] et al answered to this question by utilizing Bycroft's Solution for translation and rotation of a rigid plate on the surface of an infinite half space and subjected it to harmonic exciting forces and moments. The results of analysis of a multi-story building sitting on top of the foundation plate indicate that when the soil medium becomes sufficiently

soft or flexible, relative to the structure, there is a significant interaction. If the soil is relatively stiff, say $C_s = C_a$ 300 m/s, a rigid base analysis would provide sufficiently accurate results.

Scavuzzo et al. [5] obtained a solution to the main problem of a two-dimensional elastic half space subjected to a time-dependent uniform shearing stress representing loading by a surface structure. The structure is represented by a large base mass and several single-degree-of-freedom oscillators representing equipment attached to the base. The results have shown that the interaction depends largely on soil stiffness and on the relationship between frequency of the seismic motion and that of the structure.

The above study was the starting point of Isenberg's [4] more advanced work using finite element methods because of its ability to represent embedded structure and inelastic soil properties.

Chu et al. [6] presented a method of analysis to investigate the soil-structure interaction effect by taking into account the strain dependent soil moduli and dampings in the first step. The second step employs the modal synthesis technique in which soil and structure are considered as two subsystems having different damping values. It was pointed out that it is important to extract sufficient numbers of vibration modes from the soil subsystem to adequately evaluate the building response. Otherwise, some higher frequency contents of earthquake motion being transmitted through the basement slab to the structure above may be erroneous. Because of the lack of ability in this method to account for non-elastic soil properties of the layered soil medium, and to avoid time consuming modal synthesis of a large number of modes, the present study is intended to follow up the work of Isenberg to gain further insight into the non-linear soil-structure interaction problem.

In applying the finite element technique to the present problem, the major difficulty lies in prescribing adequate boundary conditions for the edges of the finite element grid. The top edge

is treated as a free surface which adequately represents the ground surface. The remaining edges of the grid, however, do not exactly correspond to the physical boundaries. Inappropriate treatment of these boundaries may distort the solution in the vicinity of the structure. One way of approach is to move the boundaries a considerable distance from the structure, so that the building response is not significantly affected. Another alternative approach is to regard the motions adjacent to the artificial boundaries as being associated with the waves which may be reflected back towards the structure. A procedure for absorbing such waves at artificial boundaries is outlined in this analysis.

Referring back to Isenberg's work, it is necessary to point out that the plastic flow mode adopted in representing the material properties of soil media, the kinematic or orthotropic strain hardening effect was not taken into account. The unknown proportionality constant λ (which will be discussed later) with its work hardening effect has considerable significance in determining the value of the plastic strain rate. The present work includes the work hardening effect. Another drawback in Isenberg's work is the modelling technique adopted in converting axisymmetric nuclear buildings to two dimensional finite element models. Much criticism has been made of using filling material with a considerably high E modulus to represent the trench or air gap between the outer shield building and the steel containment. In the present analysis, a more accurate modal model technique has been adopted to represent the superstructure in the two dimensional finite element model, with a frequency band width of significant interest. Finally, the linear acceleration method of integration technique used in inelastic finite element analysis interferes with interpreting responses at higher frequencies than 15-16 Hz. Responses at higher frequencies show perturbations superposed on the main structural response. In order to represent the true picture of the acceleration response, Isenberg attempted to separate the true acceleration pulse from the superposed numerical

noise. This separation was beyond the scope of work presented. In the present analysis, the numerical integration was the stable implicit integration scheme proposed by Newmark and Wilson, and spurious numerical oscillation was observed.

Unfortunately, no other previous work in the field of non-linear soil structure interaction problems appeared other than that of Isenberg's. Since the condensed version of the work incorporated in this thesis appeared in the M.I.T. Report [53], a number of papers dealing with the non-linear soil structure interaction problem were published, which show increasing concern of engineers to find more meaningful and truly representative solutions to this very complex problem.

2. Introduction

This is a theoretical study of the dynamic response of a nuclear reactor power structure subjected to earthquake motions. Dynamic response of this structure is defined here primarily as the motion and frequency response spectra of its foundation.

Due to the inherent complexity and nonlinear behaviour of soil, various approaches have been postulated to find more meaningful conclusions to this complex problem. The dynamic interrelationship between the response of structure and the characteristics of its foundation medium is commonly described as the interaction effect. The interaction phenomenon is principally attributed to the mechanism of exchange of energy between the soil and the structure, and its primary influence on the structure is to modify the mode of vibration and response.

Some factors which are considered for the present study are:

1. Soil stiffness and shear-wave velocity
2. Presence of several layers with different material properties
3. Assumed yield condition of soil
4. Time history input of earthquake motion at bedrock

Of several candidate methods of analysis for the present study, the finite element method seems the most suitable. The geometry of the embedded structure can be represented by a two-dimensional plane strain section. All contributions to the interaction, from the nearly rigid body response of the foundation to the wave effects in the soil, are included.

Since the main purpose and goal of this thesis is to gain insight into this interaction, the results of this analysis are presented in the form of a comparison between structural and free field response. For example, the frequency spectra of structural responses are compared with those of the free field to determine whether the presence of a structure suppresses free field spectra

locally. By comparing stress in the soil adjacent to the structure with the stress at the same depth when the structure is absent, the influence of the structure on the stress in the soil can be examined to see whether the structure tends to promote or retard failure in the adjacent soil. Since this is primarily a study of interaction, the details of the superstructure and equipment response are given little attention here. However, an attempt is made to relate the translation and rotation of the foundation to the translation of the elevated parts of the structure where, in an actual structure, equipment might be attached.

In the present analysis, according to geological tests in the field and under laboratory conditions, the boundary and the bottom layers are considered linearly elastic, because of the rock-like formation of this stratum, while the rest of the layers are represented by elastic/perfectly plastic soil medium. In the present analysis, the region of soil surrounding the structure is defined, and transient earthquake load is applied along one side. This method differs from the commonly used one of shaking the bottom of the soil and structure system to simulate bedrock motion. The reason for choosing this less orthodox method is that it makes best use of available techniques to prevent spurious reflections from artificial boundaries of the finite element grid. Within limits imposed by these assumptions, the present analysis appears to represent correctly the interaction between soil and structure.

Introduction and formulation of general purpose non-linear analysis

The great importance of investigation of non-linear behavior of various types of structures for adequate safety in design is rapidly being recognised. It is reported [4, 5] that in some cases, the behaviour of the materials is significantly non-linear, even at relatively small loading. For other structures, the influence of geometry changes on the response of the structure cannot be neglected [6, 7, 8].

The ultimate load behaviour of the structure which is in effect governed by the non-linear effect is a very important aspect of analysis [9, 10, 11]. If this ultimate load can be obtained accurately, the safety of the structure is increased and in many cases costs can be reduced.

In certain design problems found in the nuclear industry, extensive testing is carried out in order to assess accurately the response of the structure under consideration. However, it should be pointed out that the realisation of reliable test data is very expensive, and the need for parametric studies has increased the emphasis on reliable and exact theoretical analyses. If the appropriate analytical method is available, testing can be reduced significantly, and a better understanding of the structural behaviour can be attained.

Non-linear behaviour in structural systems is usually put in one of three categories:

- 1) Geometric nonlinearity, which arises from non-linear terms in the kinematic equations,
- 2) Material nonlinearities in the constitutive equations, and
- 3) Combined geometric and material nonlinearity.

Computationally, these categories are somewhat superficial, since, except perhaps in problems of stability or cyclic loading of inelastic elements, the mathematical techniques that can be applied successfully to treat one type of nonlinearity are, with some modification, generally applicable to the other types of nonlinearity. To provide a basis for further discussion, it is necessary to review briefly the basic notions of the finite element concept and its application to non-linear problems in solid mechanics. To start with, we view a continuous body as a collection of a finite number of elements connected together at various nodal points. For application in solid mechanics, it is generally more natural to describe the motion of this collection of elements relative to some specific reference configuration. Clearly, when one is faced with the problem of describing the behavior of a

structure of a solid body, we generally know its shape, composition at a certain time, and we wish to trace its motion relative to a configuration in which its geometry is known. After an element has undergone large displacements from its reference configuration, all kinematic variables needed to describe its motion may be written in terms of either its initial material coordinates or the current spatial coordinates.

A fundamental property of finite element models is that typical elements can be isolated from the collection and their behaviour can be studied independently of the behaviour of the other elements in the collection. The process of connecting individual elements to form a complete model is a topological problem, and is independent of the physical nature of the problem.

The earliest finite element analyses of non-linear problems have been developed for specific application by Oden [12], Fellipio [13], Martin and Carey [14], and Zienkiewicz [15]. These procedures were primarily developed in order to obtain solutions to the specific problem considered. However, to provide general analysis capabilities, much research is still required to improve the stability, accuracy and effectiveness of non-linear solutions.

In non-linear analysis, stability and accuracy are a great deal more difficult to obtain than in linear analysis and depend on various factors.

An important aspect is the use of a consistent continuum mechanics formulation, and effective finite element discretization. During recent years, the isoparametric finite element procedure has proven to be very effective in both linear and non-linear analysis.

Another aspect, as pointed out before, is the use of a material model to account for material nonlinearities, and which accurately represents the actual material under field conditions.

In dynamic analysis, it is further necessary to use numerical time integration which introduces additional errors [16, 17]. Extensive research is currently being devoted to developing stable and accurate integration schemes. However, it should be pointed out that a proper evaluation and use of an integration method is only possible if a consistent non-linear formulation is used [16].

3. Historical development of non-linear static and dynamic analysis

Now after the introduction to general purpose non-linear analysis, it is worthwhile to consider some background and interesting developments directed to the solution of non-linear dynamic problems and computer programs.

The earliest examples in the literature of the solution of dynamic problems using the finite element method are given by Klein and Sylvester [28] and Popov and Chow [30]. Turner [7] formulated the geometrical non-linear problem by using the finite element method in 1960, and almost ten years later the results were obtained for the elastic dynamic problem by Stricklin et al. [11]. There is an extensive survey made by Fulton [9] covering the area of non-linear elastic deformations, which is primarily directed to the solution of dynamic shell buckling problems.

The material nonlinearity and the combined problems of non-linear material and geometric behaviour have been extensively discussed by Marcal [29]. MacNamara and Marcal developed a base on which a general purpose finite element program could be built for analysing non-linear dynamic problems [23]. Two general methods for incorporating the elastic-plastic behaviour into a finite element analysis have been developed, and they are known as the Initial Strain Method and Tangent Modulus Method [22], [23]. Bathe et al. [17] and Wilson et al. [28] presented a general step-by-step solution technique for the evaluation of the dynamic response of structural systems with physical and geometrical nonlinearities. The algorithm is effective in non-linear analysis and in the analysis of linear systems introduces a predictable amount of errors for a specified time step. Guide-lines are given for the selection of time step size for different types of dynamic loadings. The method can be applied to the static and dynamic analysis of both discrete structural systems and continuous solids idealised as an assemblage of finite elements. Results of several non-linear analyses are presented and compared with results obtained by other methods and from experiments.

The following table of comparison shows some of the computer programs commonly used for non-linear, transient dynamic analysis. The contents of this table are obtained from a well-documented study and comparative evaluation of numerical methods for dynamic structural analysis [31].

Table 3.1

	Geometry Problem types	Geometric non-linearities	Continuum descriptions (see note)	Discretization	Integration E = explicit I = implicit	Difference formula	Energy balance	Origin
ANSYS	General purpose	Yes, but limited	Not specific	F.E.	I(T)	Houbolt	No	Proprietary
ADINA	General purpose	Yes	S - E σ - ε	F.E.	I(T)	Newmark or Willson	Yes	Bathe/M.I.T.
NONSAP	2D & some 3D capability	Yes	S - E σ - ε	F.E.	I(T)	Newmark or Willson	Yes	U. California, Berkeley
PISES	2D & 3D axl. cont.	Yes	σ - d	F. DIFF.	E	Cent. DIFF.	Yes	Proprietary
MARC	General Purpose	Yes, moderate rotations for shell plate	S - E	F.E.	I(T)	Newmark or Willson	No	Proprietary

NOTE: T = tangent stiffness
 S - E = second Piola - Kirchhoff Stress - Green Strain
 σ - ε = Cauchy stress - velocity strain
 σ - ε = Cauchy stress - Amansi strain

4. Continuum mechanics

In non-linear dynamic finite element analysis involving large deformations and material nonlinearities, it is necessary to use an incremental formulation of the equation of motion. It is assumed that the continuum can experience large displacements, large strains, and the media are described by general constitutive laws. The formulations given herein include all non-linear effects.

Let us now consider the motion of a body [Figure 1]. It is now required to evaluate the equilibrium positions of the body at the discrete time points $0, \Delta t, 2\Delta t - \text{etc.}$, where Δt is an increment in time. We now assume that the static and kinematic variables for all time steps 0 to t have been solved, and that the solution for time $t + \Delta t$ is required.

In Figure 1, the coordinates describing the configuration of this body at time 0 are ${}^0x_1, {}^0x_2, {}^0x_3$ at time t are ${}^tx_1, {}^tx_2, \text{and } {}^tx_3$, and at a time $t + \Delta t$ are ${}^{t+\Delta t}x_1, {}^{t+\Delta t}x_2, {}^{t+\Delta t}x_3$, where the left subscript denotes the time related configuration of the body, and subscripts refer to the coordinates. The notation for the displacement variable u is similar, such as ${}^{t+\Delta t}u_i, i = 1, 2, 3$. We can now describe the configuration at time t in the following manner:

$${}^tx_i = {}^0x_i + u_i \quad (4.1)$$

$$i = 1, 2, 3$$

$${}^{t+\Delta t}x_i = {}^0x_i + {}^{t+\Delta t}u_i \quad (4.2)$$

The increment in the displacements from time t to $t + \Delta t$ are denoted as follows

$$\Delta u_i = {}^{t+\Delta t}u_i - {}^tu_i \quad i = 1, 2, 3 \quad (4.3)$$

During the time the body is in motion, its mass density, surface area, and volume stresses and strains are changing continuously.

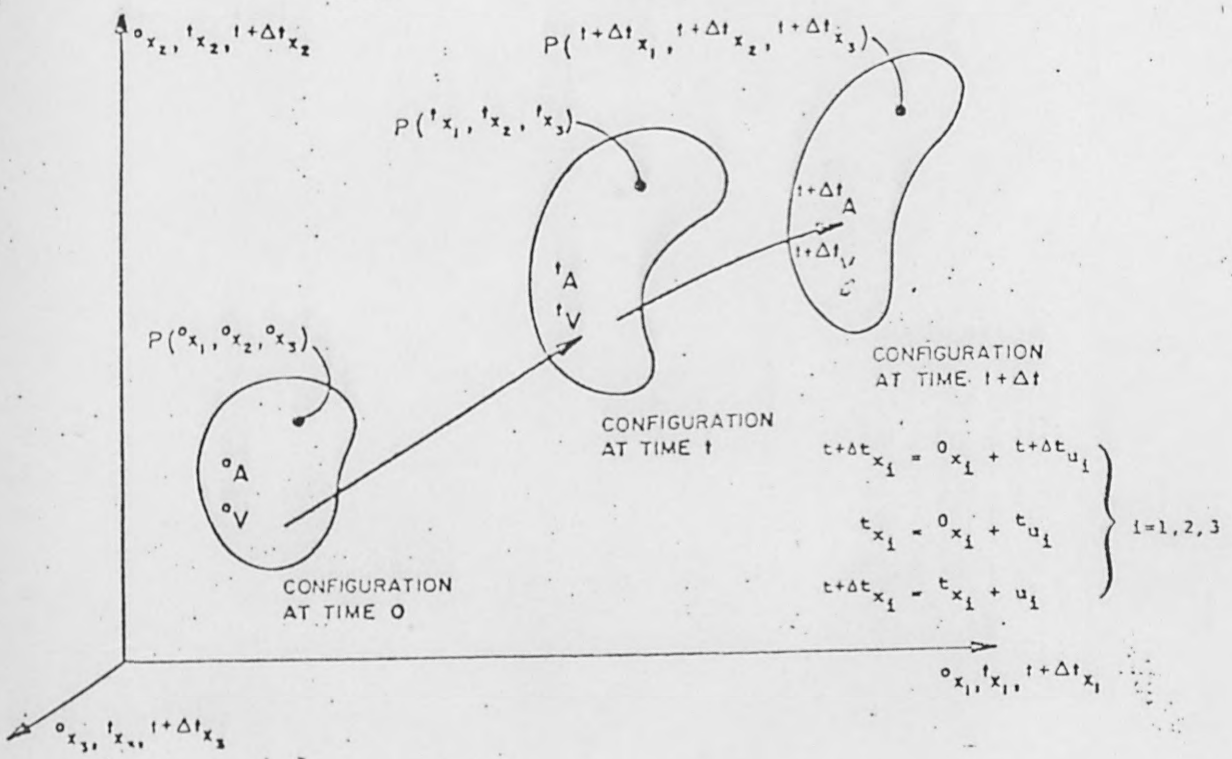


FIG. 1

We now denote these quantities at a time $0, t, t + \Delta t$ as $0_p, t_p, t + \Delta t_p, 0_A, t_A$ and $0_V, t_V$ and $t + \Delta t_V$.

Since the configuration of the body at time $t + \Delta t$ is not known, we will refer applied forces, stresses and strains to a known equilibrium configuration. Analogous to the notation already mentioned, the surface and body force components per unit mass at time $t + \Delta t$, but measured in the configuration at time t , are

$${}^t_{}{}^{t+\Delta t} \hat{t}_K = \text{surface force per unit area } (\hat{t})$$

referred to the configuration at time t .

$${}^t_{}{}^{t+\Delta t} f_K = \text{body force per unit mass } (f)$$

referred to the configuration at time t , $K = 1, 2, 3$.

Considering now the stresses, the cartesian stress components of the Cauchy stress tensor at time $t + \Delta t$ is

$${}^{t+\Delta t} \tau_{ij}$$

Since the Cauchy stresses (engineering stresses) are always referred to the configuration in which they do occur,

$${}^{t+\Delta t} \tau_{ij} = {}^{t+\Delta t} \tau_{ij}$$

The cartesian components of the second Piola-Kirchhoff stress tensor corresponding to the configuration at time $t + \Delta t$ but measured in configuration at time t by

$${}^t_{}{}^{t+\Delta t} s_{ij}$$

Considering the strains, the cartesian components of Cauchy's infinitesimal strain tensor referred to the configuration at time

$t + \Delta t$ are denoted by $t + \Delta t e_{ij}$. The reference configurations for the Kirchhoff stresses, Green-Lagrange strains are those which are referred to at times 0 and t .

In the formulation of the governing equilibrium equations, it is necessary to consider derivatives of displacement and coordinates. In the notation adopted, a comma denotes differentiation with respect to coordinates following, and the left subscripts indicate the configuration in which this coordinate is measured. Thus we have, for example

$$t + \Delta t \begin{matrix} 0 \\ u_{i,j} \end{matrix} = \frac{\partial^{t+\Delta t} u_i}{\partial^0 x_j} \quad (4.4)$$

$$t + \Delta t \begin{matrix} 0 \\ x_{m,n} \end{matrix} = \frac{\partial^0 x_m}{\partial^{t+\Delta t} x_n} \quad (4.5)$$

4.1 Principle of virtual displacements

Since the isoparametric displacement based finite element procedure shall be employed for the numerical solution, we shall use the principle of virtual displacement to express the equilibrium of the body in the configuration at time $t + \Delta t$. Assuming that the direction and magnitude of the body and surface loading is independent of the configuration, the principle of virtual displacement requires that [18]

$$t + \Delta t \int_V e_{ij}^{t+\Delta t} \delta_{t+\Delta t} e_{ij}^{t+\Delta t} dv = t + \Delta t R \quad (4.6)$$

where $t + \Delta t R$ = external virtual work and is expressed as follows

$$t + \Delta t R = \int_A^{t+\Delta t} \hat{0}^t_K \delta u_K^0 da + \int_V^0 \rho^{t+\Delta t} f_K \delta u_K^0 dv \quad (4.7)$$

δu_K is a virtual variation in the current displacement components $t + \Delta t$, and $\delta_{t+\Delta t} e_{ij}$ are the virtual corresponding variations in strains or $\delta_{t+\Delta t} e_{ij} = \delta \frac{1}{2} (t+\Delta t u_{i,j} + t+\Delta t u_{j,i})$ (4.8)

Equation 4.6 cannot be solved directly since the configuration at time $t + \Delta t$ is unknown. An approximate solution can be obtained by referring all variables to a known previously calculated equilibrium configuration, and the solution is improved by iteration [17, 20].

For the purpose of obtaining a first approximation solution, a formulation called the total Lagrangian formulation or just the Lagrangian formulation is adopted. In this solution, all static and kinematic variables are referred to the initial configuration at time $t = 0$ [18]. In the other approximate solution, all static and kinematic variables are referred to the configuration at time t . This is commonly known as the updated Lagrangian formulation. Both formulations include all the non-linear effects such as large displacement, large strains and material nonlinearities. The only advantage of using one or the other is the numerical efficiency which largely depends on the definition of the material law.

The first step in the formulation is to obtain an approximate solution to equation 4.6 by linearizing the equation about the last calculated equilibrium configuration at time t . The approximate solution is then improved by iteration [19].

Using the notations outlined before, the TL formulation is transformed to [20]:

$$\int_V^0 \delta_{t+\Delta t} S_{ij} \delta_{t+\Delta t} \epsilon_{ij}^0 dv = {}^{t+\Delta t}R \quad (4.9)$$

Similarly, in the UL formulation, equation 4.6 becomes

$$\int_V^t \delta_{t+\Delta t} S_{ij} \delta_{t+\Delta t} \epsilon_{ij}^t dv = {}^{t+\Delta t}R \quad (4.10)$$

where

$${}^0e_{ij} = \frac{1}{2} \left[\frac{\partial {}^0u_i}{\partial {}^0X_j} + \frac{\partial {}^0u_j}{\partial {}^0X_i} + \frac{\partial {}^t u_k}{\partial {}^0X_i} \frac{\partial {}^0u_k}{\partial {}^0X_j} + \frac{\partial {}^0u_k}{\partial {}^0X_i} \frac{\partial {}^t u_k}{\partial {}^0X_j} \right] \quad (4.17)$$

and

$${}^0\eta_{ij} = \frac{1}{2} \left[\frac{\partial {}^0u_k}{\partial {}^0X_i} \frac{\partial {}^0u_k}{\partial {}^0X_j} \right] \quad (4.18)$$

Using the above decompositions and linearising the equations of motion, as well as using the approximations

$${}^0S_{ij} = {}^0C_{ijrs} {}^0e_{ij} \quad (4.19)$$

$$\delta {}^0\varepsilon_{ij} = \delta {}^0e_{ij} \quad (4.20)$$

we obtain the approximate equations of motion in total Lagrangian formulation

$$\int_{{}^0V} {}^0C_{ijrs} {}^0e_{rs} \delta {}^0e_{ij} {}^0dv + \int_{{}^0V} {}^tS_{ij} \delta {}^0\eta_{ij} {}^0dv =$$

$${}^{t+\Delta t}R - \int_{{}^0V} {}^tS_{ij} \delta {}^0e_{ij} {}^0dv \quad (4.21)$$

In a similar way, we can derive the approximate linearised equations of motion in updated Lagrangian formulation as below:

$$\int_{{}^tV} {}^tC_{ijrs} {}^te_{rs} \delta {}^te_{ij} {}^tdv + \int_{{}^tV} {}^t\tau_{ij} \delta {}^t\eta_{ij} {}^tdv =$$

$${}^{t+\Delta t}R - \int_{{}^tV} {}^t\tau_{ij} \delta {}^te_{ij} {}^tdv \quad (4.22)$$

4.2 The finite element discretization

The finite element discretization of equations of motion 4.21 and 4.22 including the nonlinear material effects can be written in the following form as shown by Bathe et al. [19].

T.L. Formulation

$$\int_{0V} \rho^0 \ddot{u}_k \delta u_k^0 dv + \int_{0V} C_{ijrs}^0 e_{rs} \delta e_{ij}^0 dv + \int_{0V} t_{S_{ij}}^0 \delta n_{ij}^0 dv = {}^{t+\Delta t}R - \int_{0V} t_{S_{ij}}^0 \delta e_{ij}^0 dv \quad (4.1.1)$$

U.L. Formulation

$$\int_{0V} \rho^0 \ddot{u}_k \delta u_k^0 dv + \int_{0V} t_{ijrs}^C e_{rs} \delta t_{ij}^e dv + \int_{0V} t_{\tau_{ij}}^t \delta t_{ij}^e dv = {}^{t+\Delta t}R - \int_{0V} t_{ij}^e \delta t_{ij}^e dv \quad (4.1.2)$$

In the isoparametric finite element solution, the coordinates and displacement of an element are interpolated using

$$\begin{aligned} 0X_j &= \sum_{i=k}^N h_k^0 X_j^k & j = 1, 2, 3 \\ tX_j &= \sum_{k=1}^N h_k^t X_j^k \\ {}^{t+\Delta t}X_j &= \sum_{k=1}^N h_k^{t+\Delta t} X_j^k \\ t_{u_j} &= \sum_{k=1}^N h_k^t u_j^k; & u_j &= \sum_{k=1}^N h_k u_j^k \end{aligned}$$

The following table shows the transformation of the finite element formulation to the equivalent matrix evaluation.

The following notations are used for the calculation of the element matrices:

H_s, H = surface and volume displacement transformation matrix

${}_{0}^{t+\Delta t}t, {}_{0}^{t+\Delta t}t_f$ = vectors of surface and body forces defined per unit area and per unit mass of the body at time 0

$B_L, {}_{0}^{t}B_L, {}_{t}^{t}B_L$ = linear strain displacement matrix

${}_{0}^{t}B_{NL}, {}_{t}^{t}B_{NL}$ = nonlinear strain displacement matrix

C = stress-strain material properties (incremental or total)

${}_{t}^{t}\tau, \hat{t}_{t}^{\tau}$ = matrix and vector of Cauchy stresses

${}_{0}^{t}S, \hat{t}_{0}^{t}S$ = matrix and vector of second Piola-Kirchhoff stress

\hat{t}_{t}^{τ} = vector of stress in nonlinear material only

Table 4.1
Finite element matrices

Analysis type	Integral	Matrix Calculation
A. in all analysis	$\int_V \rho^{t+\Delta t} \mathbf{u}_k \delta \mathbf{u}_k \, dv$ ${}^{t+\Delta t} \mathbf{R} =$ $\int_A \mathbf{t}_k \delta \mathbf{u}_k \, da$ $+ \int_V \rho^{t+\Delta t} \mathbf{f}_k \delta \mathbf{u}_k \, dv$	$\mathbf{M}^{t+\Delta t} \ddot{\mathbf{u}} =$ $\int_V \rho \mathbf{H}^T \mathbf{H} \, dv$ ${}^{t+\Delta t} \mathbf{R} = \int_A \mathbf{H}_S^T \mathbf{t}_k \, da$ $+ \int_V \rho \mathbf{H}^T \mathbf{f}_k \, dv$
B. Material nonlinearity only	$\int_V C_{ijrs} e_{rs} \delta e_{ij} \, dv$ $\int_V \mathbf{t}_{\sigma_{ij}} \delta e_{ij} \, dv$	${}^t \mathbf{K} \mathbf{u} = \left(\int_V \mathbf{B}_L^T \mathbf{C} \mathbf{B}_L \, dv \right) \mathbf{u}$ ${}^t \mathbf{F} = \int_V \mathbf{B}_L^T \hat{\mathbf{t}}_{\Sigma} \, dv$
C. Total Lagrangian formulation	$\int_V C_{ijrs}^0 e_{rs} \delta e_{ij}^0 \, dv$ $\int_V \mathbf{t}_{S_{ij}}^0 \delta e_{ij}^0 \, dv$ $\int \mathbf{t}_{S_{ij}}^0 \delta e_{ij}^0 \, dv$	${}^t \mathbf{K}_L \mathbf{u} = \left(\int_V \mathbf{B}_L^T \mathbf{C}_0 \mathbf{B}_L \, dv \right) \mathbf{u}$ ${}^t \mathbf{K}_{NL} \mathbf{u} = \left(\int_V \mathbf{B}_{NL}^T \mathbf{t}_S \mathbf{B}_{NL} \, dv \right) \mathbf{u}$ ${}^t \mathbf{F} = \int \mathbf{B}_{NL}^T \hat{\mathbf{t}}_S^0 \, dv$

Table 4.1 (continued)

Analysis Type	Integral	Matrix Evaluation
D. Updated Lagrangian formulation	$\int_V t_{Cijrs} t_{e rs} \delta t_{e ij} t_{dv}$	$t_{L}^{K u} = \int (t_{L}^{B T} t_{t} C_{t}^{B L} t_{dv}) u$
	$\int_V t_{\tau ij} \delta t_{\eta ij} t_{dv}$	$t_{NL}^K = \int (t_{NL}^{B T} t_{\tau} t_{NL}^{B} t_{dv}) u$
	$\int_V t_{\tau ij} \delta t_{e ij} t_{dv}$	$t_F = \int t_{L}^{B T} t_{\tau}^{\wedge} t_{dv}$

5. Formulation of Basic Equation of Motion Due to Earthquake Excitation

In order to derive the equations of motion due to arbitrary motion at the base of the soil-structure system, it will be necessary to include support in the nodal point displacement vector. We therefore partition the total displacement vector $\{u\}_t$ into support displacements $\{u\}_b^t$ and the displacements $\{u\}^t$ for the other nodes. In matrix form the above displacements could be written as follows [21]:

$$\{u\}_t = \begin{Bmatrix} \{u\}^t \\ \{u\}_b^t \end{Bmatrix} \quad (5.1)$$

Now the nodal point displacements are made up of quasi-static displacements $\{u\}_s$ and displacements due to the dynamic effect $\{u\}$ for other nodes and supports respectively.

In matrix form:

$$\begin{Bmatrix} \{u\}^t \\ \{u\}_b^t \end{Bmatrix} = \begin{Bmatrix} \{u\}_s \\ \{u\}_{sb} \end{Bmatrix} + \begin{Bmatrix} \{u\} \\ \{u\}_b \end{Bmatrix} \quad (5.2)$$

Introducing (5.2) in the following general equation of motion

$$[M] \{\ddot{u}\} + [C] \{\dot{u}\} + [K] \{u\} = \{P_t\} \quad (5.3)$$

Now by expanding the structural property matrices, to account for support displacements, the equation of motion of the nodes not attached to the support can be stated as follows:

$$\begin{bmatrix} [M] & | & [M]_b \\ \hline & & \end{bmatrix} \begin{Bmatrix} \{\ddot{u}\}^t \\ \{\ddot{u}\}_b^t \end{Bmatrix} + \begin{bmatrix} [C] & | & [C]_b \\ \hline & & \end{bmatrix} \begin{Bmatrix} \{\dot{u}\}^t \\ \{\dot{u}\}_b^t \end{Bmatrix} + \begin{bmatrix} [K] & | & [K]_b \\ \hline & & \end{bmatrix} \begin{Bmatrix} \{u\}^t \\ \{u\}_b^t \end{Bmatrix} = 0$$

As there are no external loads applied at the nodal points, the right hand side of equation (5.3) vanishes.

Therefore, equation (5.3) can be stated as follows:

$$[M] \{\ddot{u}\} + [C] \{\dot{u}\} + [K] \{u\} = \{P_{\text{eff}}^{(t)}\} \quad (5.5)$$

where

$$\{P_{\text{eff}}^t\} = - \begin{bmatrix} [M] & [M_b] \end{bmatrix} \begin{Bmatrix} \{\ddot{u}\}_s \\ \{\ddot{u}\}_{sb} \end{Bmatrix} - \begin{bmatrix} [C] & [C_b] \end{bmatrix} \begin{Bmatrix} \{\dot{u}\}_s \\ \{\dot{u}\}_{sb} \end{Bmatrix} \quad (5.6)$$

If the damping term in the effective load vector is neglected, which is considerably smaller than the inertial term, the pseudo-static displacements may be computed most conveniently from the static relationships.

$$[K] \{u\}_s + [K]_b \{u\}_{sb} = 0 \quad (5.7)$$

In which the only loading specified is the support displacement vector $\{u\}_{sb}$ or base motion.

Solving for nodal displacements gives:

$$\{u\}_s = - [K]^{-1} [K]_b \{u\}_{sb} \quad (5.8)$$

Substituting (5.8) in (5.6) yields:

$$\{P_{\text{eff}}^{(t)}\} = \begin{bmatrix} [M] & [K]^{-1} [K]_b & - [M]_b \end{bmatrix} \{\ddot{u}^{(t)}\}_{sb} \quad (5.9)$$

For a lumped mass system, the effective load vector in (5.6) can be written as follows:

$$\{P_{\text{eff}}^{(t)}\} = [M] [R] \{\ddot{u}^{(t)}\}_{sb} \quad (5.10)$$

Because $[M]_b = 0$

and $[R] = [K]^{-1} [K]_b$ (5.11)

$[K]_b$ is the stiffness coupling matrix between the superstructure and the base support.

The influence matrix $[R]$ depends on the type of support displacement as well as on the structural configuration. When a unit static translation of the base of a structure produces directly a unit displacement of all degrees of freedom, then the matrix $[R]$ is a column vector. In other words

$$\{P_{\text{eff}}^t\} = [M] \{1\} \ddot{u}_{\text{sb}}^{(t)} \quad (5.12)$$

If we now define $\ddot{u}_{\text{sb}}^{(t)}$ as ground acceleration, then

$$\ddot{u}_{\text{sb}}^{(t)} = \ddot{u}_g^{(t)} \quad (5.13)$$

Therefore, the equation of motion at any time t due to a given base acceleration may be written as

$$\begin{aligned} [M] \{\ddot{u}(t)\} + [C] \{\dot{u}(t)\} + [K] \{u(t)\} &= [M] \{1\} \ddot{u}_g^{(t)} \\ &= \{P_{\text{eff}}^t\} \end{aligned} \quad (5.14)$$

In equation (5.14), it should be emphasized that the forces developed during an earthquake are not applied to the structure, but are applied as inertia forces resulting from the motions of the structure. Equation (5.14) is identical with that which would apply to a stationary structure subjected to an effective force

$$\{P_{\text{eff}}^t\} = [M] \{1\} \ddot{u}_g^{(t)} \quad (5.15)$$

6 Methods of Temporal Integration

Since the subject matter of this thesis is the non-linear dynamic analysis, it is essential and appropriate, to take a good look at some of the most commonly used numerical integration scheme in engineering problems. Question is often asked which is the most powerful integration scheme, that will solve almost every kind of non-linear problem static or dynamic. The author of this thesis feels that there is no unique answer to this question. Researches in this area are still continuing in various institutions, and the answer is yet to be found, that is to say an universal integration scheme suitable for all kinds of non linear problems. In this section essential factures of some commonly used integration scheme will be discussed, and recommendation of their proper usage will be made, which may help practicing engineers and researchers in selecting suitable numerical scheme.

It is necessary to be pointed out that the discussion will be limited within the scope of this thesis.

The methods which are to be discussed here are as follows:

1. Houbolt method
2. Newmark method
3. Load extrapolation method
4. Central difference method

1 Houbolt Method

The nonlinear system of ordinary differential equations that represent the structural dynamic model are

$$M\ddot{u} + C\dot{u} + K(u)u = F(t) \quad (6.1)$$

where M is the mass matrix, C is the damping matrix, K is the stiffness matrix, and $F(t)$ is the generalized force vector. Note that the stiffness term is nonlinear through the dependence of the stiffness matrix K on the displacement vector u .

We develop step by step solution algorithms by defining a partition of the time axis into discrete points. We call this partition P .

$$P = 0, \Delta t, 2\Delta t, \dots, n\Delta t \quad (6.2)$$

We denote the vector of displacements u evaluated at the points of partition P by

$$u^0, u^{\Delta t}, u^{2\Delta t}, \dots, u^{n\Delta t} \quad (6.3)$$

Similarly the velocity and acceleration are given by

$$\dot{u}^0, \dot{u}^{\Delta t}, \dot{u}^{2\Delta t}, \dots, \dot{u}^{n\Delta t} \quad (6.4)$$

and

$$\ddot{u}^0, \ddot{u}^{\Delta t}, \ddot{u}^{2\Delta t}, \dots, \ddot{u}^{n\Delta t} \quad (6.5)$$

The Houbolt method (47) is obtained by fitting a cubic polynomial of the current value of displacement and the three previous values. Then we get at a typical time point $t = i\Delta t$

$$\dot{u}^{i\Delta t} = \frac{1}{6\Delta t} \left\{ 11u^{i\Delta t} - 18u^{(i-1)\Delta t} + 9u^{(i-2)\Delta t} - 2u^{(i-3)\Delta t} \right\} \quad (6.6)$$

and

$$\ddot{u}^{i\Delta t} = \frac{1}{\Delta t^2} \left\{ 2u^{i\Delta t} - 5u^{(i-1)\Delta t} + 4u^{(i-2)\Delta t} - u^{(i-3)\Delta t} \right\} \quad (6.7)$$

Evaluating 6.1 at $t = i\Delta t$ and introducing (6.6) and (6.7), we get

$$\begin{aligned} \left\{ M + \frac{11}{12}\Delta t C + \frac{1}{2}\Delta t^2 k(u^{i\Delta t}) \right\} u^{i\Delta t} = \\ = \frac{1}{2}\Delta t^2 F^{i\Delta t} + \left(\frac{5}{2}M + \frac{3}{2}\Delta t C \right) u^{(i-1)\Delta t} - \left(2M + \frac{3}{4}\Delta t C \right) u^{(i-2)\Delta t} \\ + \left(\frac{M}{2} + \frac{1}{6}\Delta t C \right) u^{(i-3)\Delta t} \end{aligned} \quad (6.8)$$

This is the Houbolt algorithm. It must be started by a special procedure which will not be discussed here. Eq. (6.8) is a system of nonlinear algebraic equations. It can be solved for example by the Newton-Raphson method. Thus for each time point in the partition P we must iteratively solve a system of nonlinear algebraic equations.

2 Newmark Method

In the method developed by Newmark (46) the velocity vector $\dot{u}^{i\Delta t}$ and the displacement vector $u^{i\Delta t}$ are assumed to have the following form

$$\begin{aligned} \dot{u}^{i\Delta t} &= \dot{u}^{(i-1)\Delta t} + (1-\delta)\Delta t \ddot{u}^{(i-1)\Delta t} + \delta \Delta t \ddot{u}^{i\Delta t} \\ u^{i\Delta t} &= u^{(i-1)\Delta t} + \Delta t \dot{u}^{(i-1)\Delta t} + \left(\frac{1}{2} - \alpha \right) \Delta t^2 \ddot{u}^{(i-1)\Delta t} \\ &\quad + \alpha \Delta t^2 \ddot{u}^{i\Delta t} \end{aligned} \quad (6.9)$$

where α and δ are constants. The constant, acceleration case is the case in which $\alpha = \frac{1}{4}$ and $\delta = \frac{1}{2}$ in (6.9). Evaluating (6.1) at $t = i\Delta t$ and $t = (i-1)\Delta t$ and using (6.9), we get for $\delta = \frac{1}{2}$.

$$\begin{aligned}
 & \left\{ M + \frac{\Delta t}{2} C + \alpha \Delta t^2 k(u^{i\Delta t}) \right\} u^{i\Delta t} \\
 &= \Delta t^2 \left\{ \alpha F^{i\Delta t} + (1-2\alpha) F^{(i-1)\Delta t} + \alpha F^{(i-2)\Delta t} \right. \\
 & \quad \left. + 2 \left\{ M - \Delta t^2 \left(\frac{1}{2} - \alpha \right) K(u^{(i-1)\Delta t}) \right\} u^{(i-1)\Delta t} \right. \\
 & \quad \left. - \left\{ M - \frac{\Delta t}{2} C + \alpha \Delta t^2 k(u^{(i-2)\Delta t}) \right\} u^{(i-2)\Delta t} \right. \quad (6.10)
 \end{aligned}$$

This is the Newmark method. Equation (6.10) represents a system of nonlinear algebraic equations. For each step in the step by step time integration process (6.10) must be solved by an iterative process such as Newton-Raphson.

3 Load Extrapolation

In the load extrapolation schemes we simplify (6.8) and (6.10) and for that matter any implicit scheme by carrying out the following procedure: We place all nonlinear terms on the right-hand side of the equation, consider these terms as applied loads, and use a backwards difference approximation to express the applied loads in terms of values at previous time points. This approach has been used by Weeks (48) and Stricklin (11). Suppose in (6.8) and (6.10) we denote all the nonlinear terms plus the applied loads when transposed to the right hand side of the equation and $i\Delta t$ evaluated at time point $t = i\Delta t$ by $H(t, u)$.

We let

$$H(t, u) = H(t, u)^{(i-1)\Delta t} + \Delta t \frac{\partial}{\partial t} H(t, u)^{(i-1)\Delta t} \quad (6.11)$$

Then using the backwards difference approximation

$$\frac{\partial}{\partial t} H(t, u)^{(i-1)\Delta t} = \frac{H(t, u)^{(i-1)\Delta t} - H(t, u)^{(i-2)\Delta t}}{\Delta t} \quad (6.12)$$

We get

$$H(t, u)^{i\Delta t} = 2 H(t, u)^{(i-1)\Delta t} - H(t, u)^{(i-2)\Delta t} \quad (6.13)$$

As an illustration of the application of this type algorithm let

$$H(t, u)^{i\Delta t} = \frac{1}{2} \Delta t^2 (F^{i\Delta t} - k(u^{i\Delta t}) u^{i\Delta t}) \quad (6.14)$$

Using (6.14) and (6.13) in conjunction with (6.8) (The Houbolt algorithm), we get a Houbolt algorithm with load extrapolation.

$$\begin{aligned} \left(M + \frac{11}{12} \Delta t C \right) u^{i\Delta t} &= \Delta t^2 \left(F^{(i-1)\Delta t} - K(u^{(i-1)\Delta t}) u^{(i-1)\Delta t} \right) \\ &\quad - \frac{\Delta t^2}{2} \left(F^{(i-2)\Delta t} - K(u^{(i-2)\Delta t}) u^{(i-2)\Delta t} \right) \\ &\quad + \left(\frac{5}{2} M + \frac{3}{2} \Delta t C \right) u^{(i-1)\Delta t} - \left(2M + \frac{3}{4} \Delta t C \right) u^{(i-2)\Delta t} \\ &\quad + \left(\frac{M}{2} + \frac{1}{6} \Delta t C \right) u^{(i-3)\Delta t} \end{aligned} \quad (6.15)$$

4 Central Difference Method

Let us evaluate (6.1) at time point

$$t = (i-1)\Delta t$$

$$M \ddot{u}^{(i-1)\Delta t} + C \dot{u}^{(i-1)\Delta t} + K(u^{(i-1)\Delta t}) u^{(i-1)\Delta t} = F^{(i-1)\Delta t} \quad (6.16)$$

Now in the central difference approximation we let

$$\ddot{u}^{(i-1)\Delta t} = \frac{u^{i\Delta t} - 2u^{(i-1)\Delta t} + u^{(i-2)\Delta t}}{\Delta t^2} \quad (6.17)$$

and we let

$$\dot{u}^{(i-1)\Delta t} = \frac{u^{(i-1)\Delta t} - u^{(i-2)\Delta t}}{\Delta t} \quad (6.18)$$

Introducing (6.17) and (6.18) into (6.16) we get the central difference algorithm.

$$\begin{aligned} M u^{i\Delta t} = & 2M u^{(i-1)\Delta t} - M u^{(i-2)\Delta t} - \Delta t C u^{(i-1)\Delta t} \\ & + \Delta t C u^{(i-2)\Delta t} - \Delta t^2 K (u^{(i-1)\Delta t})' u^{(i-1)\Delta t} \\ & + F^{(i-1)\Delta t} \end{aligned} \quad (6.19)$$

This scheme is explicit for the case when the mass matrix is lumped. This implies that no iteration during a time step is required with the central difference algorithm. This is its main benefit. Its drawbacks are that it is only conditionally stable. The time step must be less than a certain critical value.

$$\Delta t \leq \Delta t^{\text{CRIT}} \quad (\text{ca. } 1/10 \text{ of lowest eigen period})$$

to obtain a stable approximation. In addition the scheme is not self starting.

We do not discuss the starting scheme here because it is normally the same as is used in the linear analysis. However we do make this comment: The starting scheme for the central difference approximation pollutes the solution with error because it is normally very inaccurate. (24)

5 Numerical Experiments (Weeks (48))

Weeks (48) has performed numerical experiments to determine the relative efficiency of the following schemes:

- . Houbolt {
 - Newton-Raphson
 - Load Extrapolation

- . Newmark {
 - Newton-Raphson
 - Load Extrapolation
 ($\alpha = \frac{1}{4}$)

- . Central Difference

The sample problem is shown in Figure 6.1

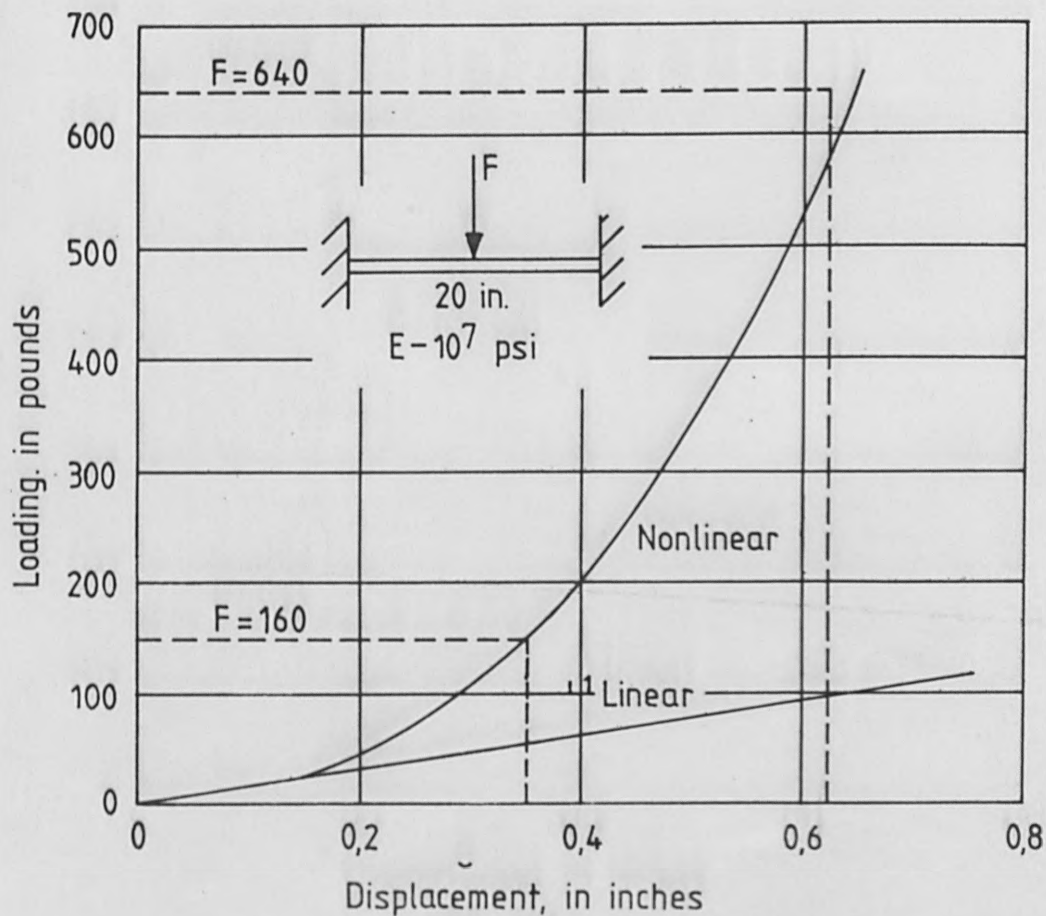


Fig. 6.1

Two finite elements are used to model the system giving it one degree of freedom. In Figure 6.2 the solution to the undamped problem using the three methods with Newton-Raphson iteration is shown.

Conclusion:

- . Houbolt too damped to be of use
- . Central difference has amplitude error
- . Newmark has a phase error

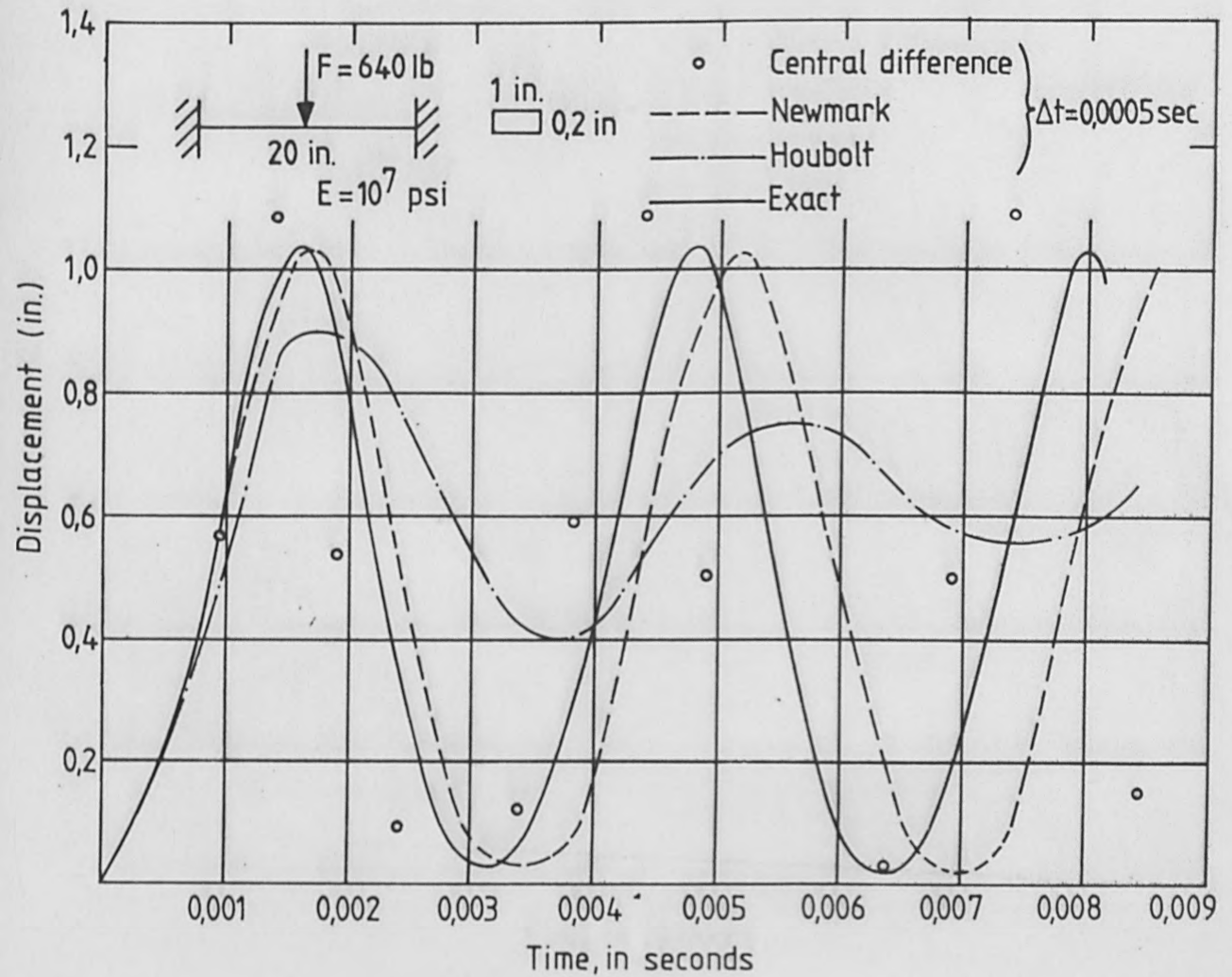


Fig. 6.2

In Figure 6.3 the solution to the damped problem using load extrapolation is compared to the results using Newton-Raphson both using the Houbolt scheme.

Note that Weeks tried the Newmark load extrapolation scheme for these time step sizes but the scheme was unstable.

Conclusions:

- . Newmark load extrapolation scheme is unstable at large time steps.
- . Houbolt load extrapolation scheme does not have this problem.
- . Houbolt load extrapolation scheme attenuates the amplitude of the response.
- . Houbolt Newton-Raphson is always stable
- . In this case load extrapolation is actually better than Newton-Raphson

Recommendation: Use Newmark method with small step size. This contradicts Stricklin's recommendation to use Houbolt's method (highly dissipative). (11)

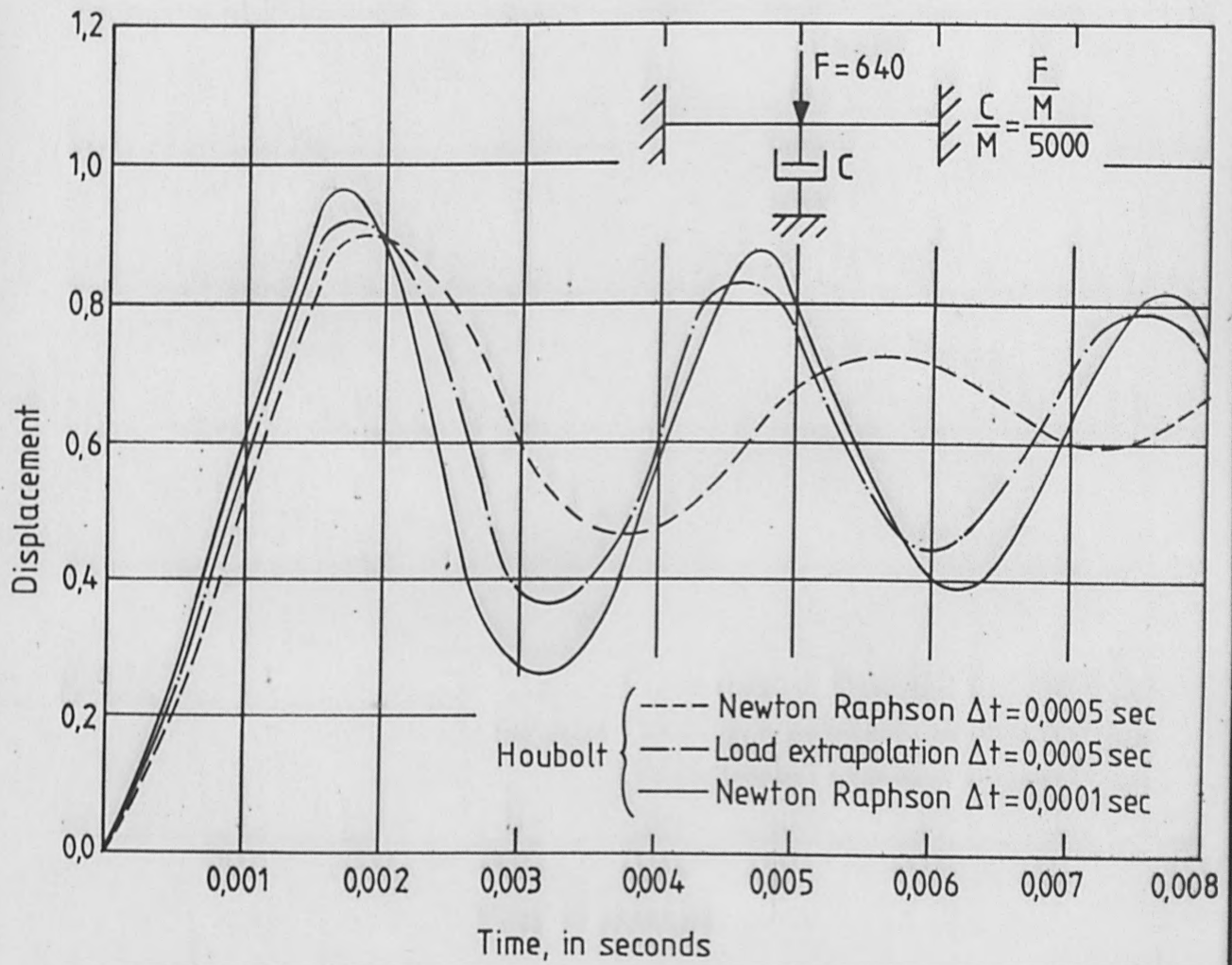


Fig. 6.3

7. Temporal integration of assembled finite elements

In the previous section, the method of temporal integration of a simplified damped system has been explained. In this section, the temporal integration of the equilibrium equation in matrix form will be explained.

Using the matrix evaluation given in Table 4.1 we have, for linear analysis at a time $t + \Delta t$

$$M^{t+\Delta t} \ddot{u} + K^{t+\Delta t} u = {}^{t+\Delta t} R \quad (7.1)$$

In nonlinear analysis including nonlinear material effects only

$$M^{t+\Delta t} \ddot{u} + {}^t K u = {}^{t+\Delta t} R - {}^t F \quad (7.2)$$

Using the TL formulation

$$M \cdot {}^{t+\Delta t} \ddot{u} + \begin{pmatrix} {}^t K \\ {}^t O_L \end{pmatrix} + \begin{pmatrix} {}^t K \\ {}^t O_{NL} \end{pmatrix} u = {}^{t+\Delta t} R - {}^t F \quad (7.3)$$

Using the UL formulation

$$M^{t+\Delta t} \ddot{u} + \begin{pmatrix} {}^t K \\ {}^t L \end{pmatrix} + \begin{pmatrix} {}^t K \\ {}^t NL \end{pmatrix} u = {}^{t+\Delta t} R - {}^t F \quad (7.4)$$

M = time independent mass matrix; either a lumped mass matrix M_l or a consistent mass matrix M_c can be used.

K = time independent linear elastic, small displacement stiffness matrix

$\begin{pmatrix} {}^t K \\ {}^t O_L \end{pmatrix}, \begin{pmatrix} {}^t K \\ {}^t L \end{pmatrix}$ = linear strain incremental stiffness matrices

$\begin{pmatrix} {}^t K \\ {}^t O_{NL} \end{pmatrix}, \begin{pmatrix} {}^t K \\ {}^t NL \end{pmatrix}$ = nonlinear strain (geometric or initial stress) incremental stiffness matrices

$\begin{pmatrix} {}^t K \\ {}^t L \end{pmatrix}$ = linear strain incremental stiffness matrix, not including the initial displacement effect

- $t+\Delta t$ R = vectors of externally applied element nodal loads
 t F , t F = vectors of nodal point forces equivalent to the element stresses at time t
 t F = vector of nodal point forces equivalent to the element stresses at time t , not including the initial displacement effect
 u = vector of incremental nodal displacements, assembled from u_j^k
 $t+\Delta t$ u = vector of total nodal displacements at time $t + \Delta t$, assembled from $u_j^{t+\Delta t k}$
 $t+\Delta t$ u = vector of nodal point accelerations

7.1 Equilibrium iteration

It is important to note that in nonlinear analysis Equation 7.2 is only an approximation to the actual equation to be solved in each time step, which is Equation 4.6. Equation 7.2 was obtained by linearising the equations of motion as shown in Tables 4.1 and 7.1. Depending on the nonlinearities in the system and the magnitude of the time step Δt , the linearisation may introduce serious errors and, indeed, solution instability. It should also be noted that the step-by-step solution may become unstable although an integration operator is used which is unconditionally stable in linear analysis [6, 7, 23].

A common observation is that the errors introduced as a consequence of the linearisation cause the calculated solution to "drift away" from the exact solution. This is much more serious in dynamic analysis than in static analysis, since, in dynamic analysis, the solution for any prescribed load at a specific time is always dependent on the history of the solution [10, 11, 23].

In order to avoid large integration errors, we may choose to iterate in each load step until, within the necessary assumptions on the variation of the material constants and the numerical time integration

scheme used, Equation 4.6 is satisfied within a required tolerance [10]. The equations solved in the iteration depend on the nonlinear finite element formulation used, and are extensions of the incremental equations. Considering, as before, a single element, in the T.L. formulation the equation used for the iteration is obtained from Equation 7.3 and is written as

$$\begin{pmatrix} t_{0L} \\ t_{0NL} \end{pmatrix} \Delta u^{(i)} = t+\Delta t_{0R} - t+\Delta t_{0F}^{(i-1)} - M t+\Delta t_{0\ddot{u}}^{(i)} \quad (7.1.1)$$

$$i = 1, 2, 3, \dots$$

where

$$t+\Delta t_{0u}^{(i)} = t+\Delta t_{0u}^{(i-1)} + \Delta u^{(i)}$$

It should be noted that for $i = 1$, Equation 7.1.1 corresponds to Equation 7.3, i.e.

$$\begin{aligned} \Delta u^{(1)} &= u, & t+\Delta t_{0\ddot{u}}^{(1)} &= t+\Delta t_{0\ddot{u}}, & (7.1.2) \\ t+\Delta t_{0u}^{(0)} &= t_u, & \text{and } t+\Delta t_{0F}^{(0)} &= t_F \end{aligned}$$

The calculation of the acceleration approximation $t+\Delta t_{0\ddot{u}}^{(i)}$ is the finite element evaluation of

$$\int_{0V} t+\Delta t_{0S_{ij}}^{(i)} \delta t+\Delta t_{0\varepsilon_{ij}}^{(i)} dv \quad (7.1.3)$$

where the superscript (i) shows that stresses and strains are evaluated using $t+\Delta t_{0u}^{(i)}$. Since

$$t+\Delta t_{0\varepsilon_{ij}} = \frac{1}{2} (\delta_{0u_{i,j}} + \delta_{0u_{j,i}} + t+\Delta t_{0u_{k,i}} \delta_{0u_{k,j}} + t+\Delta t_{0u_{k,j}} \delta_{0u_{k,i}}) \quad (7.1.4)$$

we have

$$t+\Delta t_{0F}^{(i)} = \int_{0V} t+\Delta t_{0B_L}^{(i)T} t+\Delta t_{0S}^{(i)} dv \quad (7.1.5)$$

where the matrices $t+\Delta t_{0B_L}^{(i)}$ and $t+\Delta t_{0S}^{(i)}$ correspond to the matrices $0B_L^t$ and $0S^{\wedge}$ in Table 4.1 respectively.

In the U.L. formulation, the equation used for a single element with equilibrium iteration is

$$\begin{pmatrix} t_{K_L} \\ t_{NL} \end{pmatrix} \Delta u^{(i)} = \begin{matrix} t+\Delta t_R \\ t+\Delta t_F^{(i-1)} \end{matrix} - M \begin{matrix} t+\Delta t_{\ddot{u}}(1) \\ t+\Delta t_{\ddot{u}}(i) \end{matrix} \quad (7.1.6)$$

$$i = 1, 2, 3 \dots$$

in which the i 'th displacement and acceleration approximations are calculated as above and $\begin{matrix} t+\Delta t_F^{(i)} \\ t+\Delta t \end{matrix}$ is the finite element evaluation of

$$t+\Delta t_V(i) = \int \begin{matrix} t+\Delta t_{\tau_{ij}}(i) \\ t+\Delta t_{\tau_{ij}} \end{matrix} \delta_{t+\Delta t} e_{ij}^{(i)} t+\Delta t_{dv}(i); \quad \text{i.e.} \quad (7.1.7)$$

$$\begin{matrix} t+\Delta t_F \\ t+\Delta t \end{matrix} = \frac{\int \begin{matrix} t+\Delta t_{B_L}(i)T \\ t+\Delta t_{B_L} \end{matrix} t+\Delta t_{\tau}^{(i)} t+\Delta t_{dv}(i)}{t+\Delta t_V(i)} \quad (7.1.8)$$

where the matrices $\begin{matrix} t+\Delta t_{B_L}(i) \\ t+\Delta t_{B_L} \end{matrix}$ and $t+\Delta t_{\tau}^{(i)}$ correspond to the matrices t_{B_L} and t_{τ} in Table 4.1 respectively.

The equation used in the analysis with material nonlinearities only is obtained from Equation 7.1.1 or Equation 7.1.6, by assuming that the configuration of the element does not change and that all strains are small, i.e. products of displacement derivatives in the strain calculations can be neglected. In this case, we obtain, with the previously used notation

$$t_{K_L} \Delta u^{(i)} = \begin{matrix} t+\Delta t_R \\ t+\Delta t_F^{(i-1)} \end{matrix} - M \begin{matrix} t+\Delta t_{\ddot{u}}(1) \\ t+\Delta t_{\ddot{u}}(i) \end{matrix} \quad (7.1.9)$$

$$i = 1, 2, 3 \dots$$

where $\begin{matrix} t+\Delta t_F^{(i)} \\ t+\Delta t \end{matrix}$ is the finite element evaluation of

$$\int_{O_V} \begin{matrix} t+\Delta t_{\sigma_{ij}}(i) \\ t+\Delta t_{\sigma_{ij}} \end{matrix} \delta e_{ij}^{(i)} dv, \quad \text{i.e.}$$

$$t+\Delta t_F(i) = \frac{\int_{O_V} B_L^T t+\Delta t_{\Sigma}^{(i)} dv}{O_V} \quad (7.1.10)$$

For an assemblage of elements which are described as linear, materially nonlinear only, by the T.L. or the U.L. formulations, we have corresponding to Equation 5.14 the following equilibrium iteration,

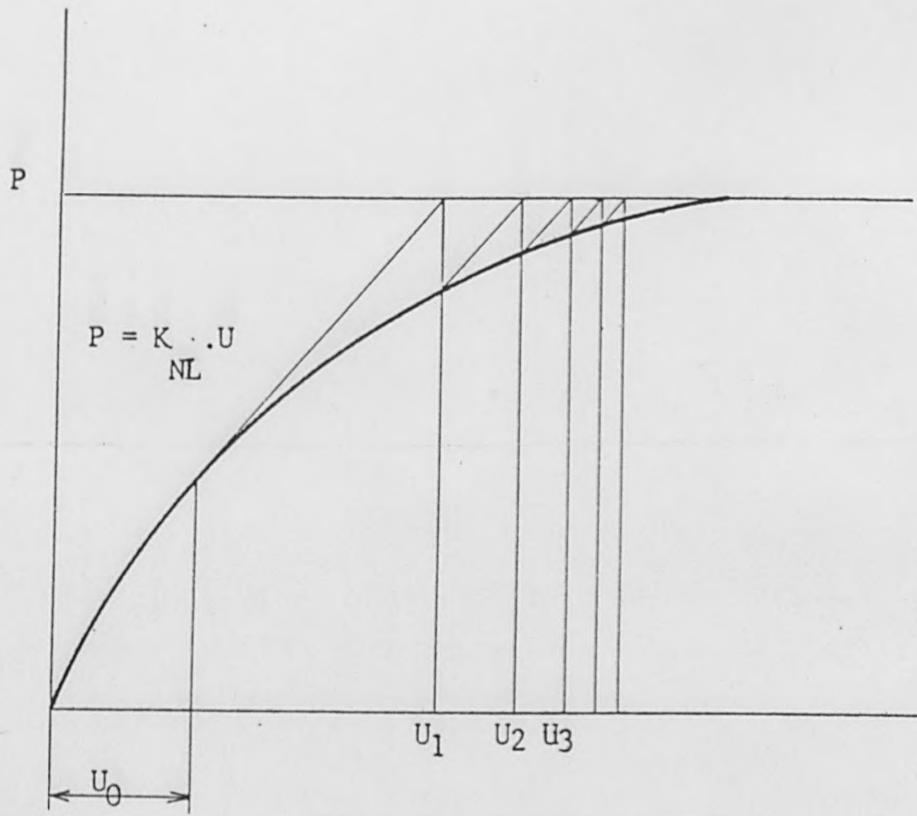
$${}^t_K \Delta u = {}^{t+\Delta t}_R - {}^{t+\Delta t}_{F(i-1)} - M {}^{t+\Delta t}_{\ddot{u}(i)} - C {}^{t+\Delta t}_{\dot{u}(i)} \quad (7.1.11)$$

$$i = 1, 2, 3 \dots$$

in which the iteration vectors are now defined for the element assemblage, and an appropriate convergence measure need be employed [12]. Equation 7.1.11 is used in the Newmark integration scheme, whereas using the Wilson θ -method, the equilibrium iteration is performed for time $t + \tau$ [17, 18].

The equilibrium iteration in Equation 7.1.11 (and Equations 7.1.1 and 7.1.6) corresponds to a Newton iteration with a constant stiffness matrix [19]. It should be noted that, provided convergence occurs, and the material description used is not path dependent, i.e. the material is elastic or hyperelastic, the "exact" solution within the assumption of the time integration operator and the convergence tolerance is obtained. It follows also that in the dynamic analysis of geometrically nonlinear systems with elastic or hyperelastic materials, we do not need to form a new stiffness matrix in each time step, but can assure solution accuracy by using equilibrium iteration. In the analysis of systems with path dependent material properties, however, the solution path is determined by the tangent stiffness matrix and sufficiently small load steps are required for solution accuracy. The above procedure is illustrated in the revised flow chart made by the author of the NONSAP program vol 2 of the thesis.

In the computer program NONSAP, one can specify an interval of time steps for formation of a new tangent stiffness matrix, and a second interval of time steps in which equilibrium iterations are to be performed. Table 7.1 gives the step-by-step time integration scheme used in the program. It is noted that the same constants are defined for the Wilson θ -method and the Newmark method in order to have one computer algorithm for both integration schemes. In the iteration



U_0 = Assumed Initial Displacement.

the convergence tolerance used is the ratio of the Euclidean norms of incremental displacements and total displacements [16, 17].

The importance of equilibrium iteration depends on the problem considered and is more pronounced in problems which allow relatively large load steps, i.e. the solution is not highly path dependent [23, 22].

Table 7.1 Summary of Step-by-Step Integration

INITIAL CALCULATIONS

1. Form linear stiffness matrix K , mass matrix M and damping matrix C ; initialize $u_0, \dot{u}_0, \ddot{u}_0$

2. Calculate the following constants:

$\text{tol} \leq 0.01$; $\text{nitem} \geq 3$; in static analysis $\theta = 1$ and goes to 3.

Wilson θ -method: $\theta \geq 1.37$, usually $\theta = 1.4$, $\tau = \theta \Delta t$

$$a_0 = 6/\tau^2 \quad a_1 = 3/\tau \quad a_2 = 2a_1 \quad a_3 = 2 \quad a_4 = 2 \quad a_5 = \tau/2$$

$$a_6 = a_0/\theta \quad a_7 = -a_2/\theta \quad a_8 = 1 - 3/\theta \quad a_9 = \Delta t/2 \quad a_{10} = \Delta t^2/6$$

Newmark method: $\theta = 1.0$, $\delta \geq 0.50$, $\alpha \geq 0.25 (0.5 + \delta)^2$, $\tau = \Delta t$

$$a_0 = 1/(\alpha \Delta t^2) \quad a_1 = \delta/(\alpha \Delta t) \quad a_2 = 1/(\alpha \Delta t) \quad a_3 = 1/(2\alpha) - 1 \quad a_4 = \delta/\alpha - 1$$

$$a_5 = \Delta t(\delta/\alpha - 2)/2 \quad a_6 = a \quad a_7 = -a_2 \quad a_8 = -a_3$$

$$a_9 = \Delta t(1 - \delta) \quad a_{10} = \delta \Delta t$$

3. Form effective linear stiffness matrix: $\hat{K} = K + a_0 M + a_1 C$

4. In linear analysis, triangularize \hat{K}

FOR EACH TIME STEP

A. IN LINEAR ANALYSIS

(i) Form effective load vector:

$${}^{t+\tau}\hat{R} = {}^tR + \theta({}^{t+\Delta t}R - {}^tR) + M(a_0^t u + a_2^t \dot{u} + a_3^t \ddot{u}) + C(a_1^t u + a_4^t \dot{u} + a_5^t \ddot{u})$$

(ii) Solve for displacement increments:

$$\hat{K}^{t+\tau} u = {}^{t+\tau}\hat{R} ; \quad u = {}^{t+\tau}u - {}^t u$$

(iii) Go to C.

B. IN NONLINEAR ANALYSIS

(i) If a new stiffness matrix is to be formed, update \hat{K} for nonlinear stiffness effects to obtain ${}^{t+\tau}\hat{K}$; triangularize ${}^{t+\tau}\hat{K}$;

$${}^{t+\tau}\hat{K} = LDL^T$$

(ii) Form effective load vector:

$${}^{t+\tau}\hat{R} = {}^tR + \theta({}^{t+\Delta t}R - {}^tR) + M(a_2^t \dot{u} + a_3^t \ddot{u}) + C(a_4^t \dot{u} + a_5^t \ddot{u}) - {}^t F$$

(iii) Solve for displacement increments using latest D,L factors:

$$LDL^T u = t+\tau_R^{\wedge}$$

(iv) If required, iterate for dynamic equilibrium; then initialize $u^{(0)} = u, i = 0$

(a) $i = i + 1$

(b) Calculate (i-1)st approximation to accelerations, velocities, and displacements:

$$t+\tau_{\ddot{u}}(i-1) = a_0 u^{(i-1)} - a_2 \dot{u}^t - a_3 \ddot{u}^t; \quad t+\tau_{\dot{u}}(i-1) = a_1 u^{(i-1)} - a_4 \dot{u}^t - a_5 \ddot{u}^t;$$

$$t+\tau_u(i-1) = t_u + u^{(i-1)}$$

(c) Calculate (i-1)st effective out-of-balance loads:

$$t+\tau_R^{\wedge}(i-1) = t_R + \theta(t+\Delta t t_R - t_R) - M^{t+\tau_{\ddot{u}}(i-1)} - C^{t+\tau_{\dot{u}}(i-1)} - t+\tau_F(i-1)$$

(d) Solve for the i'th correction to the displacement increments:

$$LDL^T \Delta u(i) = t+\tau_R^{\wedge}(i-1)$$

(e) Calculate new displacement increments:

$$u(i) = u^{(i-1)} + \Delta u(i)$$

(f) Iteration convergence if $\|\Delta u^{(i)}\|_2 / \|u^{(i)}\|_2 + \|u^{(i)}\|_2 < \text{tol}$

If convergence: $u = u^{(i)}$ and go to C;

If no convergence and $i < \text{nitern}$: go to (a); otherwise restart using new stiffness matrix and/or a smaller time step size.

C. CALCULATE NEW ACCELERATIONS, VELOCITIES AND DISPLACEMENTS

Wilson θ -method:

$${}^{t+\Delta t}\ddot{u} = a_6 u + a_7 \dot{u} + a_8 \ddot{u}$$

$${}^{t+\Delta t}\dot{u} = \dot{u} + a_9 ({}^{t+\Delta t}\ddot{u} + \ddot{u})$$

$${}^{t+\Delta t}u = u + \Delta t \dot{u} + a_{10} ({}^{t+\Delta t}\ddot{u} + 2\ddot{u})$$

Newmark method:

$${}^{t+\Delta t}\ddot{u} = a_6 u + a_7 \dot{u} + a_8 \ddot{u}$$

$${}^{t+\Delta t}\dot{u} = \dot{u} + a_9 \ddot{u} + a_{10} {}^{t+\Delta t}\ddot{u}$$

$${}^{t+\Delta t}u = u +$$

8. Modal equivalence of super-structure

In earthquake engineering the dynamic analysis of structures is carried out using generalized coordinates in such a way that the equation of motion for the system will be decoupled. Each equation represents a mode of the system. The response is found for each mode and the final result is obtained by superimposing the results. This method is known as the modal analysis.

When a lumped mass model has been set up for a complex structure containing more than one component (or branches), it can be useful to select the significant modes for each component or branch before they are coupled to build the total structure.

This section shows how an approximate model can be set up using component mode substitution. This model is more accurate, especially in the higher modes, than a reduced lumped mass model with the same number of degrees of freedom.

The concept of modal equivalence is described in references (25) through (26). We will use an independent formulation applied to the systems involved; a reactor power station. The modelling technique described below was used to model the superstructure in this case study.

8.1 Equations of Equilibrium:

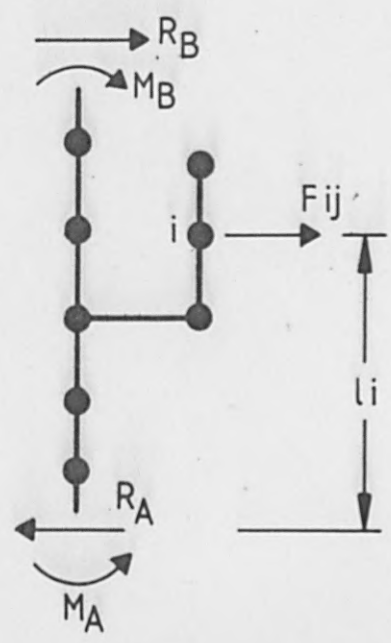
Considering horizontal accelerations only, we find that a necessary condition for a modal equivalent system to replace the subsystem is that the reactions from R_A , R_B , M_A and M_B in Figure (8) shall be the same for the same mode in the subsystem and its equivalent system.

With the reactions from the two systems equal, we have

$$\sum_{i=1}^N F_{ij} = F'_j \quad (8.1.1)$$

F_{ij} is the dynamic force of the i^{th} mass in the j^{th} mode in the subsystem

SUBSYSTEM



MODAL EQUIVALENT SYSTEM

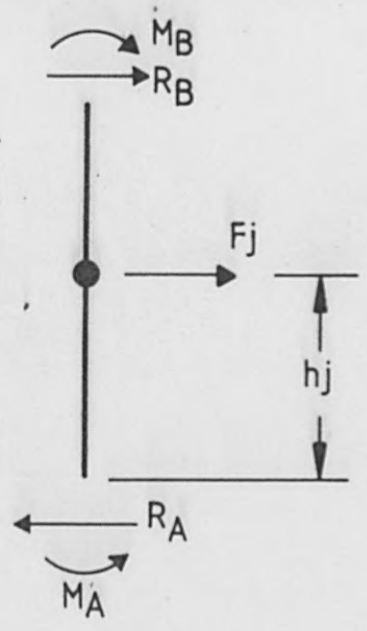


Fig. 8. Subsystem and Equivalent System for Mode j

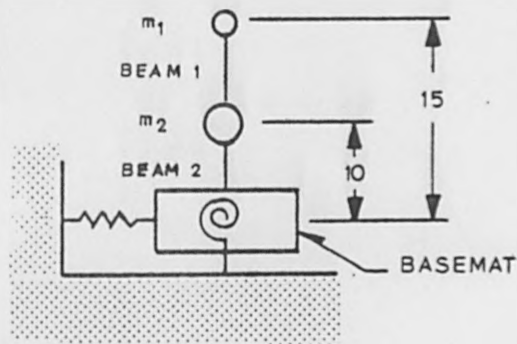


Figure 8 a. Unmodified Two-Degree-of-Freedom Model

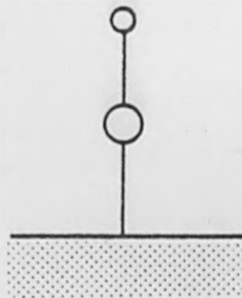


Figure 8 b. Fixed Base Two - Degree - of - Freedom Model

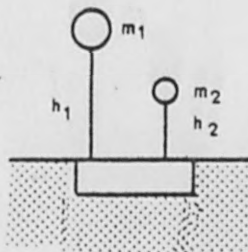


Figure 8 c. Fixed Base Modal Equivalent Model

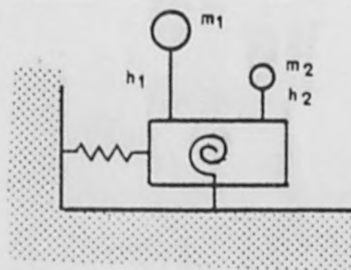


Figure 8 d. Complete Modal Equivalent Model

F'_j is the dynamic force of the single mass of the equivalent system in the j^{th} mode

N is the number of modes in the subsystem

Neglecting the rotational inertia, and taking the moment about A in both systems, we have:

$$\sum_{i=1}^N F_{ij} l_i = F'_j \cdot h_j \quad (8.1.2)$$

The equation determined by the moment about B is linearly dependent on Equations 8.1.1 and 8.1.2.

8.2 Modal Mass :

The name "modal mass" is introduced for the mass m_j of the modal equivalent system shown by Figures (8c) (8d) We have

$$F_{ij} = m_i \phi_{ij} \ddot{q}_j \quad (8.2.1)$$

m_i is the mass of the i^{th} nodal point

ϕ is the normalized modal matrix ($\phi^T M \phi = I$)

ϕ_{ij} is the normalized displacement of the i^{th} nodal point in the j^{th} mode

q_j is the j^{th} generalized response of the j^{th} mode with frequency ω_j

The generalized response is given by

$$\ddot{q} + 2\lambda\omega\dot{q} + [\omega^2]q = -\phi^T M \ddot{u}_g \quad (8.2.2)$$

\ddot{u}_g is the ground acceleration

$\phi^T M = S$ is the participation vector

λ = the modal damping factor

$$q_j = (1/\omega_j) S_j \int_0^t e^{-\lambda\omega(t-t')} \ddot{u}_g \sin[\omega_j(t-t')] dt' \quad (8.2.3)$$

The right side of 8.1.1 is

$$F'_j = m'_j \ddot{x}_j \quad (8.2.4)$$

where m'_j = modal mass j

$$x_j = (-1/\omega_j) \int_0^t \ddot{u}_g e^{-\lambda\omega(t-t')} \sin[\omega_j(t-t')] dt' \quad (8.2.5)$$

Equation 8.2.3 and 8.2.5, we obtain

$$\ddot{q}_j = S_j \ddot{x}_j \quad (8.2.6)$$

which, when inserted in 8.2.1 and further in 8.2.4 and 8.2.1 will give the modal mass as the square of the participation factor.

$$\sum_{i=1}^N m_i \phi_{ij} \cdot S_j = m'_j \quad (8.2.7)$$

$$m'_j = S_j^2 \quad (8.2.8)$$

8.3 Modal Elevation :

An elevation of the modal mass can be easily determined once the modal mass is known.

For the subsystem

$$\sum_{i=1}^N F_{ij} \cdot \ell_i = \sum_{i=1}^N m_i \phi_{ij} S_j \ddot{x}_j \cdot \ell_i \quad (8.3.1)$$

For the modal equivalent system

$$F'_j \cdot h_j = m'_j \cdot \ddot{x}_j \cdot h_j \quad (8.3.2)$$

Therefore on using Equations 8.2.1 and 8.2.8, and equating the right hand sides of the two equations above, we have

$$h_j = \left[\sum_{i=1}^N m_i \phi_{ij} \ell_i \right] / S_j \quad (8.3.4)$$

Modal Damping

Modal damping is defined by the strain energy weighted damping:

$$\beta_j = \frac{\sum_{i=1}^M \phi_i^{jT} \beta_i K_i \phi_i^j}{\sum_{i=1}^M \phi_i^{jT} K_i \phi_i^j} \quad (8.3.5)$$

Sample problem:

Two degrees of freedom of Super Structure.

Input to problem:

$$m_1 = 2 \quad m_3 = \text{Basemat mass} = 20$$

$$m_2 = 5 \quad m_4 = \text{Basemat Rotary Intertia } 10 \cdot 15$$

$$\text{Base Translational spring} = 2 \times 10^5$$

$$\text{Base Rotational spring} = 1.0 \times 10^6$$

$$\text{Beam 1} \quad EI = 10 \times 10^4$$

$$\text{Beam 2} \quad EI = 10 \times 10^4$$

Any consistent set of units may be used.

Eigen value analysis of fixed base model gives dynamic properties;

$$w_1 = 5.11 \quad \text{rad/sec}$$

$$\phi_1 = (0.538, 0.290)$$

$$w_2 = 33.22 \quad \text{rad/sec}$$

$$\phi_2 = (-0.459, 0.340)$$

Table 8.1

DYNAMIC PROPERTIES OF THE ORIGINAL MODEL

MATRIX A (MASS)

2.0000000E+00	0.	0.	0.
0.	5.0000000E+00	0.	0.
0.	0.	2.0000000E+01	0.
0.	0.	0.	1.0150000E+01

MATRIX B (STIFFNESS)

9.6014000E+02	-1.6803200E+03	-2.4010300E+03	7.2018000E+02
-1.6803200E+03	3.2407200E+03	7.2023600E+03	-1.5604000E+03
-2.4010300E+03	7.2023600E+03	1.3600750E+05	-4.8012900E+03
7.2018000E+02	-1.5604000E+03	-4.8012900E+03	2.0084020E+05

EIGENVALUE 1 2.0943994E+01
 $\eta = 4.5764608E+00$ RAD/SEC
 $F = 7.233595E-01$ HZ
 VECTOR 1.0000000E+00 6.6418504E-01 -1.2242601E-02 5.0538455E-04
 EIGENVECTOR FACTOR = 5.2744754E-01

EIGENVALUE 2 9.9143397E+02
 $\eta = 3.1487044E+01$ RAD/SEC
 $F = 5.0113230E+00$ HZ
 VECTOR 1.0000000E+00 -7.0342222E-01 6.3947623E-02 -7.9190253E-03
 EIGENVECTOR FACTOR = -4.6847598E-01

EIGENVALUE 3 6.9029029E+03
 $\eta = 3.3033710E+01$ RAD/SEC
 $F = 1.3223194E+01$ HZ
 VECTOR -2.1600932E-01 2.3987218E-01 1.0000000E+00 4.1765610E-02
 EIGENVECTOR FACTOR = 2.2141521E-01

EIGENVALUE 4 1.9800517E+04
 $\eta = 1.4071431E+02$ RAD/SEC
 $F = 2.2395396E+01$ HZ
 VECTOR 2.0515179E-02 -1.8097213E-02 -1.9157987E-02 1.0000000E+00
 EIGENVECTOR FACTOR = 3.1373054E-01

Table 8.2

DYNAMIC PROPERTIES OF THE MODAL EQUIVALENT MODEL

MATRIX A (MASS)			
6.3391413E+00	0.	0.	0.
0.	6.1085850E-01	0.	0.
0.	0.	2.0000000E+01	0.
0.	0.	0.	1.0150000E+01
MATRIX B (STIFFNESS)			
1.6700530E+02	0.	2.0252790E+03	-1.6700530E+02
0.	6.7321230E+02	2.7760090E+03	-6.7321230E+02
2.0252790E+03	2.7760090E+03	1.3600750E+05	-4.8012880E+03
-1.6700530E+02	-6.7321230E+02	-4.8012880E+03	2.0084020E+05
EIGENVALUE 1			
2.0944107E+01			
$\omega =$	4.5764732E+00 RAD/SEC		
$F =$	7.2836893E-01 HZ		
VECTOR	1.0000000E+00	6.9340417E-02	-1.6332725E-02 6.7422680E-04
EIGENVECTOR FACTOR =	3.9536445E-01		
EIGENVALUE 2			
9.9143450E+02			
$\omega =$	3.1467054E+01 RAD/SEC		
$F =$	5.0113244E+00 HZ		
VECTOR	-7.8411519E-03	1.0000000E+00	-2.3636627E-02 2.9270922E-03
EIGENVECTOR FACTOR =	1.2674361E+00		
EIGENVALUE 3			
6.9029031E+03			
$\omega =$	3.3033711E+01 RAD/SEC		
$F =$	1.3223194E+01 HZ		
VECTOR	4.5940514E-02	7.7566715E-01	1.0000000E+00 4.0765533E-02
EIGENVECTOR FACTOR =	2.2141521E-01		
EIGENVALUE 4			
1.9300518E+04			
$\omega =$	1.4071431E+02 RAD/SEC		
$F =$	2.2395397E+01 HZ		
VECTOR	-1.6289690E-03	-6.3595566E-02	-1.9157779E-02 1.0000000E+00
EIGENVECTOR FACTOR =	3.1373055E-01		

The computer output in table 8.1 shows that A is a diagonal mass matrix having three horizontal degrees of freedom and one rotational degree of freedom due to rotational motion of the basemat. Matrix B is the resultant stiffness matrix. From the eigenvalue analysis of the original model in fig. 8a, we obtained four modes of vibrations, three horizontal modes and one rotational mode.

The modal equivalent comprehensive model is obtained by using Cantilevers from fig. 8c and the basemat and spring properties from fig. 8a. Computer out-puts in table 8.1. and 8.2. show the agreement between the original model and the modal equivalent model to more significant figures.

9. Prevention of unwanted reflected wave from the Finite element boundary of the soil model

Introduction

It is a recognised fact, that in soil-structure interaction problem, the effect of seismic waves reflecting from the artificial boundary (Finite element representation of infinite continuum) causes much of the difficulties in evaluating correct structural response. Thus in order to obtain adequate evaluation of response it has been necessary to assume necessary boundary conditions in the finite element model of soil mass supporting the structure, which would adequately represent infinite media. Clearly the main limitation of this approach is that not all boundary conditions can be applied satisfactorily.

For the simple reason is that seismic waves are not one dimensional or plane waves but spherical waves consisting various components such as 'P' waves, 'S' waves, Rayleigh waves and not necessarily the incident waves are normal to the surface. In short, the problem of preventing unwanted reflected wave from the finite element boundary is very complex.

However in recognition of these facts and associated difficulties, Lysmer (49) proposed that boundaries of the finite element model should be removed far away from the structure, so that full effects of radiation damping are correctly represented. Alternatively Kausel (50) proposed, that analytical model may be provided with transmitting boundaries which absorb any wave effects emanating from the structure and thus simulates the effects of an extensive soil deposit.

Huang (51) proposed another alternative method which involves the use of viscous boundaries along the planar surfaces of a slice of soil on which one or more structures are located. Tzung and Lee (52) proposed improved transmitting boundaries for time domain analysis to account for highly non-linear foundation medium. Authors in ref. (2) and (4) used forced boundary conditions to eliminate the effect of wave reflection. These can be achieved by imposing zero displacement (fixed) or zero stress (free) boundary conditions for sides of the grid and to apply earthquake shaking at the bottom of the grid. The bottom behaves as a rigid boundary with respect to waves. This appears to be satisfactory as long as the period of the wave motions are long enough that wave effects are negligible. To use the above method, authors in ref. (2) and (6), proposed, that the critical depth of soil mass measured from the bedrock to the bottom of the Basemat should be determined first. If the critical depth is sufficiently larger than the distance from the structure then the wave effect can be neglected. To determine the critical length, the authors proposed that if the minimum rise time of the periods of interest t_r is known, then the following relation holds

$$L_{\text{critical}} = C_s \cdot t_r \qquad C_s = \text{Shearwave velocity}$$

This approach appears to be too idealized. Because sub soil layers are not homogenous. Each soil layer has its own physical properties, such as shear modulus, mass density and poisson's ratio. Therefore propagation velocity of shear wave is not constant through the layers. Furthermore at the interface between the layers, the effects of multiple reflections and dissipations of waves cannot be ruled out.

Kunar and Rodrigues-Ovejero (57) proposed non-reflecting boundaries at the base and vertical faces of a two dimensional finite element or finite different soil mesh by introducing viscous dashpots as energy absorbers at the base of the model where the seismic excitation is applied. For the lateral boundaries a superposition non-reflecting boundary formulation is recommended. To simulate non-reflecting boundary on the lateral surfaces, the authors introduced two overlapping but independent boundaries A and B, connected to the main grid. The wave that propagate into the boundary zones will be reflected off the boundaries of region A and B, which are then constrained. Using constrained conditions the reflections are eliminated by averaging the stresses and velocities in two boundary regions.

Basically, the idea of prevention of reflection of waves from the finite element boundary is similar to the one proposed by the author of this thesis, but the present technique used in the analysis is different. The quiet boundary technique incorporated in the computer program for the purpose of reducing unwanted reflection from the boundaries is based on the theory of one dimensional wave propagation. The underlying idea is to compute the motion which a nodal point on the boundary of the finite element grid would have if there were no boundary, that is the motion which the same point would have in an infinite continuum and to force the point to have that velocity. It may be easier for the reader to conceive of this as anticipating a reflection and cancelling it as it occurs by superposing signal of equal in magnitude but opposite in sign. The technique is exact for one dimensional wave propagation problem and has given satisfactory results in the type of two dimensional calculation performed in the present and previous study (53) as well as in three dimensional problem (54).

The advantages of the present method over the one proposed in ref (57) are as follows:

- 1) Simplicity of solution algorithm
- 2) Use of virgin input (acceleration, or velocity time history from the seismograph. Whereas the method described in ref. (57) requires deconvolution process using a program similar to SHAKE to generate stress on force time history at the base from the acceleration time history. This can pollute the prescribed acceleration time history input. The reason for using force time history is that the input acceleration time history implies prescribed velocities and displacements, along the base nodes, to which the dashpots are connected. This renders the dashpots ineffective as they are no longer free to move to respond to the radiation waves caused by interaction between the structure and soil.
- 3) In the present method P and S waves can be treated equally effectively.
- 4) The present method is a one step process, where as the method proposed in ref. (57) requires two steps namely deconvolution and elimination of reflection.

9.1 Method of preventing unwanted reflections from artificial boundaries

The present quiet boundary technique is most clearly illustrated in the one-dimensional propagation case. This is shown in Figure 9-1 with the aid of the common conception of real and "phantom" waves. A dilatation wave (p-wave) is shown travelling in a finite element rod from the left toward a fixed boundary. This wave has a partner "phantom" wave travelling from the right. As these waves meet each other at the boundary, they superpose to produce zero particle velocity at the boundary. At later times, the incident wave has travelled out of the finite element grid and has become a "phantom" wave, while the original "phantom" wave has entered the grid and has become a reflected wave which may interfere with the response calculations within the grid. The aim of the quiet boundary technique is to minimize or prevent boundary reflections. The analytical technique used is to calculate the motion of the boundary surface as it would occur if the rod were continuous [32]. The computer then imposes this motion on the boundary. Inputs to the calculation are the velocity- or acceleration-time history of the incoming wave and the material properties of the rod. The calculation is based on the solution to the wave equation in one-dimension.

The effect of the quiet boundary technique is illustrated in Figure 9-2. It may be considered that the reflection occurs, but that it is exactly cancelled by a wave of equal magnitude and opposite sign. Hence, the problem in the quiet boundary technique becomes one of defining the amplitude of the correction wave and its phasing relative to the reflected wave.

To illustrate the application of the quiet boundary technique, let us first consider the problem of representing an infinitely long one-dimensional continuum by an elastic rod of finite length. In this, it is desired to determine the boundary conditions at the far end of the rod, such that the response in the interior of the rod corresponds to that for the infinitely long continuum.

In this problem, it is assumed that at a time $t = t_0$, the particle velocity at point i and $i-1$ are known. i is a point far away at the boundary, and point $i-1$ is located adjacent to it. The distance between the two points is Δx .

$t_0 v_{i-1}$ = particle velocity at point $i-1$, at time $t = t_0$

$t_0 v_i$ = particle velocity at point i , at time $t = t_0$

The solution of the one dimensional wave equation gives the particle velocity at i at a time

$$t = t_0 + \Delta x / C_p \quad (9.1)$$

as

$$(t_0 + \Delta x / C_p)_{v_i} = t_0 v_{i-1} \quad (9.2)$$

C_p is the speed of propagation of the pressure wave.

Through linear interpolation, the velocity v_i at a time $t = t_0 + 2 \Delta t$ is found as follows:

$$(t_0 + 2\Delta t)_{v_i} = \frac{t_0 v_i \{ \Delta x / C_p - 2\Delta t \} + (t_0 + \Delta x / C_p)_{v_i} \{ 2 \Delta t \}}{\Delta x / C_p} \quad (9.3)$$

For this to be the solution of the wave equation

$$2\Delta t \leq \Delta x / C_p \quad (9.4)$$

At every time step, $(t + 2\Delta t)_{v_i}$ is computed and applied to the nodal points, where it is regarded as the prescribed velocity at time $t = t_0 + 2\Delta t$. In Figure [9.2] is shown the effectiveness of this method when treating one dimensional wave propagation in a rod of finite length. In this example, the motion at the center of the rod is compared when the quiet boundary technique is applied with the motion when the technique is not applied.

One more point that also needs to be discussed is the motion arising due to the interaction with the structure in the middle of the grid, which must be cancelled to avoid unwanted reflection. The term "scattered velocity" will now represent such motion. The term "boundary velocity" will represent input motion, which is computed prior to finite element analysis.

At the node $i-1$ in Figure [9.1], the particle velocity at time $t = t_0$ is composed of boundary velocity and scattered velocity. This is indicated below

$$t_{0v_{i-1}} = t_{0v_{i-1}}^b + t_{0v_{i-1}}^s \quad (9.5)$$

Now $t_{0v_{i-1}}^b$ is found from $(t_0 - x/C_p)_v^b$ for all time and is expressed as follows:

$$t_{0v_{i-1}}^b = (t_0 - \Delta x/C_p)_v_i^b \quad (9.6)$$

Thus, the scattered motion propagating toward the boundary at point $i-1$ and time $t = t_0$ is

$$t_{0v_{i-1}}^s = t_{0v_{i-1}} - (t_0 - \Delta x/C_p)_v_i^b \quad (9.7)$$

Now using the wave equation to find the scattered wave velocity at point i and at a time $t = (t_0 + \Delta x/C_p)$ gives the following:

$$(t_0 + \Delta x/C_p)_v_i^s = t_{0v_{i-1}}^s \quad (9.8)$$

or

$$(t_0 + \Delta x/C_p)_v_i^s = t_{0v_{i-1}} - (t_0 - \Delta x/C_p)_v_i^b \quad (9.9)$$

The correction to be made to the prescribed boundary velocity at time $t = t_0 + 2\Delta t$ in order to prevent reflection of the scattered wave is

$$t_0 + 2\Delta t_{v_i}^s = \frac{t_{0v_i}^s \times (\Delta x/C_p - 2\Delta t) + (t_0 + \Delta x/C_p)_v_i^s \times 2\Delta t}{\Delta x/C_p} \quad (9.10)$$

Then the adjusted boundary condition at time $t = t_0 + 2\Delta t$ thus

becomes

$$(t_0 + 2\Delta t) v_i^b = (t_0 + 2\Delta t) v_i^b + (t_0 + 2\Delta t) v_i^s \quad (9.11)$$

In the discussion above, the quiet boundary technique is applied to incoming pressure waves. The above method is equally effective when dealing with incoming shearwaves. This can be done just by merely changing C_p to C_s in equation (9.10).

Based on the theory of one dimensional wave propagation, and the derived formula to suppress the unwanted wave from the finite element of the soil model a computer program VELCOR (vol. 2) was written, and used with the modified version of NONSAP, to analyse non-linear soil-structure interaction problem. The computer program VELCOR in its present form (submitted for thesis) can be used in one and two dimensional problems quite effectively, and will be demonstrated in the actual problem dealing with the non-linear response of embedded structure.

VELCOR is written in such a way, that the program can be used as a subroutine with any other program dealing with structural dynamics. The interface with VELCOR and other program having dynamic capabilities, can be formed without any difficulty, by using a labelled common, with the variables that are already in use in the program which is to be coupled with VELCOR. Guidance to implementation, and additional input data are explained in VELCOR.

VELCOR can be used in non-linear problem such as elasto-plastic deformation of material such as soil. We especially mentioned soil as material because the problem under investigation in this thesis makes the use of soil sublayer as supporting medium of the embedded structure, and non-linear response of structure is mainly due to non-linear (elasto-plastic) behaviour of soil under earthquake loading.

Most commonly used criteria for yielding of soil, is the generalised Drucker-Prager yield criteria. For two dimensional problems such

as the case we are investigating in this thesis, this is reduced to Mohr-Coulomb yield criteria, and the yield function is calculated accordingly. Subroutine "STRESS" computes the present Stress level, which in turn calls subroutine CANDE, which computes the incremental corner displacements and Strains and prepare to enter into Elastic-Plastic analysis, by setting up Stress and Strain vectors, and form the material matrix using the constitutive laws by calling "ELPAL". The subroutine YLDFUN is called in ELPAL, which adjusts the Stress deviators so that Stresses exactly satisfy the yield condition. A flow chart for VELCOR is included in the VOL2 of the thesis.

For two or three dimensional problem $V_i^b(x)$ and $V_i^b(y)$, $V_i^b(z)$ to account for boundary velocities at any grid point in x, y and z direction. Similar notation can be applied to scattered wave velocity $V_i^s(x)$, $V_i^s(y)$ and $V_i^s(z)$ in three orthogonal directions. The equations (9, 10) and (9, 11) are solved simultaneously for two or three dimensional cases (53, 54).

We monitored Element No. 41. and computed the vertical Stress time-history response. For the check problem utilising two dimensional quiet boundary technique, we used the soil model (without structure) in Fig. 12.2 A. The element 41 is located at a distance of 105.0 m from the left hand end of the boundary.

An arbitrary triangular Stress pulse of 6000 N/m^2 was assumed. The duration of pulse including rise and decay time was assumed to be 0.01 Sec. The pulse is assumed moving at a constant speed over the surface of the plane.

The integration time step was selected according to the following formula:

$$\begin{aligned} C_p &= \text{Velocity of pressure wave propagation } 1373.0 \text{ m/s.} \\ f &= \text{Highest response frequency under consideration} = 15 \text{ Hz} \\ \lambda &= \text{Wave length or element-length} = 15.0 \text{ m} \end{aligned}$$

$$\text{Maximum time step} = \Delta t = \frac{1}{10} \cdot \frac{\lambda}{C_p}$$

$$\text{or } \Delta t = \frac{1}{10} \frac{15.0}{1373.0} = 0.001 \text{ Sec.}$$

Number of integration steps = 300 (0.3 Sec.)

In Fig. (9.3) it shows that the initial Stress peak remains virtually unaffected by incomplete canceling of reflection. Reflections of about 25 % (150 Kp/m^2) of the peak signal appears in the finite element solution. These reflections are complicated signals containing P and S waves. Maximum amplitude of any one of these waves is governed by the maximum amplitude of the incident P wave which is 600 Kp/m^2 (6000 N/m^2). Therefore it is not surprising to see significant Stress oscillations in the free field Stress time-history. The solution obtained by finite element method is then compared with the analytical solution given by Cole-Huth (45). Authors in ref. (45) postulated that if the motion of line load producing pressure (Stress) on the surface of an elastic half plane is known, then the resulting Stresses and displacements can be estimated. To use the solution technique given by Cole-Huth, we must assume the velocity of the pressure pulse, or moving load and Mach numbers M_L & M_T with respect to longitudinal and transversal elastic waves must be known. We assume a supersonic case in which $M_L > 1$ and $M_T > 1$. For example we assume the velocity of pressure pulse as 1500.0 m/sec. The velocity of longitudinal wave in the middle layer is 1373 m/s, and the transversal wave is 800 m/s. (See 12 table 12)

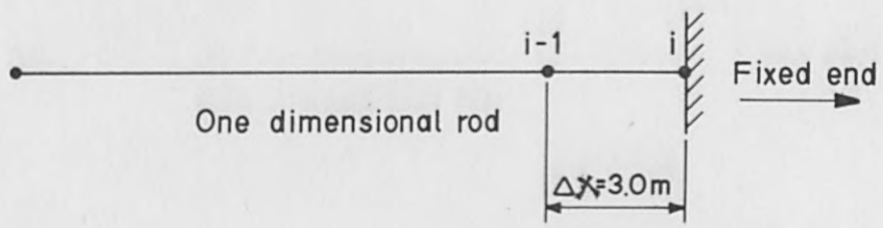
$$\begin{aligned} \text{Therefore } M_L &= \frac{1500}{1373} > 1 \\ \text{and } M_T &= \frac{2000}{800} > 1 \end{aligned}$$

Once our assumptions are fixed we use the equations 51, 52 and 53, of ref. (45) to derive the resultant vertical, shear and horizontal Stresses. In Fig. 9.3 and 9.4 only the resultant vertical and horizontal stress time-histories are plotted.

As far as the drawback of this method, it was found that there is impedance mismatch at the interface between plastic element and elastic element near the boundary when the computation was extended beyond 10 seconds of earthquake input. This is because the boundary elements were forced to remain elastic, while adjacent to the boundary

elements were allowed plastic deformation.

However in the vicinity of the Basemat, no such restriction was made and therefore, no significant error was allowed to occur.



$E = 2.305 \times 10^8 \text{ N/m}^2$
 $\rho = 1520 \text{ kg/m}^3$

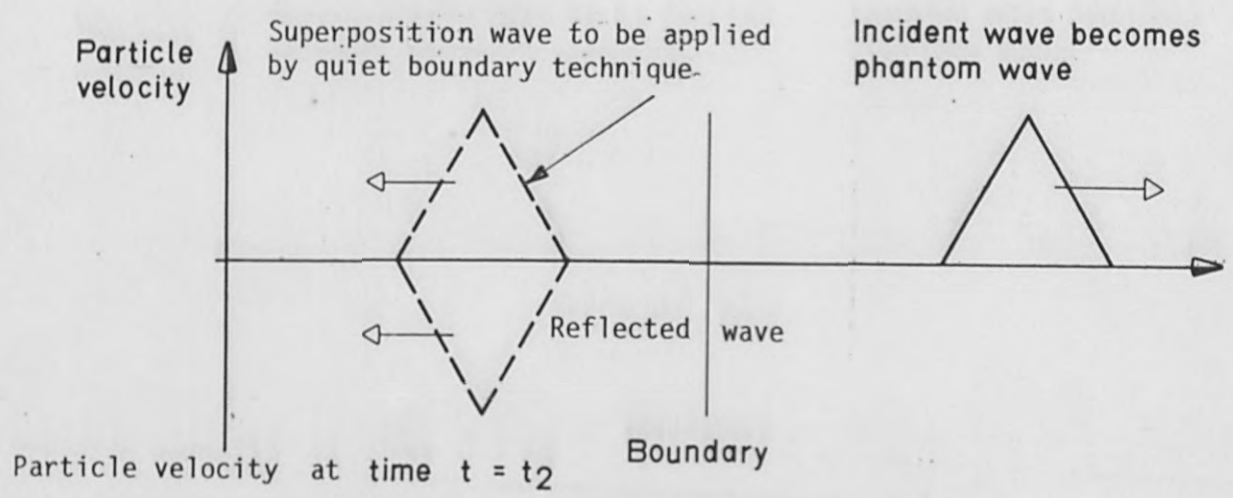
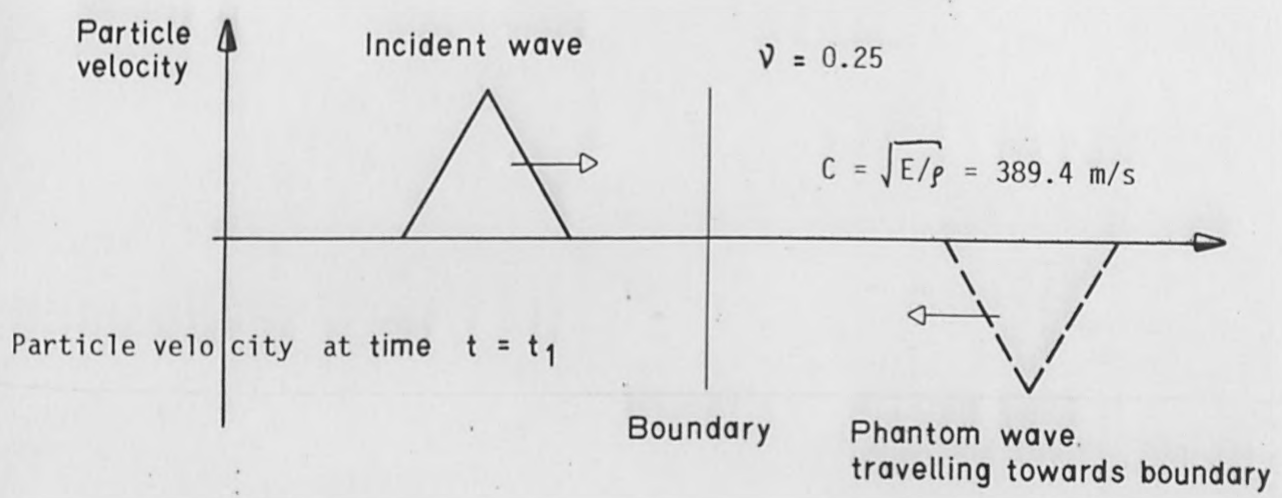
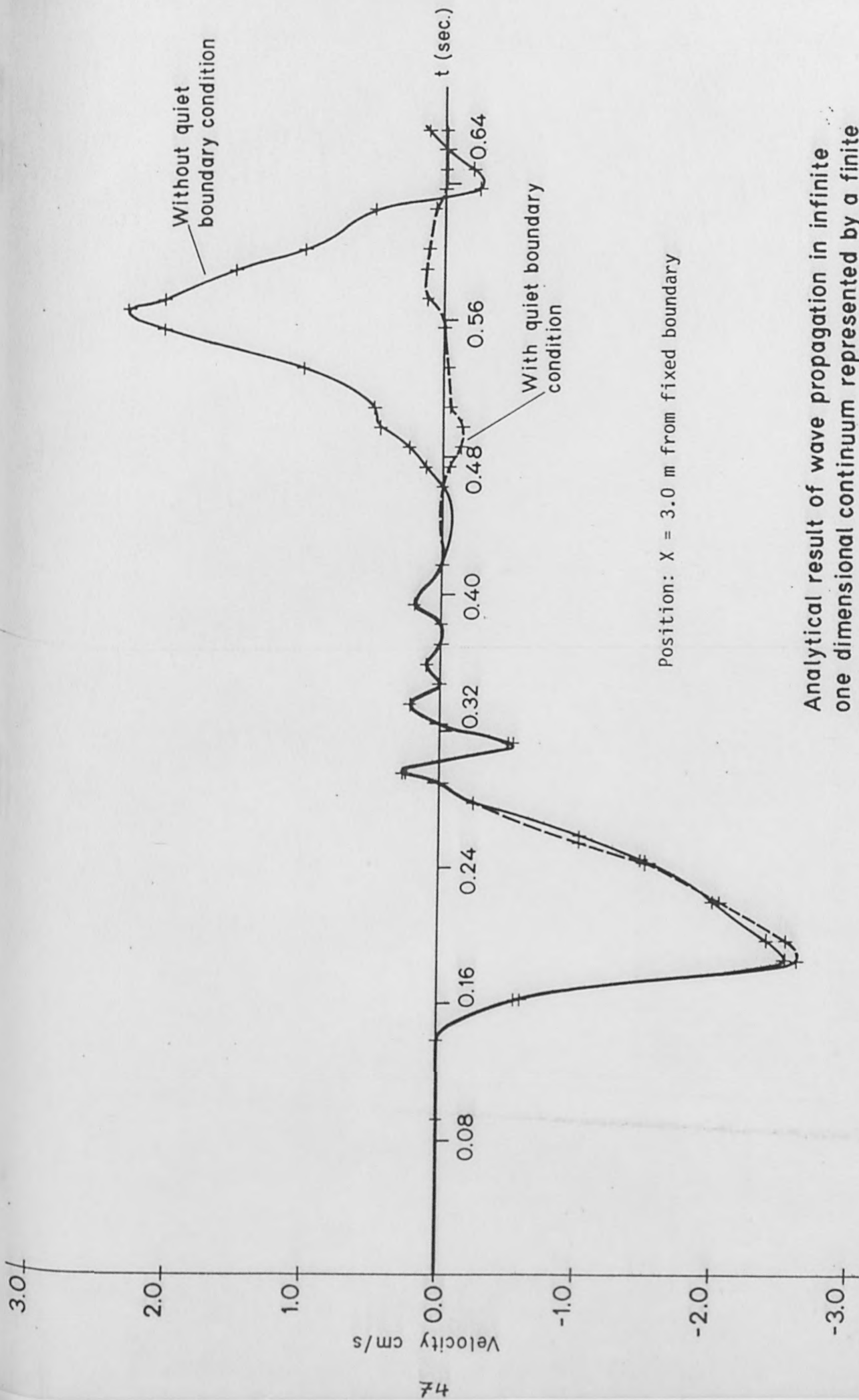


Illustration of quiet boundary technique

Fig. 9.1



Analytical result of wave propagation in infinite one dimensional continuum represented by a finite length of rod.

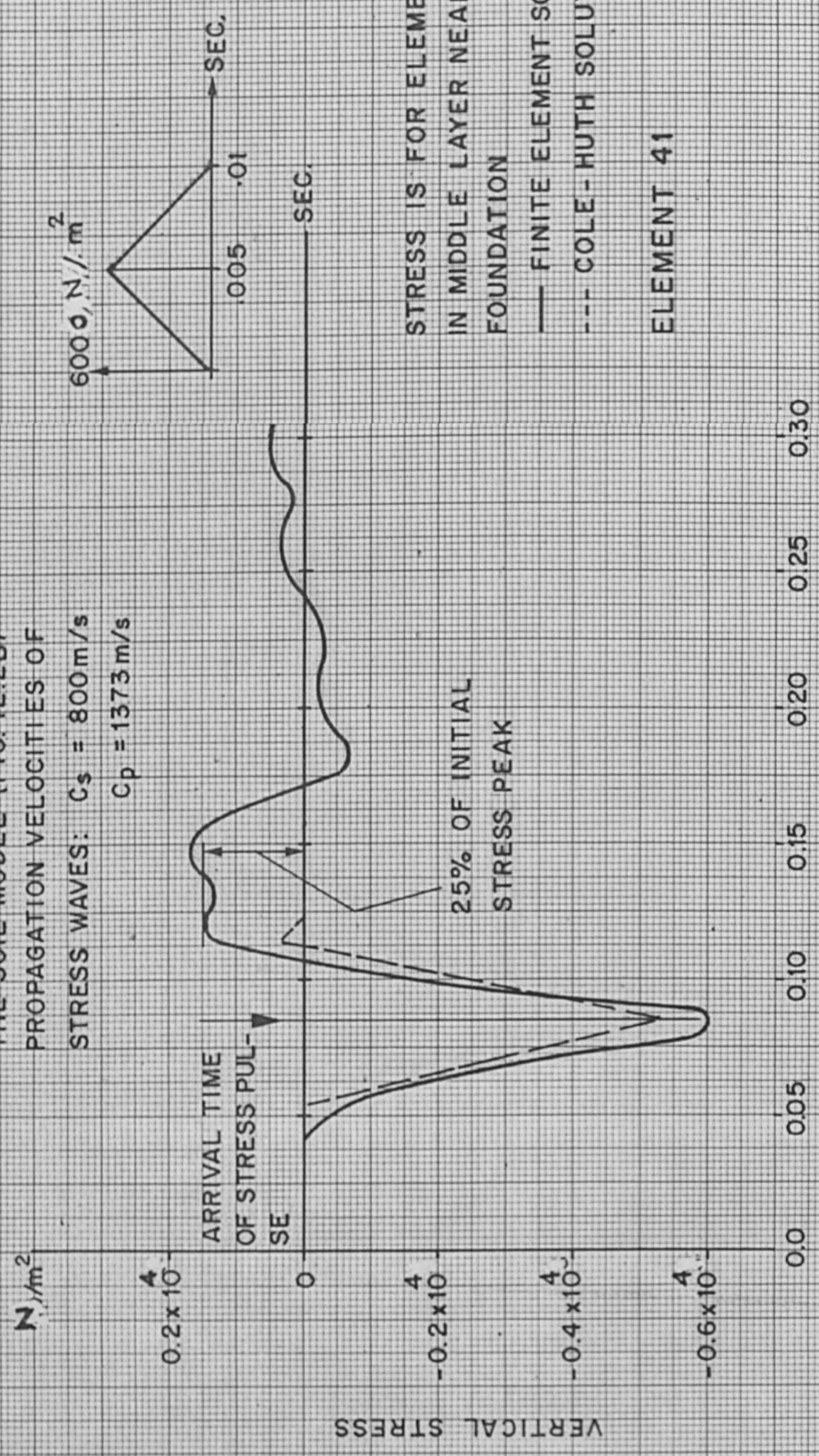
Fig. 9.2

CHECK PROBLEM UTILISING TWO DIMENSIONAL QUIET BOUNDARY TECHNIQUE

APPLIED STRESS PULSE AT LEFT HAND END OF FE BOUNDARY OF

THE SOIL MODEL (FIG. 12.2B)
PROPAGATION VELOCITIES OF

STRESS WAVES: $C_s = 800 \text{ m/s}$
 $C_p = 1373 \text{ m/s}$

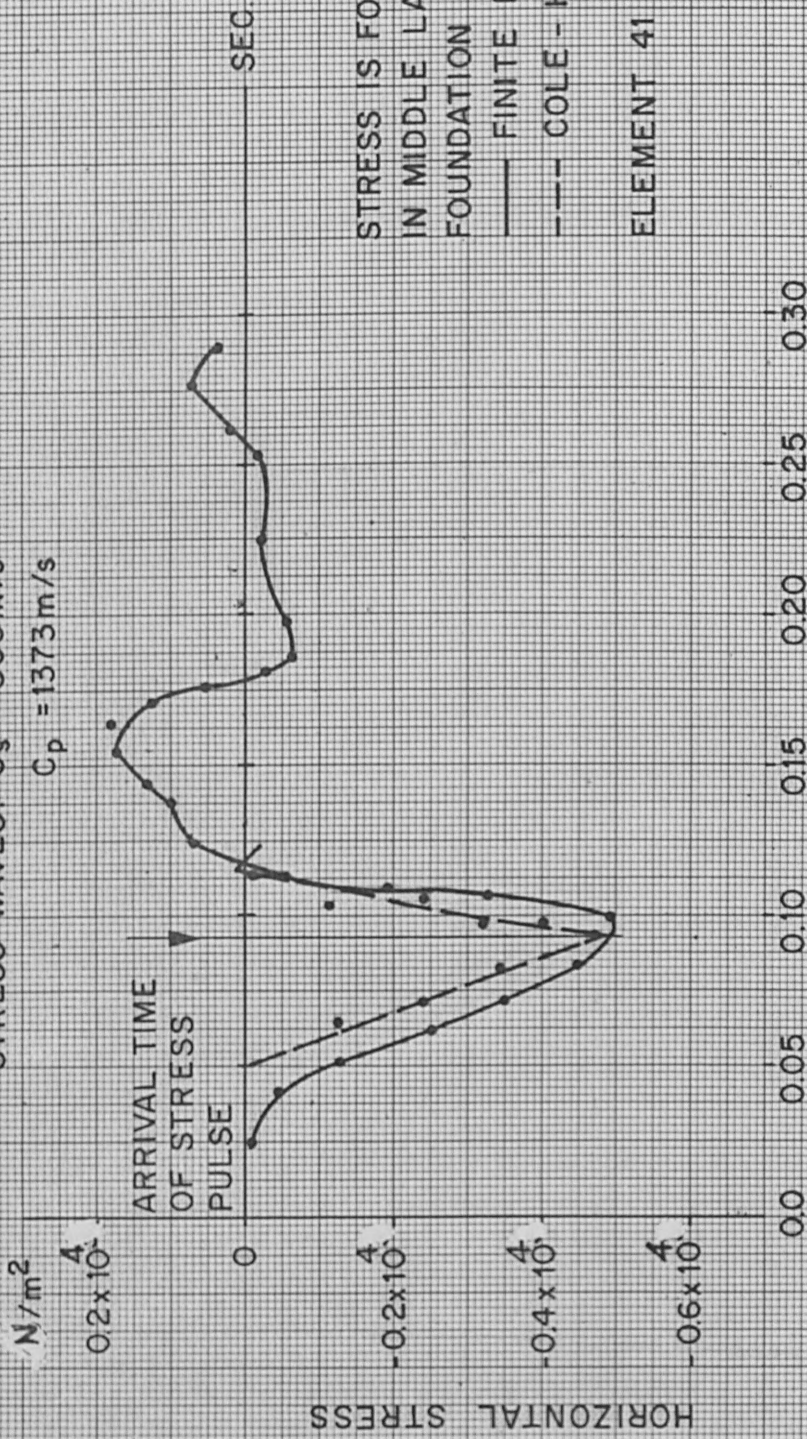


FE ELEMENT MODEL OF SOIL

FIG. 9.3

CHECK PROBLEM UTILISING TWO DIMENSIONAL QUIET BOUNDARY TECHNIQUE

APPLIED STRESS PULSE AT LEFT HAND END OF FE BOUNDARY OF THE SOIL MODEL (FIG. 12.28)
 PROPAGATION VELOCITIES OF STRESS WAVES: $C_s = 800 \text{ m/s}$
 $C_p = 1373 \text{ m/s}$



FE ELEMENT MODEL OF SOIL

FIG. 9.4

10. Comparison of Finite element solution with closed form solution of soil-structure interaction problem

Two attempts, identified as cases 1 and 2 were made to compare the present methods of computing interaction effects with those of previous investigators. We consider a cantilever structure embedded in a strip of soil fig. (10.1) and is reported by Scavuzzo in Ref. (34). The present results are compared with those of Ref. (34) in fig. (10.3).

Comparison is made in Fig. 10.4 between present results and those reported in Ref. (35). The comparison is qualitatively favourable. The quantitative differences are partly due to distortion of input in the analysis of Ref. (35). Where as the input is 5*c/s harmonic motion and the present analysis faithfully preserve this. The analysis of Ref. (35) distorts the input to predominately 4 CPS motion by using excessively large element in the soil. This data is also presented in Table 10.2.

* Note:

Dominant exciting frequencies of input of cases 1 and 2 are found by plotting spectral density against frequency. This was done by authors Program SEMON (Simulated earthquake motion) BBC Program No HT2192/79.

A second comparison is made with Scavuzzo's closed form method in Ref. (34). Scavuzzo's analysis represents the horizontal translation degree of freedom of the base mass and of the 4 CPS and 5 CPS oscillators. His analysis differs from the present case 2 in that he omits rocking motion of the foundation. The rocking motion is produced by differential vertical motion of nodal points 27 and 28 (Fig. 10.1).

The input to Scavuzzo's analysis was 5 CPS harmonic defined in table (10.1). Now when the strip foundation was analysed without the structure (free field) it was found that the peak acceleration at

nodal points 11, 27, 28, 31 (on the surface) was in average 1.29 times greater than that computed by Finite element analysis. Now what causes such discrepancy? One possible argument is that the boundary reflection could not be efficiently eliminated due to the size of the FE Grid which distorts the results. Furthermore Scavuzzo considered the Strip foundation infinitely long, so as to allow the wave train pass without reflection. Secondly momentum being changed from all horizontal to part horizontal and part vertical as the input motion propagates through the grid. To compare the two methods the scaling factor should be taken into account as mentioned before, when output is evaluated. This is done by scaling upward the foundation response of the present case (2) by 1.29 Fig. (10.2) and table (10.3), which include scaling factor. These shows that the two methods give similar results especially at 5 C/s which is the fixed base fundamental mode of the structure alone.

The input to our present problem is shown in the following table:

Table 10.1 Case Elastic soil

Case 1

$$V_H = (60,5) \left\{ 1 - \frac{0,6t}{2\pi} (0,6 \sin 2\pi t + 0,2 \cos \pi t) \right\}$$

inch/sec

Case 2

$$0 < t < 0,8 \text{ sec}$$

$$V_H = \left(\frac{1}{16\pi}\right) [-t \cos 10\pi t + \left(\frac{1}{10\pi}\right) \sin 10\pi t]$$

inch/sec

$$0,8 < t < 2 \text{ sec}$$

$$V_H = \left(\frac{1}{14\pi}\right) [-\cos 10\pi t + 0,5 (t \cos 10\pi t) - \left(\frac{1}{10\pi}\right)] \sin 10\pi t.$$

$$t > 2 \quad V_H = 0.$$

inch/sec

10.1 CLOSED FORM SOLUTION OF SOIL-STRUCTURE INTERACTION

During shock motion, inertia forces of large structures will influence the foundation motion locally. Scavuzzo [34] has presented an analytical solution to the problem by coupling a N-Mass structure with a one-dimensional wave, the resulting solution is formulated as a Volterra integral equation. By using an input wave similar to those encountered in earthquake motions, the significance of this interaction was investigated. Results show that the reduction in spectrum acceleration is significant and depends both on structure frequency and weight for a given foundation input.

The theoretical formulation is based on the propagation of one dimensional wave in the elastic medium, Fig.(10.1) The interaction between the structure and elastic wave is taken into account in a one-dimensional manner. Thus the spectrum curves of the free ground motion U_p and the motion at the base of the structure U can be analysed and compared.

The assumptions made in this mathematical model however are significant. It is well known that surface waves from the earthquake force are not one dimensional, and there are three types of waves associated with the earthquake wave propagation, namely pressure waves (P), shearwave (S) and Rayleigh wave (R). The structure may also excite all three of these waves in its response. However, these simplifications enable us to form a closed form solution and thereby leading us towards a step forward to the solution of more complex problems.

10.2 ONE DIMENSIONAL WAVE SOLUTION

The one dimensional wave solution is divided into two portions. The solution to the free wave and the solution to an infinitely long bar subjected to a transient force at the origin. Since one half of the total force will act on each half of the infinite bar, a semi-infinite bar was used in the derivation.

The governing differential equation with the following initial and boundary conditions

$$a^2 \frac{\partial^2 U}{\partial x^2} = \frac{\partial^2 U}{\partial t^2} \quad (10.2.1)$$

the boundary conditions are

$$U(x, 0) = 0.0$$

$$\frac{\partial U(x, 0)}{\partial t} = 0$$

$$U(\infty, t) = 0$$

$$EA \frac{\partial U(0, t)}{\partial x} = \frac{F(t)}{2} \quad (10.2.2)$$

where

a = wave velocity in bar

A = bar cross section

E = elastic modulus

U = displacement

$U(x, t)$ = displacement in function of space (co-ordinate) and time

$F(t)$ = inertia force at the structure foundation

By making use of Laplace transform the solution can be shown as:

$$U(x, t) = \frac{a}{2EA} \int_0^{t - (x/a)} F(\lambda) d\lambda \quad t > \frac{x}{a} \quad (10.2.3)$$

$$U(x, t) = 0 \quad t < \frac{x}{a} \quad (10.2.3)$$

Where λ is a parameter, and is defined as follows:

$$\lambda_j = (a m_j w_j^2 / 2 EA) \text{ and has unit}$$

1/sec., where

m_j = ith mass of a multi-mass system

w_j = ith frequency

superimposing this result onto a wave travelling in the bar the following is obtained for $t > x/a$

$$U(x, t) = \frac{a}{2EA} \int_0^{t - (x/a)} F(\lambda) d\lambda + U_p(x - at) \quad (10.2.4)$$

where U_p is free ground displacement.

The forces acting at the base of a structure caused by Jth mode of Jth multi-mass structure can be written .

$$F_j(t) = - M_j W_j \int_0^t \ddot{U}(0, \tau) \sin W_j (t - \tau) d\tau \quad (10.2.5)$$

where M_j is the modal mass of the Jth mode

$$M_j = \frac{(\sum_i m_i x_{ij})^2}{\sum_i m_i x_{ij}^2}$$

where x_{ij} mode shape of Ith mass and Jth mode.

Therefore the total base force from all modes is .

$$F(t) = - \sum_j M_j W_j \int_0^t \ddot{U}(0, \tau) \sin W_j (t - \tau) d\tau \quad (10.2.6)$$

Now substituting eqn 10.2.6 into eqn 10.2.4 the following integro-differential equation is obtained for $t - \frac{x}{a}$

$$U(x, t) = - \sum_j \frac{\lambda_j}{W_j} \int_0^{t-(x/a)} \int_0^r \ddot{U}(0, \tau) \sin W_j (r - t) d\tau dr + U_p(x-at) \quad (10.2.7)$$

The above equation can be changed into standard form of the volterra integral equation by taking the second derivative with respect to time. Furthermore the base acceleration is obtained from the resulting equation. This acceleration can be directly used to determine the shock spectrum. Thus, by taking the second derivative with respect to time, the following is obtained

$$\ddot{U}(x, t) = - \sum_j \lambda_j \int_0^{t-(x/a)} \ddot{U}(0, \tau) \cos W_j (t - \frac{x}{a} - \tau) d\tau + \ddot{U}_p(x-at) \quad (10.2.8)$$

At the base of the multi mass system the equation 10.2.8 becomes ($x = 0$)

$$\ddot{U}(0, t) = - \sum_j \lambda_j \int_0^t \ddot{U}(0, \tau) \cos W_j (t-\tau) + \ddot{U}_p(t) \quad (10.2.9)$$

The equation used to represent $\ddot{U}_p(t)$ = Free ground motion, see table 10.1, case 1.

Velocity response spectra using case 2 input

Comparison of results of author's computed value with those given in Ref. (35).

Velocity response spectra (Foundation/Freefield surface response)

Table 10.2

Frequency CPS	Horizontal		Vertical	
	Author	Ref. (35)	Author	Ref. (35)
1	0,24	0.70	0.30	0.45
2	0,38	0.63	0.22	0.39
3	0.30	0.4	0.21	0.28
4	0.30	0.4	0.19	0.44
5	0.22	0.16	0.20	0.44
6	0.19	0.22	0.18	0.36

The results of the comparative analysis are shown in the following table:

Table 10.3

Case 2 Elastic soil

Frequency	Spectral velocity (cm/S)	
	Author	Scavuzzo
1	0.84	3.0
2	2.84	6.0
3	5.4	7.32
4	12.19	12.24
5	45.03	47.02
6	9	22.40
8	3.6	5.31

10.3 CALCULATIONS

By making use of the free wave motion in equation (10.2.9) the response spectrum was calculated. The resulting curve is shown in Fig. (10.3) and then compared with the present finite element solution technique. As seen from fig. (10.3) the amount of reduction in free wave passage response depends both on the natural frequency and lambda value. The values used in the calculation of lambda, assuming the building to be represented by first mode.

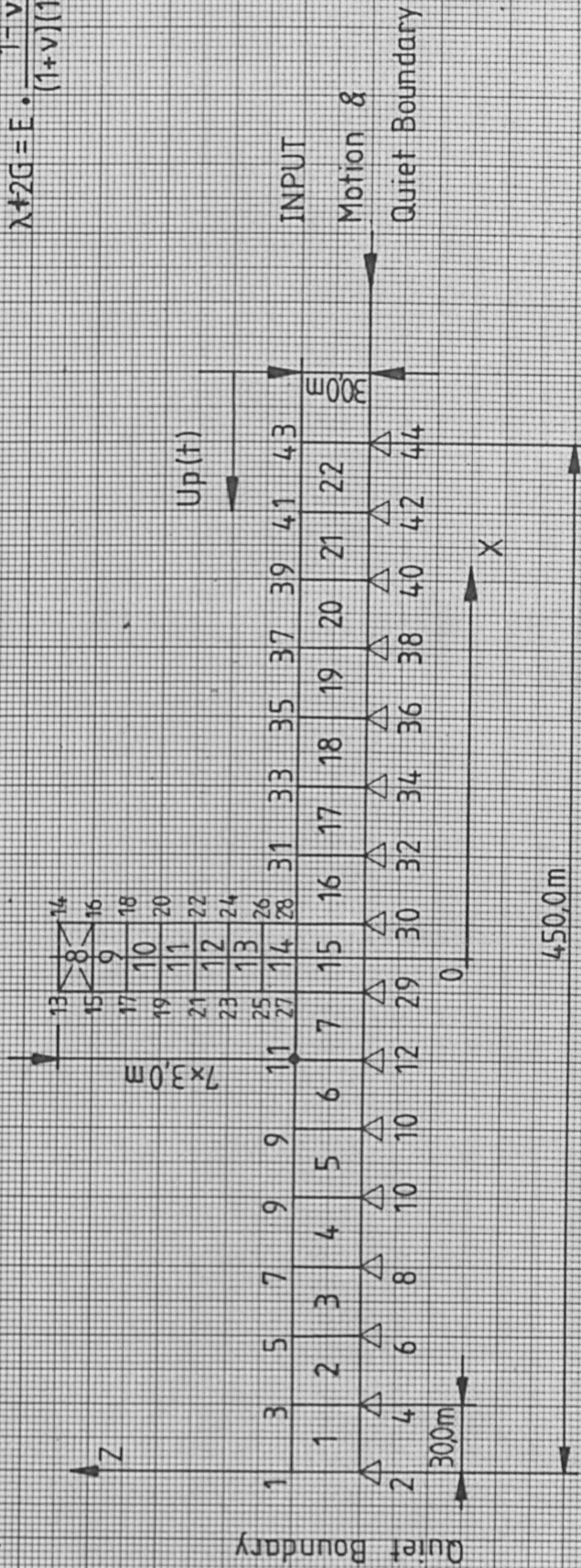
Identifi- cation	EL NUMBER	ν	E N/m ²	P Kg/m ³	Cp m/s	Cs m/s
Foundation	1-7, 15-22	0,4	$2,9 \times 10^8$	1296	473	291
Structure	9-14	0,17	$2,9 \times 10^9$	1296	1380	977
Concentra- ted Mass	8			$1,9 \times 10^5$ kg		

$$Cp = \sqrt{\frac{\lambda + 2G}{\rho}}$$

$$Cp = \sqrt{\frac{G}{\rho}}$$

$$G = \frac{E}{2(1+\nu)}$$

$$\lambda + 2G = E \cdot \frac{1-\nu}{(1+\nu)(1-2\nu)}$$



FINITE ELEMENT - GRID WITH STRUCTURE FIG. (10.1)

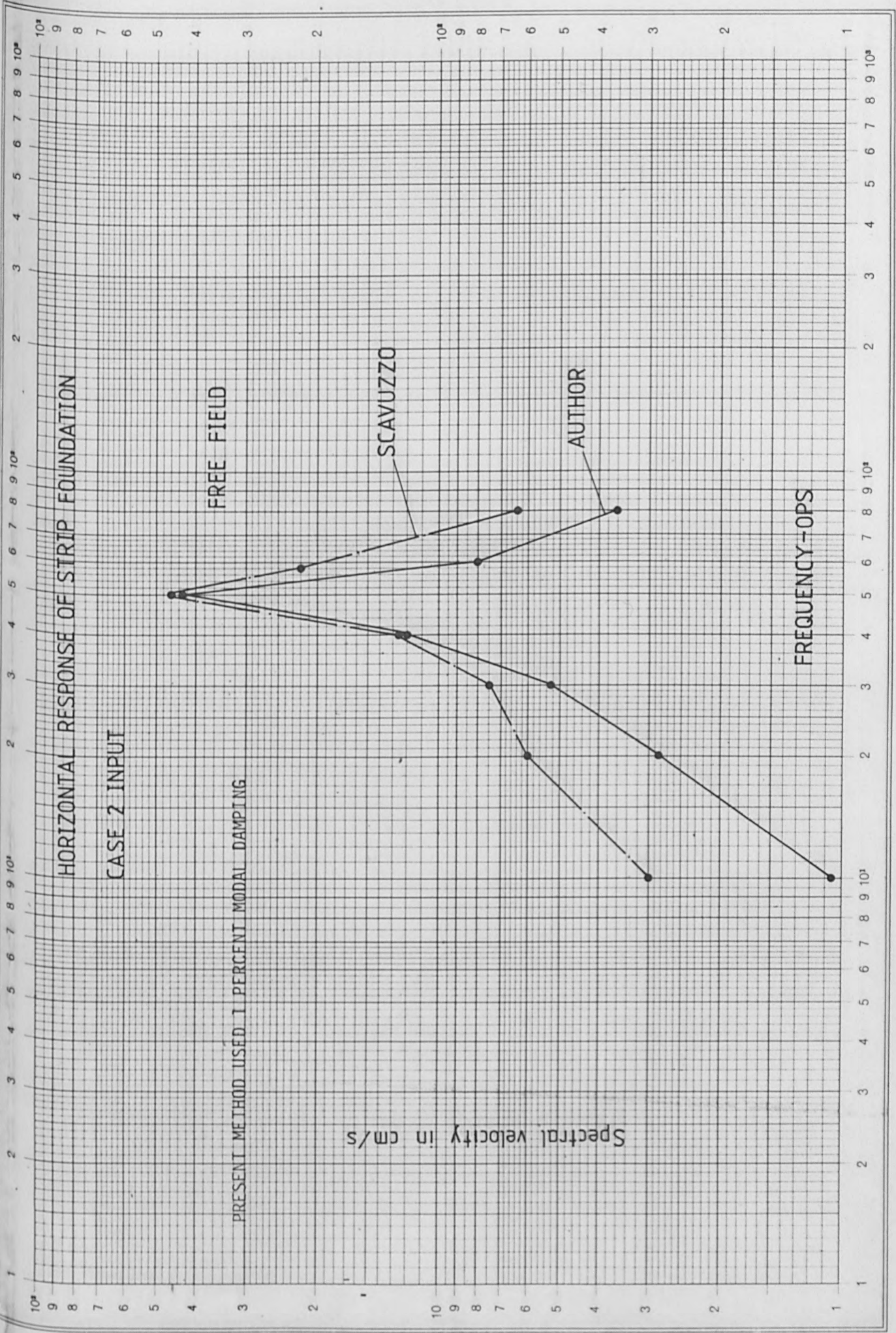


Fig. 10.2

PRESENT METHOD USED 1 PERCENT MODAL DAMPING

Case 1 input

Author without Structure

ACCELERATION RESPONSE SPECTRA

Scavuzzo without Structure

$\lambda = 2$

Author with Structure

Scavuzzo with Structure

Acceleration in "G"

FREQUENCY CPS

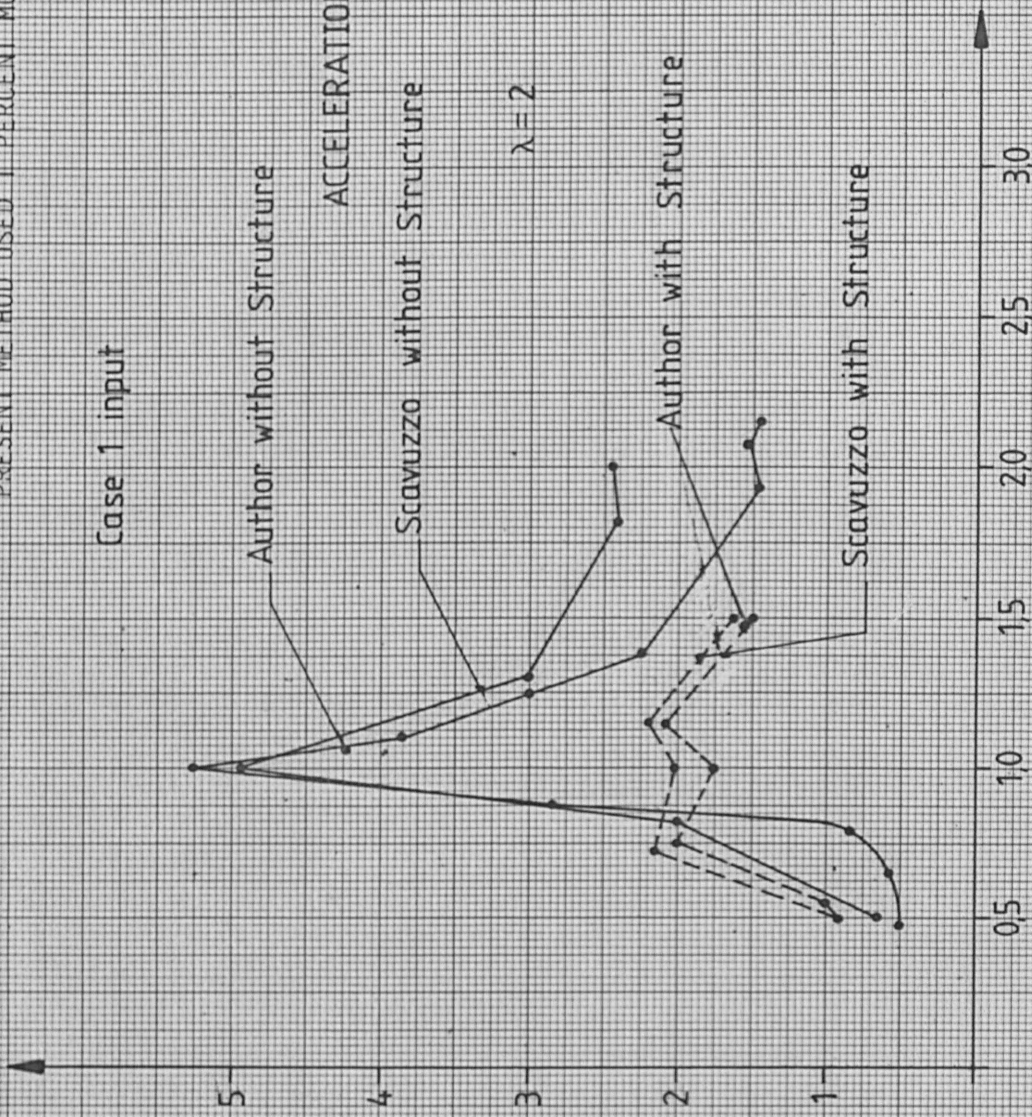


Fig. (10,3)

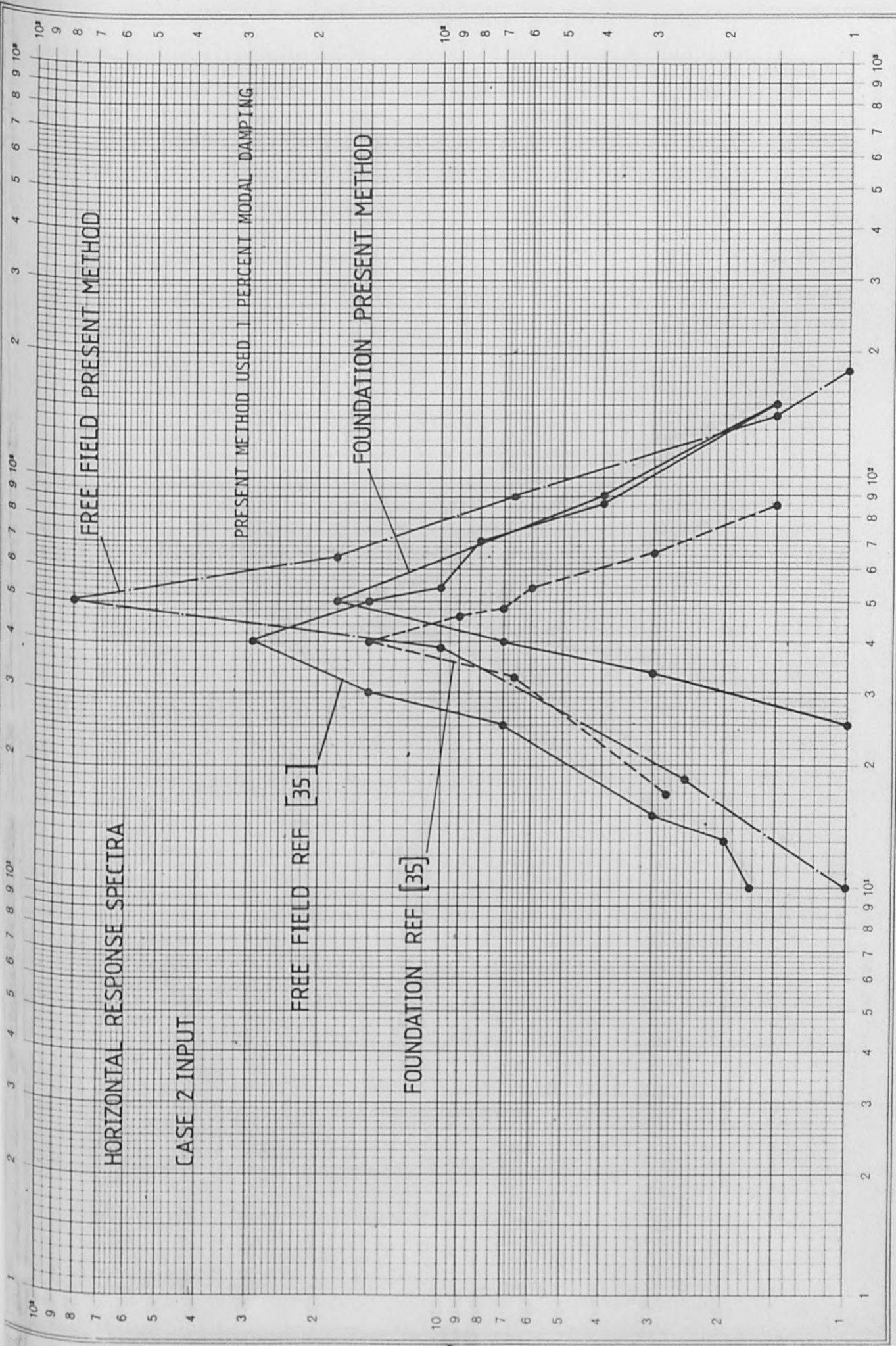


Fig. 104

11. COMPARISON BETWEEN ELASTIC AND INELASTIC FINITE ELEMENT SOLUTION AND CLOSED FORM SOLUTION

In the previous section (sec. 9) we demonstrated the importance of suppression of reflected wave from the finite element boundary, when the soil mass is subjected to transient disturbance. In section 10, we demonstrated how the response analyses by finite element method of a hypothetical structure on a strip foundation agree with the results obtained by closed form solution technique of soil structure interaction problem. In the finite element analysis we used quiet boundary technique described in sec. 9 and obtained results which agree fairly well with those given by closed form solution. So far the investigations are mainly concerned with the elastic deformation of material and response analysis in elastic domain.

As we will see later on that soil sublayers can be subjected to plastic deformation, due to earthquake shaking, and thereby influence the soil-structure interaction analysis considerably. Basically this means that due to localised plastic deformations and spreading of plastic zones within the soil sublayers affect the propagation velocities of stress waves, and consequently the degree of response. In fig. 12.3 the interaction response spectra shows the difference between the linear and non-linear analysis. A close look at the fig. 12.3., will reveal the frequency shift of peak responses and suppression of peak responses in non-linear soil-structure interaction analysis.

Therefore in this section we would like to demonstrate the capabilities of modified NONSAP program using finite element method to solve the wave propagation problem in elastic and elastic-plastic medium. Our aim therefore is to study the convergence of solution obtained by finite element method to true solution using exact theory.

The term convergence is used here to denote the tendency for a solution by present finite element method to approach the exact solution.

The problems used to illustrate convergence are as follows:

1. Plane, one dimensional wave propagation in an elastic rod.
2. Plane, one dimensional wave propagation in an inelastic rod.

The case of a plane, one dimensional wave propagating in an elastic bar is illustrated in fig. (11.1).

The governing equation used in the exact solution is as follows:

$$\frac{\partial^2 U}{\partial t^2} = \left(\frac{k}{\rho_0} \right) \frac{\partial^2 U}{\partial x^2} \quad (11.1)$$

where the wave velocity $a = \sqrt{\frac{k}{\rho_0}}$

For longitudinal wave K equals Young's modulus E . If the rod is clamped rigidly or otherwise forms part of an infinite medium then $K = K + 4G/3$ where K is the bulk modulus of the solid, and G is the modulus of rigidity.

The stress profiles calculated by the present finite element method at various times are compared with the exact solution. The quiet boundary procedure mentioned in secn (9) is used to absorb the waves at the bottom boundary. Its effectiveness is demonstrated by the apparent absence of reflection at 0.03 sec.

11.1 PROPAGATION OF ELASTIC-PLASTIC WAVES IN ROD

In order to make a convergence study on the propagation of elastic-plastic wave, a general solution technique due to Kachanow (40) will be used in this study. The solution technique is modified, and applied to a specified problem, and the results are then compared with present finite element solution method.

General Remark

At the end of the second world war great interest developed in problems of propagation of disturbances through the elastic-plastic media. Real media are not completely elastic (for example in Seismology) and it is necessary to take into account plastic properties. Finally, dynamical problems can be of great significance in the analysis of high speed technological process.

The first problems in the propagation of compressive elastic-plastic waves in rod were considered by Rakhmatulin [35] von Karman and Duwez [36] and Taylor [37]. Various generalisations of this problem exist.

11.2 BASIC ASSUMPTION

We consider the problem of waves propagating in a thin prismatic rod whose longitudinal axis coincides with the global X axis, and make the following fundamental assumption.

- 1) The cross section of the rod remains plane and normal to X axis.
- 2) Deformation is small, so that we can neglect the change in dimension of rod, and therefore the geometric stiffness property.
- 3) Inertia forces corresponding to the motion of particles of the rod in the transverse direction as a result of expansion and contraction of section can be neglected.
- 4) The influence of strain rates on the relationship between σ_x and ϵ_x can be neglected.

Now within the elastic limit, the material obeys Hooke's law:

$$\sigma = E \cdot \epsilon \quad \text{for } |\epsilon| < \epsilon_0$$

We shall assume that the compression curve is similar to the tension curve unloading proceeds along a straight line. A classical example of stress-strain curve, in keeping with the experimental data is reproduced in fig (11).

In dynamical problems the strain rates are large, and their influence on the deformation curve can be substantial. This influence is therefore neglected here in order to obtain a closeform solution to elastic-plastic wave propagation. Therefore, the assumed relationship $\sigma = \sigma(\epsilon)$ is only a first approximation, and relates to average strain rate in the given interval. To calculate the influence of the strain rate it is necessary to consider elastic viscoplastic model of the medium (see appendix A).

11.3 EQUATION OF MOTION

The differential equation of motion for a continuous medium

$$\frac{\partial \sigma}{\partial x} = \rho \frac{\partial^2 U}{\partial t^2} \quad (11.3.1)$$

Because deformation is small, $\rho = \text{constant}$, since

$$\frac{\partial \sigma}{\partial x} = \frac{\partial \sigma}{\partial \epsilon} \cdot \frac{\partial \epsilon}{\partial x} \cdot \frac{\partial \epsilon}{\partial x} = \frac{\partial^2 U}{\partial x^2} \quad (11.3.2)$$

We obtain
$$\frac{\partial^2 U}{\partial t^2} = a^2 \frac{\partial^2 U}{\partial x^2} \quad (11.3.3)$$

where the constant a is the wave velocity =
$$\sqrt{\frac{1}{\rho} \cdot \frac{d\sigma}{d\epsilon}} \quad (11.3.4)$$

In the elastic region the propagation speed is constant.

$$a = \sqrt{\frac{E}{\rho}} = a_0 \quad (11.3.5)$$

In the plastic region the propagation speed decreases with increasing deformation Fig (11.2).

The second order differential eqn (11.3.3) can be conveniently replaced by a system of two first order equations.

$$\frac{\partial v}{\partial t} = a^2 \frac{\partial \epsilon}{\partial x}, \quad \frac{\partial \epsilon}{\partial t} = \frac{\partial v}{\partial x} \quad (11.3.6)$$

We now suppose the function v and ε are prescribed along L , thereby combining the relations

$$d\varepsilon = \frac{\partial \varepsilon}{\partial t} dt + \frac{\partial \varepsilon}{\partial x} dx \quad (11.3.7)$$

$$dv = \frac{\partial v}{\partial t} dt + \frac{\partial v}{\partial x} dx \quad (11.3.8)$$

We obtain along L a system of four linear algebraic equations with respect to the first derivatives.

$$\frac{\partial \varepsilon}{\partial t}, \quad \frac{\partial \varepsilon}{\partial x}, \quad \frac{\partial v}{\partial t}, \quad \frac{\partial v}{\partial x}$$

We then find

$$\frac{\partial \varepsilon}{\partial t} = \frac{\Delta_1}{\Delta}, \quad \dots \quad \frac{\partial v}{\partial x} = \frac{\Delta_4}{\Delta} \quad (11.3.9)$$

Δ is the determinant of the system and $\Delta_1 \dots \Delta_4$ are the approximate co-factors. It is easy to see

$$\Delta = dx^2 - a^2 dt^2 \quad (11.3.10)$$

If L is a characteristic curve then the derivatives are intermediate along it, i.e.

$$\Delta = 0, \quad \Delta_1 = \Delta_2 = \Delta_3 = \Delta_4 = 0 \quad (11.3.11)$$

Consequently

$$dx \pm a dt = 0 \quad (11.3.12)$$

The condition that Co-factors are zero, now leads to the relationship

$$a d\varepsilon \pm dv = 0 \quad (11.3.13)$$

We now introduce the following function

$$(\epsilon) = \int_0^{\epsilon} a(\epsilon) d\epsilon \quad (11.3.14)$$

Then

$$d[v \pm \psi(\epsilon)] = 0 \quad (11.3.15)$$

Thus the system of differential equations under consideration has two distinct real families of characteristics

$$dx - a dt = 0 \quad (11.3.16)$$

$$v - \psi(\epsilon) = \text{const} = \xi \quad (11.3.17)$$

$$dx + a dt = 0 \quad (11.3.18)$$

$$v + \psi(\epsilon) = \text{const} = \eta \quad (11.3.19)$$

The relation (11.3.16-17) refer to forward wave propagation and (11.3.18-19) refer to backward wave.

If the quantities ϵ , v are continuous but the derivatives are discontinuous then the wave part is said to have weak discontinuity. If these functions ϵ and v are discontinuous themselves then the waves are called shock waves [9].

11.4 IMPACT LOAD ON A SEMI INFINITE ROD

We now consider a semi infinite rod $x > 0$ which is at rest at $t = 0$. At the end $x = 0$ we prescribe the velocity $v = v(t)$
or the stress $\sigma = \sigma(t)$

If a body of mass m impinges on the end of the rod with the initial velocity V_0 then

$$m \cdot \frac{\partial v}{\partial t} = \sigma \cdot S \quad \text{when} \quad x = 0 \quad (11.4.1)$$

Where S = cross-sectional area and $v = v_0$ at $t = 0$.

We consider now that at $t = 0$ the rod experiences a tension or equivalently some strain

The initial and boundary conditions are

$$t = 0 \quad u(x, t) = 0 \quad (x \geq 0)$$

$$\frac{\partial u}{\partial t} = 0 \quad (x > 0)$$

$$x = 0 \quad \sigma = \text{Constant} = \sigma_x \quad (0 \leq t < t_1)$$

$$\sigma = 0 \quad (t \geq t_1)$$

11.5 PROPAGATION OF ELASTIC WAVES

We now first consider the propagation of elastic waves.

The solution of wave equation given by d'Alembert is

$$U = f(x - a_0 t) + \psi(x + a_0 t) \quad (11.5.1)$$

Where f, ψ are arbitrary function determined by boundary conditions.

When $\sigma^* < \sigma_0$ the deformation of the rod is elastic, the wave speed is constant ($a = a_0$) the eqn (11.3.3) becomes the classical wave equation. This solution, in the form given by D,Alembert

$$x - a_0 t = \text{const}, \quad x + a_0 t = \text{const} \quad (11.5.2)$$

since the displacement is continuous on the wave front. The solution then has the form $U = \epsilon^* (x - a_0 t)$ [40] . (11.5.3)

11.6 PROPAGATION OF ELASTO PLASTIC WAVE

We turn now to the propagation of elasto plastic waves when $\sigma^* > \sigma_0$. The system of non-linear differential equations (11.3.6) is reduceable and can be transformed analogously to the equations of the plane problem.

Changing to the new variables ξ, η we obtain

$$\frac{\partial \xi}{\partial t} + a \frac{\partial \xi}{\partial x} = 0 \quad \frac{\partial \eta}{\partial t} - a \frac{\partial \eta}{\partial x} = 0 \quad (11.5.4)$$

The system can be linearized by an inversion of the variables if the Jacobian

$$\Delta(\xi, \eta) = \frac{D(\xi, \eta)}{D(x, t)} = \frac{\partial \xi}{\partial x} \frac{\partial \eta}{\partial t} - \frac{\partial \xi}{\partial t} \cdot \frac{\partial \eta}{\partial x} \neq 0 \quad (11.5.5)$$

We can now obtain the canonical system

$$\frac{\partial x}{\partial \eta} - a \frac{\partial t}{\partial \eta} = 0 \quad \frac{\partial x}{\partial \xi} + a \frac{\partial t}{\partial \xi} = 0 \quad (11.5.6)$$

It should be pointed out that this canonical system is not equivalent to the original system.

With the aid of eqn. (11.5.4) we can obtain the solution for which the Jacobian $\Delta(\xi, \eta) = 0$

Therefore

$$\Delta(\xi, \eta) = 2a \frac{\partial \xi}{\partial x} \frac{\partial \eta}{\partial x} = - \frac{2}{a} \frac{\partial \xi}{\partial t} \frac{\partial \eta}{\partial t} = 0$$

$$\Delta(\xi, \eta) = |J| = 2a \frac{\partial \xi}{\partial x} \cdot \frac{\partial \eta}{\partial x} = 0 \quad (11.5.7)$$

$$\Delta(\xi, \eta) = |J| = - 2a \frac{\partial \xi}{\partial t} \cdot \frac{\partial \eta}{\partial t} = 0 \quad (11.5.8)$$

The above solutions were lost in the process of inverting the variables. Hence it follows that the lost solutions have the form:

1. $\xi = \text{const} = \xi_0 \quad \eta = \text{const} = \eta_0$
2. $\eta = \text{const} = \eta_0$
3. $\xi = \text{const} = \xi_0$

In the first case it follows from (11.5.4) that $v = \text{constant}$, $\epsilon = \text{constant}$ i.e. a state of constant strain (a state of rest).

In the second case one of the equations in (11.5.4) is satisfied since $\eta = \eta_0$ while the other after substitution of $\xi = \eta_0 - 2\psi(\epsilon)$ takes the form

$$\frac{\partial \epsilon}{\partial t} + a \frac{\partial \epsilon}{\partial x} = 0 \quad (11.5.9)$$

The differential equation of the characteristics

$$\frac{dt}{1} = \frac{dx}{a} = \frac{d\epsilon}{0}$$

The integrals are

$$\epsilon = c_1 \quad x - at = c_2$$

C_1 and C_2 are arbitrary constants. The solution of the original system of equation is

$$\eta = \psi(\epsilon) + v = \eta_0$$

$$x - at = \phi(\epsilon)$$

where ϕ is an arbitrary function. Hence the characteristics are straight lines. The third case ($\xi = \text{constant}$) is analogous to second except that here the waves move in the opposite direction.

11.7 PROPAGATION OF AN ELASTO-PLASTIC LOADING WAVE

When the end of the rod is subjected to suddenly applied load, a simple extension wave $v + \psi(\epsilon) = \eta_0$ begins to propagate, ahead of the wave there is state of rest, hence $\eta_0 = 0$ and $v + \psi(\epsilon) = 0$

Different deformations will propagate with different speeds: elastic deformations with maximum speed (a_0), deformations beyond the elastic limit with least speed.

At the wave front $X - a_0 t = 0$ the strain experiences a jump from zero to ϵ_0 and the particle velocity from zero to $v = -\Psi(\epsilon_0) = -a_0 \epsilon_0$ immediately after this a central expansion wave passes:

$$v + \Psi(\epsilon) = 0, \quad x - a_0 t = 0$$

This can be characterised in $x - t$ plane. A pencil of straight characteristics emanating from the coordinate origin. The speed of propagation of strain is constant along each ray fig (11.2). The speed obviously decreases for the characteristic with large slope. At any fixed point $x = x'$ we have a state of rest the wave front arrives at the instant $t = x'/a_0$.

Next, in the interval $x'/a_0 < t < x'/a(\epsilon_*)$ plastic deformation appears and gradually increases at the moment $t = x'/a(\epsilon^*)$. This deformation reaches maximum value and does not change subsequently.

11.8 UNLOADING WAVE

At instant $t = t_1$ a new wave begins to propagate in the positive x direction. This is unloading wave. In the unloading region the differences in stresses and strains are related by Hooke's law.

$$\sigma - \sigma_m = E (\epsilon - \epsilon_m)$$

Where σ_m and ϵ_m are the values of stresses and strain attained in a given section of the rod at the instant when the unloading begins fig. (11)

These values are unknown functions of x . Substituting in the equation of motion we have

$$\frac{\partial^2 U}{\partial t^2} = a_0^2 \frac{\partial^2 U}{\partial x^2} + \psi(x) \quad (11.8.1)$$

Where

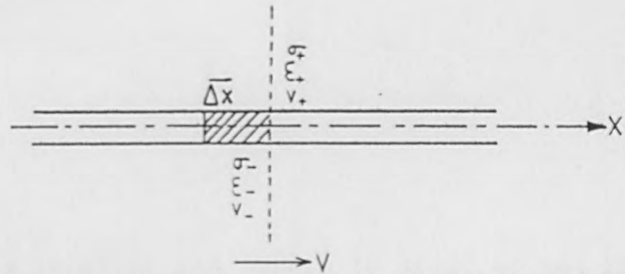
$$\psi(x) = \frac{1}{\rho} \frac{\partial}{\partial x} (\sigma_m - E \cdot \epsilon_m) \quad (11.8.2)$$

is known.

We now consider that the unloading wave moves with the velocity a_0 of the elastic waves. With passage of the front the stress and strain experience discontinuities [4].

$$\sigma_+ - \sigma_- = [\sigma]$$

$$\epsilon_+ - \epsilon_- = [\epsilon]$$



Where σ_+ , ϵ_+ , σ_- , ϵ_- are values of stresses and strain in front of and behind the front. Which is moving with some velocity V . Applying Hooke's law

$$[\sigma] = E [\epsilon] \quad (11.8.3)$$

At the wave front the condition of continuity of displacement must be satisfied.

Now consider an element of length Δx after passage of this wave the length of the element is $\bar{\Delta x} = \Delta x - (\epsilon_+ - \epsilon_-) \Delta x$

on the other hand $\bar{\Delta x} = \Delta x + (v_+ - v_-) \cdot \Delta x / v$ (11.8.4)

Thus the discontinuities in strain and velocity are connected by the relation

$$- [v] = v [\epsilon] \quad (11.8.5)$$

Next, the change in momentum of the element Δx on passage of the unloading wave must obey a dynamical law by conservation of momentum theorem.

$$- \rho \Delta x [v] = [\sigma] \Delta x / v \quad (11.8.6)$$

Eliminating the discontinuities with the aid of (11.8.3) and (11.8.5) we find that unloading wave propagates with the elastic wave

$$v = \sqrt{E/\rho} = a_0$$

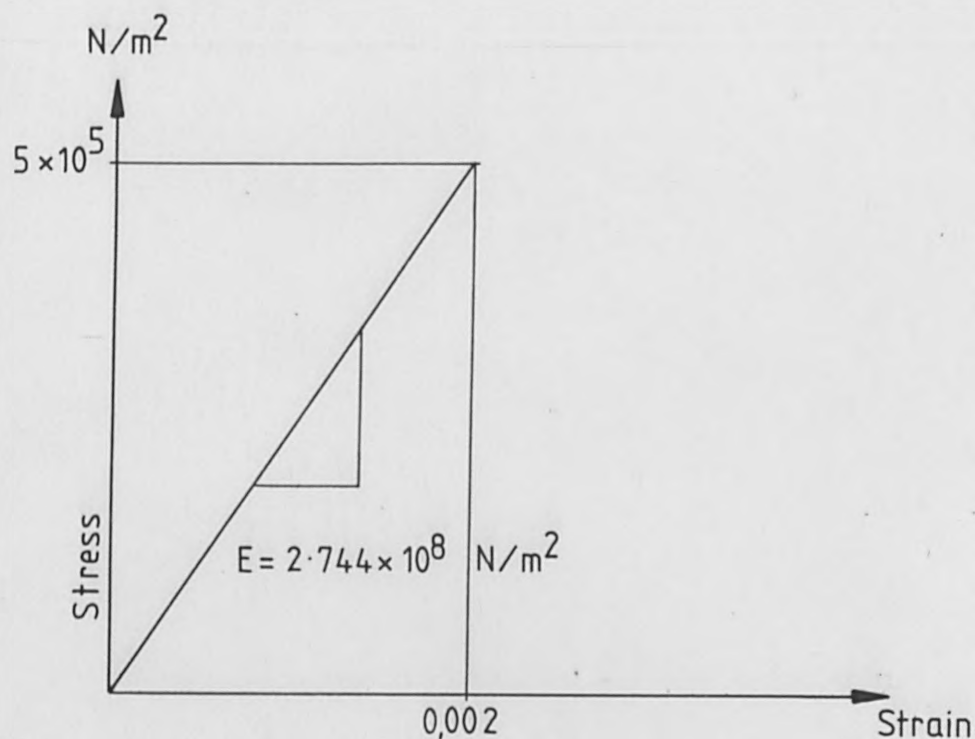
We shall now present a FE solution of a selected problem, in which a rod is subjected to a triangular load. The results of the analyses are then compared with the elastic and with the help of method of characteristics the plastic wave propagation problems (Fig. 11.1,11.2,11.3)

The stress profiles calculated by using quiet boundary condition for the elastic case fig. 11.1 are compared at various times with the exact solution. The quiet boundary procedure is used to absorb the waves at the bottom of the boundary. Absence of reflections at 0.03 sec. shows the effectiveness of the procedure.

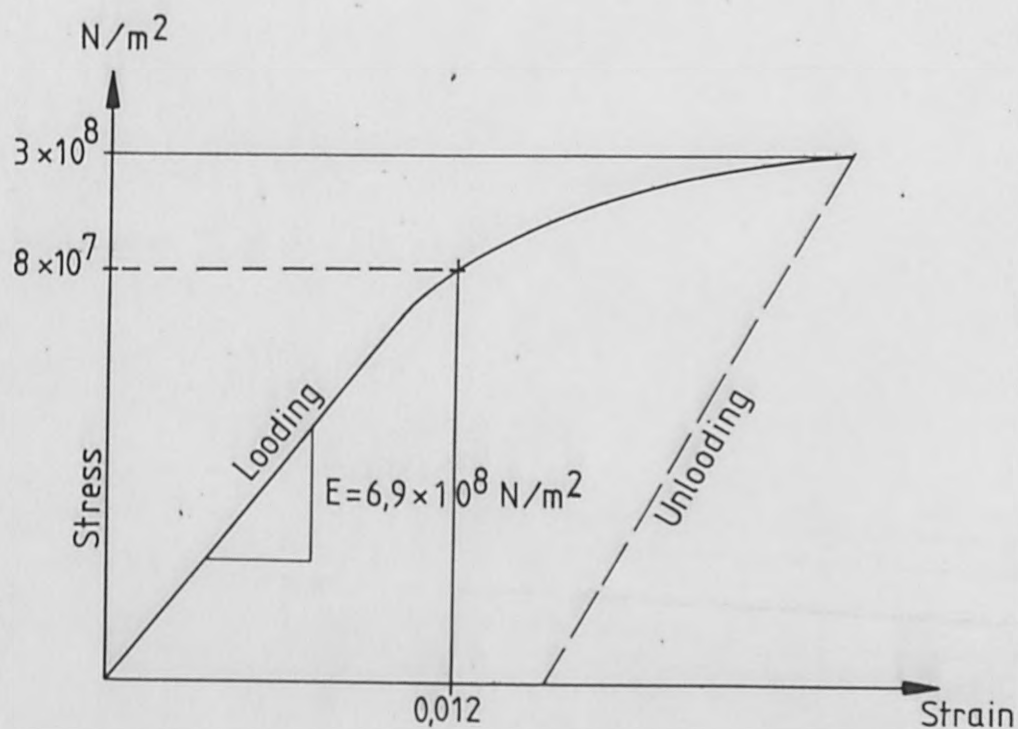
For the problem involving inelastic deformation is illustrated in fig. 11.3. The solution for the triangular pulse represents reasonably well the loading phase of the pulse, including the elastic precursor. The unloading phase is represented less well. The quiet boundary procedure was not used in this calculation, which was stopped before the reflection reached the stations on the horizontal scale. To reduce or eliminate solution oscillation there are two possibilities, namely reduce the time step or reduce the element size. The time step used in this analysis was 1×10^{-5} sec. which is sufficiently small. A further reduction of time step $\Delta t = 0.5 \times 10^{-5}$ did not help much. Therefore it was tentatively concluded that the element size will have to be reduced in order to improve agreement with the exact solution.

IBC
WV BOVERI

The Constitutive relation used in elastic and elasto-plastic wave propagation Problem.

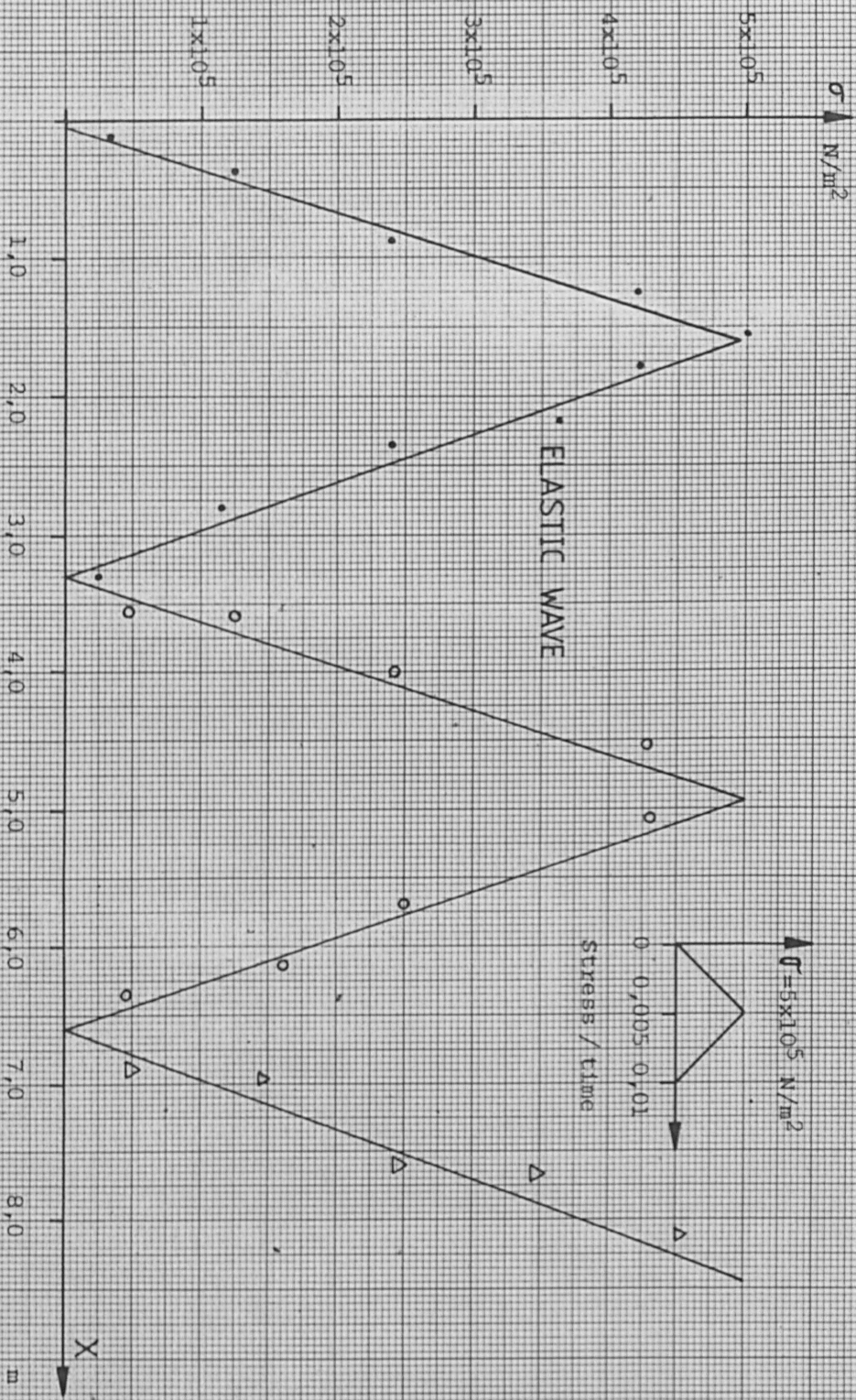


Elastic problem (ref. to Fig. 11.1)



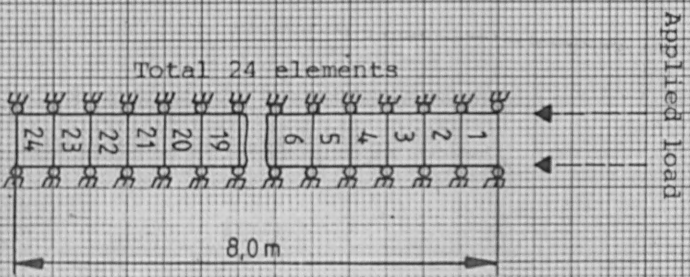
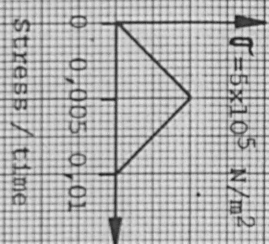
Elasto-plastic problem (ref. to Fig. 11.3)

PLANE ONE DIMENSIONAL WAVE PROPAGATION Fig. (11.1)



- Exact solution
- Finite element $t = 0,01s$
 - Finite element $t = 0,02s$
 - △ Finite element $t = 0,03s$

Bulk modulus = $1,7 \times 10^8 \text{ N/m}^2$
 Modulus of rigidity = $9,8 \times 10^7 \text{ N/m}^2$
 $P = 3207 \text{ Kg/m}^3$

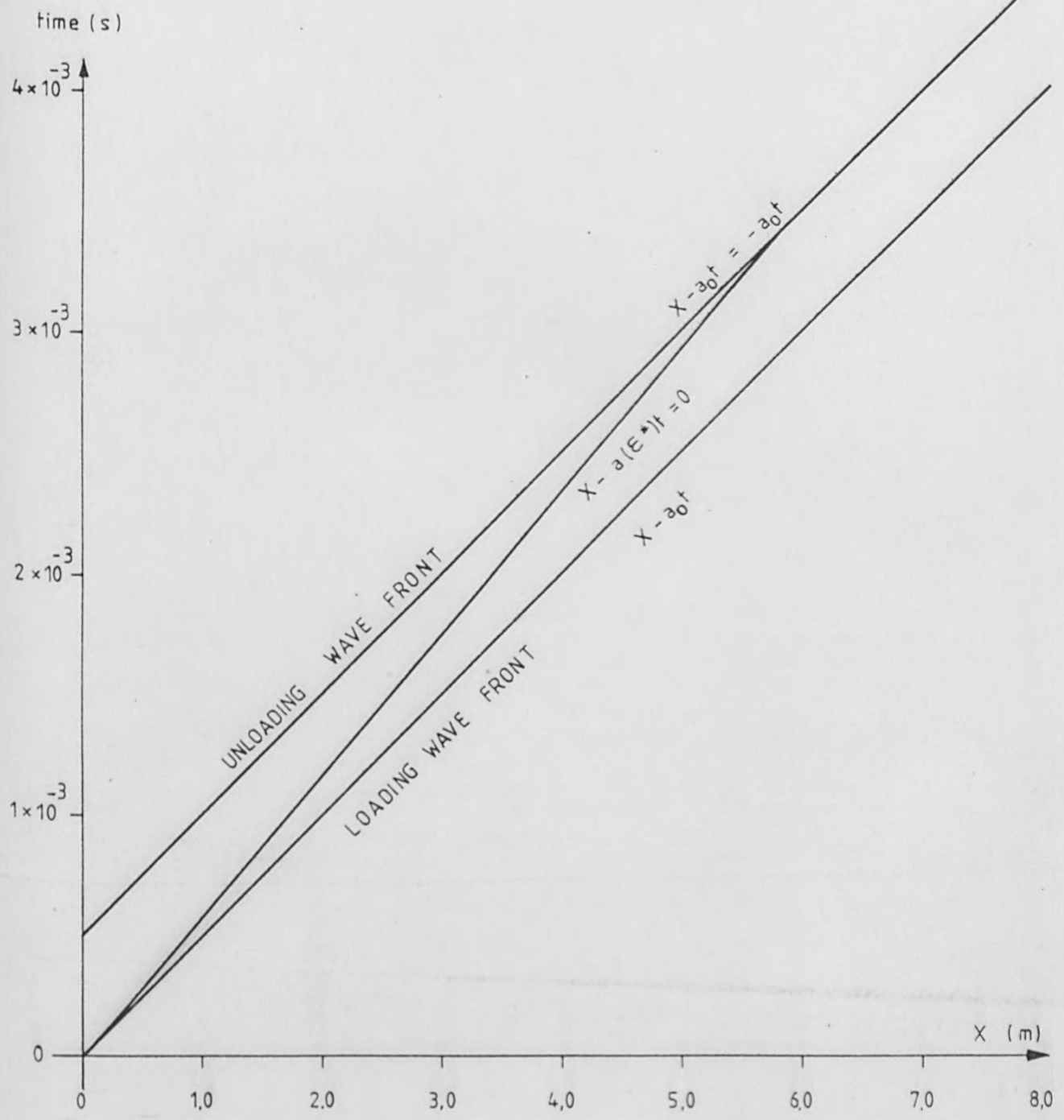


$$t_0 < \frac{L}{a_0}$$

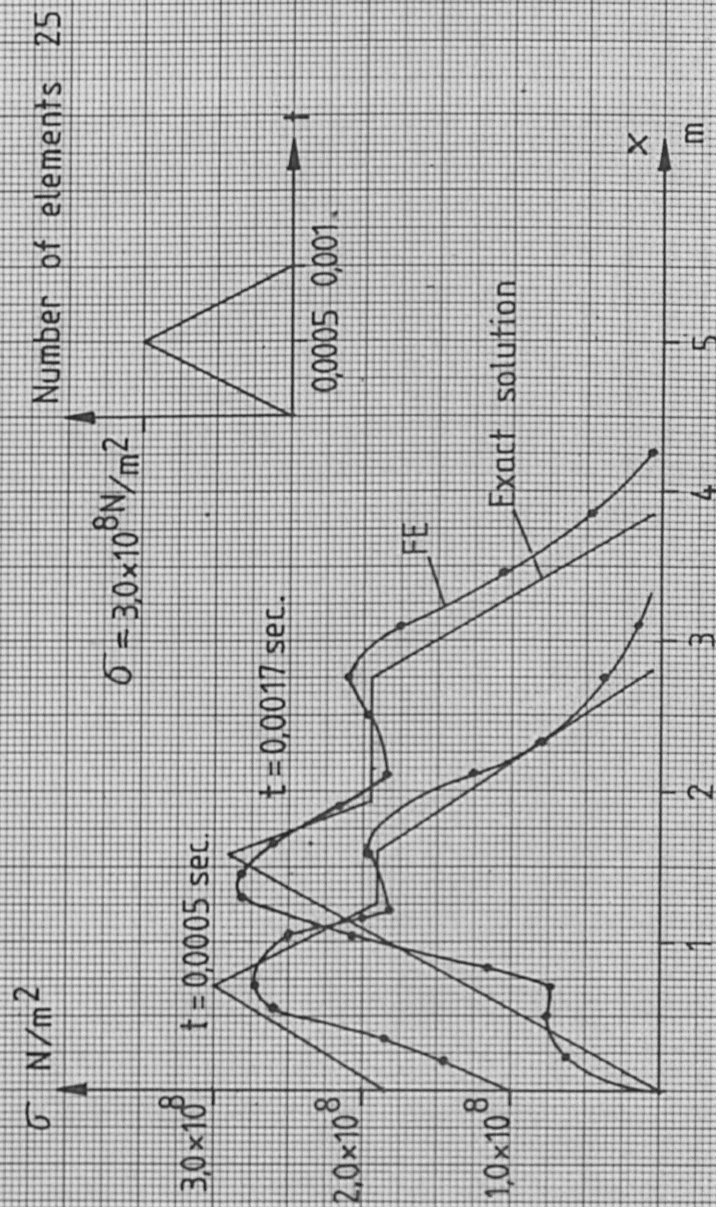
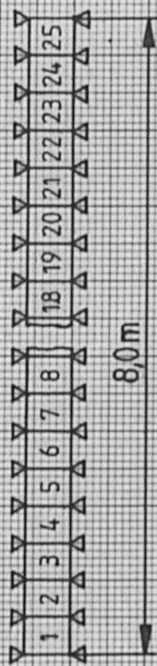
$$\frac{L}{a_0} = \frac{8}{1915} = 0,0041 \text{ sec}$$

$$t = 0,001 \text{ sec}$$

$$a(E^*) = 1600 \text{ m/s}$$



METHOD OF CHARACTERISTICS Fig. (11.2)



Number of elements 25

Density = 2138 Kg/m^3
 Bulk modulus = $4,5 \times 10^9 \text{ N/m}^2$
 Shear modulus = $2,5 \times 10^9 \text{ N/m}^2$
 Yield Stress = $8,0 \times 10^7 \text{ N/m}^2$
 $\mu = 0,38$

COMPARISON BETWEEN CLOSED FORM AND F.E. SOLUTION, FIG. (11.3)

12. Modelling of Soil-Structure System

The soil structure interaction calculations have been performed in terms of the following parameters:

- a) Finite element representations of free field and structures surrounded by soil.
- b) Soil and structural properties.
- c) Input and boundary conditions.

a+b) The containment and support structures are represented by a cantilever fastened to the upper surface of the basemat using two-dimensional 4-node isoparametric plane strain elements. The main purpose of the structural model is to represent only the lower modes of vibrations from 2 c/s up to 6 c/s are generally found to contribute to the maximum response of nuclear structures due to earthquake loading with dominant frequency content of 2.5 to 5 c/s.

The basemat is considered flexible and the depth of embedment was taken to be 10 m. The soil media is divided into three layers. The bottom layer is the bedrock, two layers above are of hard soil, and the layers below the foundation and around the structure are soft. The shear wave velocities and moduli of elasticity used for this study are given below.

Table 12

	u m/s	N / m^2	ρ kg/m ³	ν
Structure	2422	3.5×10^{10}	2550	0.17
Soil bottom layer	1190	1.086×10^{10}	2650	0.45
Soil middle layer	800	5.0×10^9	2650	0.47
Soil top layer	400	9.1×10^8	1960	0.45

In order to study the extent of inelastic deformation of the soil due to earthquake loading, non-linear material properties are assumed. The formation of plasticity and its growth over the extended region of the soil mass were observed by using Drucker-Prager Yield Criteria.

- c) The earthquake motion in the form of acceleration Time-history with a peak acceleration of 0,25 g is prescribed at the bedrock level. (fig. 12.2) The method of input and boundary conditions follow from the present assumption that earthquake loading may be regarded as a train of waves which propagate through soil and engulf a structure. The input is applied as horizontal acceleration or velocity time history to one edge of the mesh and the waves which encounter other artificial boundaries of the finite element mesh are transmitted through the boundary by the quiet boundary procedure in sec 9.

Due to rather coarse finite element model of the soil media, a significant part of the response of the foundation and structure beyond 10 c/s could not be accurately represented. However, it is well known that the high frequency part in structural response due to earthquake loading is considerably less than the low frequency response, and therefore no serious error would be expected in the response calculation.

Table 12.1

Following numerical values are used to evaluate the Yield coefficients
see appendix A.

$$1 \text{ PSI} = 6895 \text{ N/m}^2$$
$$1 \text{ PSI} = 712 \text{ kg/m}^2$$

	ϕ	C	α	K
Top layer	0	16.7 PSI	0	2,77 PSI
Middle layer	16.1	8.68 PSI	0.118	1,53 PSI
Bottom layer	Does	not	yield	

No parametric studies have been done to show the influences of yield parameters on Yield criteria, and consequently their effects on response analysis. However, an attempt is made here to show the significance of the variations of yield parameter in terms of invariant J_1 which affects the yield criteria (Fig. 12). Therefore changes in yield parameter means changes in soil strength which affect the predicted response.

Yield Criteria

Drucker Prager = $\alpha J_1 + K = \sqrt{J_2}$

Mohr-Coulomb = $\alpha J_1 + C = \sqrt{J_2}$

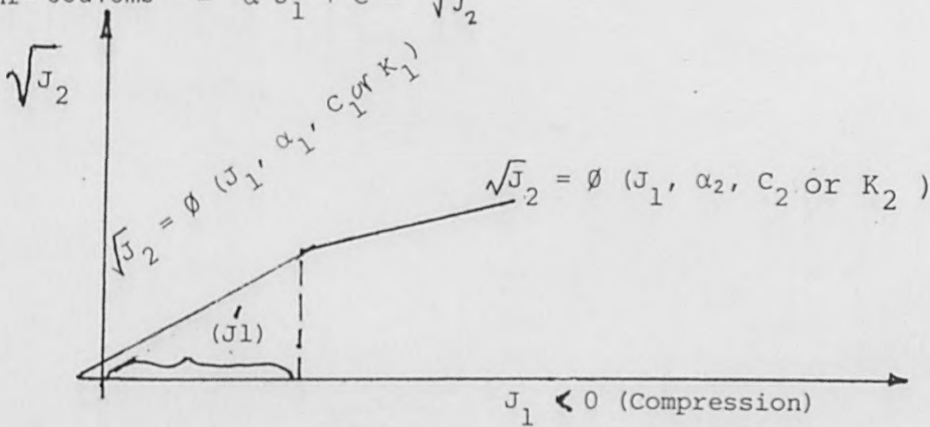


Fig. 12

$$J_1 = \sigma_1 + \sigma_2 + \sigma_3$$

$$= \sqrt{J_2} = \left\{ \frac{1}{6} \left[(\sigma_1 - \sigma_2)^2 + (\sigma_3 - \sigma_2)^2 + (\sigma_3 - \sigma_1)^2 \right] \right\}^{\frac{1}{2}}$$

J_2 = Second invariant of deviatoric stress

α_1 and α_2 = Coefficients of frictions

C_1 and C_2 = Cohesion

(J_1) = Mean stress at which the yield criteria changes from (α_1, C_1, K_1) to (α_2, C_2, K_2)

12.1 Case Study

A hypothetical nuclear power plant has been considered for this particular case study. A description of the model and assumptions are given in previous sections. Information on soil properties in Table 12.1 is obtained from actual cross-hole testing of a site for a proposed nuclear power plant.

12.2 Discussion

The results of the investigation are presented in the form of response spectra, to show and to gain further insight into the non-linear material behaviour of soil and its effect upon the interaction between soil and structure.

In Figure 12.3 the free-field response spectra at the soil surface and at the boundary layer (rock surface) are given, and compared with the interaction response spectra at a point near the reactor building and under the basemat.

The study shows that there is a shift in peak acceleration response towards higher frequency from 5 c/s to 8.3 c/s. The response above 10 c/s is anomalous, and this is due to the fact that rather coarse finite element model of the soil and structure system is unable to produce a high frequency response accurately. In the lower frequency range, the case study shows a strong deamplification of acceleration response. This could be contributed to the absorption of kinetic energy by the soil due to the progressive formation of a plastic region under the basemat and in the surrounding soil media. Chu and others [6] reported that deamplification or amplification could be expected depending on soil properties. Isenberg [4] also made a similar observation, but the deamplification was not so large as it is reported here. Isenberg used constant G module and shear wave velocities in all the layers to account for the inelastic properties of the soil.

Figures 12.2 A & B show the beginning of plasticity in the soil (shaded elements) and the spreading of plasticity in an extended region under the basemat respectively. The duration of earthquake motion at the bedrock was only 10 seconds, which was considered sufficient for this study. It has been reported by Trifunac (55) that strong motion part of the earthquake (high peak acceleration, low frequency) occurs within 10 seconds of the time history record. As most of the Nuclear Structures have frequencies within the band width of 2 - 6 c/s, the peak response of these structures have been found to occur within 10 seconds. For this reason 10 seconds earthquake input was considered sufficient. For the case of structure-equipment response it is advisable to consider a duration of 20 seconds, to include the high frequency components of earthquake record, because most items of equipment have fundamental frequencies of 15 c/s above.

We now focus our attention to the time history responses under the basemat for an extended period up to 3. sec. Now let us have a close look at the time history input in fig. 12.1. It will be observed that the rise time of peak acceleration input 0.25 g is about 2.5 sec. The next highest peak acceleration 0.24 g is noticeable at about 13 sec. Therefore we expect that the peak time history responses must occur within 2.5 sec. Figures 12.11A, 12.10A and 12.12.A and 12.10 confirm this observation. Furthermore, earthquake time-history records beyond 10.0 sec. have almost invariably high frequency content (55). In practice it was observed that any structure which is expected to reach its maximum response values beyond 10.0 sec time - history input has in general fundamental frequency equal to or higher than 10 c/sec. In this particular case we are now investigating, the structure and soil model has a fundamental frequency of about 5 c/s. To summarize, it can be said that we are not expecting higher response values beyond 2.5 sec. for this particular case.

Some explanations to fig. 12.11A and 12.10A are necessary. Notice that in fig. 12.10A, at the on set of plastic deformation (0.3 sec.) of the soil under the basemat, the structure makes a steplike motion up to about 0.6 sec. and from then on, makes a steady rigid body like motion (sliding motion) up about 0.9 sec. After a few load reversal, the soil regains its strength (strain-hardening), and from then on familiar saw tooth like response curve becomes apparent. Similar observations could be made in fig. 12.11A. At the on set of plastic deformation of soil beneath the basemat, and for about 0.6 sec., the structure does not respond to earthquake input, and has practically no vertical motion (Loss of contact?) After the soil regains its strength vertical time-history response is again restored.

12.3 Results

The present analytical results are used to study three main subjects. The first is the relation between motion of the foundation and that of the free field. Also included in the study are the influence of soil stiffness, including plasticity and frequency content of the earthquake input relative to frequency of the structure. The second object is the relation between stresses in the soil adjacent to the structure and those corresponding to points in the free field. The third major finding is the influence of plasticity of soil on the response of the superstructure, and comparison with the response using linear elastic theory of soil.

12.4 Relation between motions of the foundation and the free field

The ratios of acceleration spectra at the foundation to the spectra of the free field are shown for the embedded structure. These results clearly indicate that the horizontal response of

the foundation is less than that of the free field. The influence of plasticity on the interaction forces seems to be important, relative to energy dissipation, for vertical displacement more than for horizontal displacement. This is illustrated in Figures 12.4 and 12.5. The main interaction forces at $t = 0.3$ seconds is provided by shear stresses, acting along the edge of the superstructure. If the soil adjacent to the edge is allowed to be elastic, as shown in Figure 12.4, larger vertical displacements are expected. The amount of suppression is greatest in the region of 5 c/s in the interaction spectra, when the free field response is defined at the surface. It may also be observed that at higher frequency near 10 c/s, the free field response is lower, and that is so to say an amplification of response. This may be attributed to the fact that, due to overburden pressure, the soil mass becomes comparatively stiffer, and the response of the soil-structure system behaves as if the superstructure is sitting on a rock-like formation of soil, i.e. so-called hard soil condition. It is well known from linear analysis, that the response due to hard soil conditions is always higher than soft-soil conditions.

12.5

Relation between stress in free fields and stress adjacent to the structure

The study presented in this thesis indicates that stresses in the soil adjacent to the structure in general differ from stress which would develop at the same point if the structure were not present. One general finding for this particular case (due to typical formation and physical characteristics of the soil mass below the basemat) is that stresses in the soil beneath the foundation at the early stage of shaking due to earthquake, remain compressive. After several cycles of stress reversal due to the vertical motion of the soil and structure complex, the sign of instability of the soil (plasticity) was observed at 0.6 seconds. Where as in the next layer of soil, the instability was observed at 0.3 seconds. The reason is that due to overburden pressure, the strength of the soil layer immediately beneath the basemat is

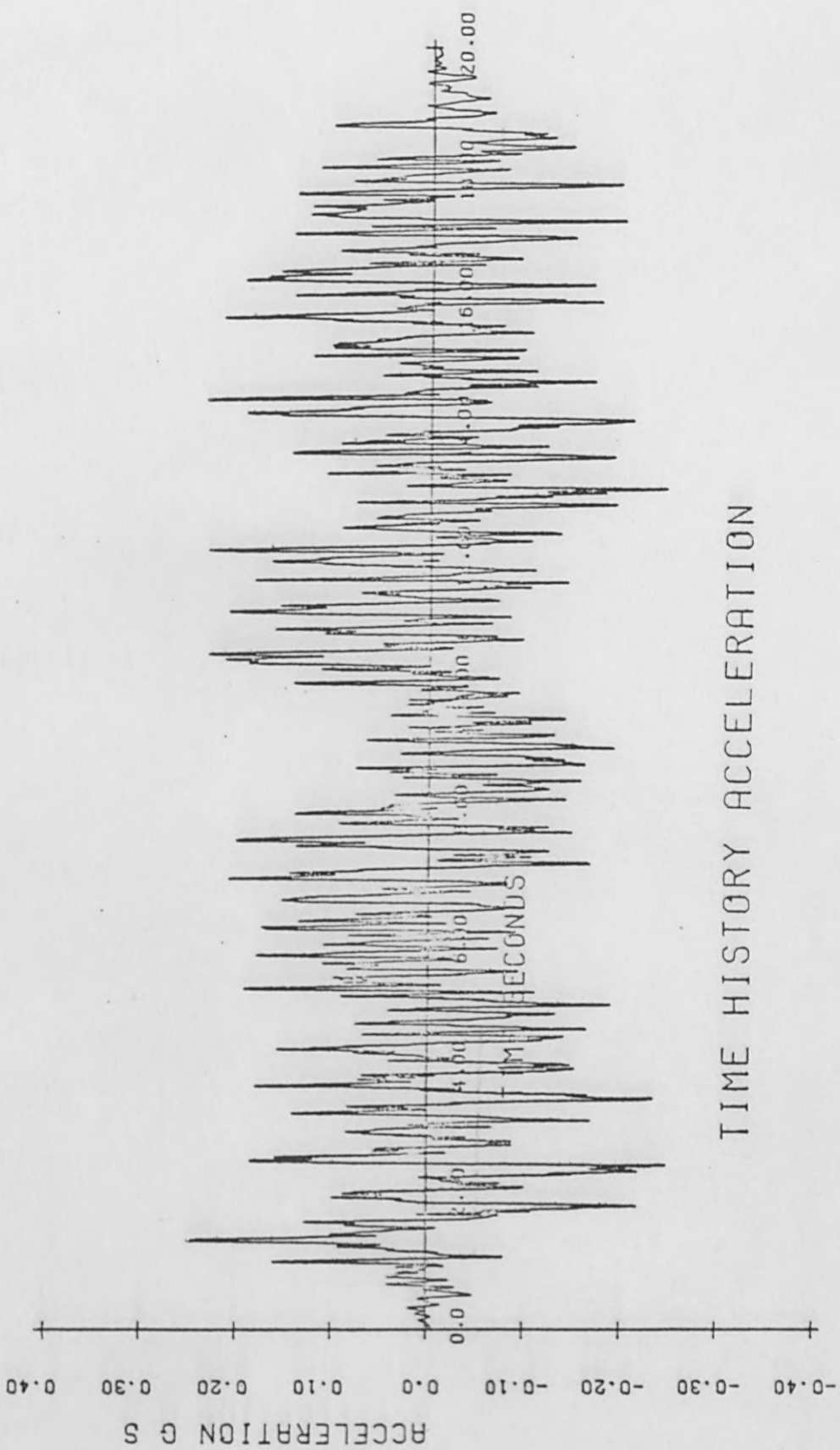
increased and therefore the instability was observed much later. One general finding is that there is a unique relation between the vertical motion of the basemat and the vertical stress history. A similar unique relation was found in the case of the shear stress time history and the horizontal motion of the basemat.

As far as the free field stress-history and the free field motion are concerned, Fig. 12.8 and 12.9 show that no apparent correlation could be found between these two results. It is probably due to the fact that unwanted scattered wave due to reflection at the artificial boundary was not allowed to travel back and distort the motion of the elements (nodal points), and therefore fairly smooth velocity time histories could be computed. On the other hand, the resultant stresses (vertical stress and shear stress) due to the motion of the elements near the boundary were not corrected when the unwanted scattered velocity was suppressed.

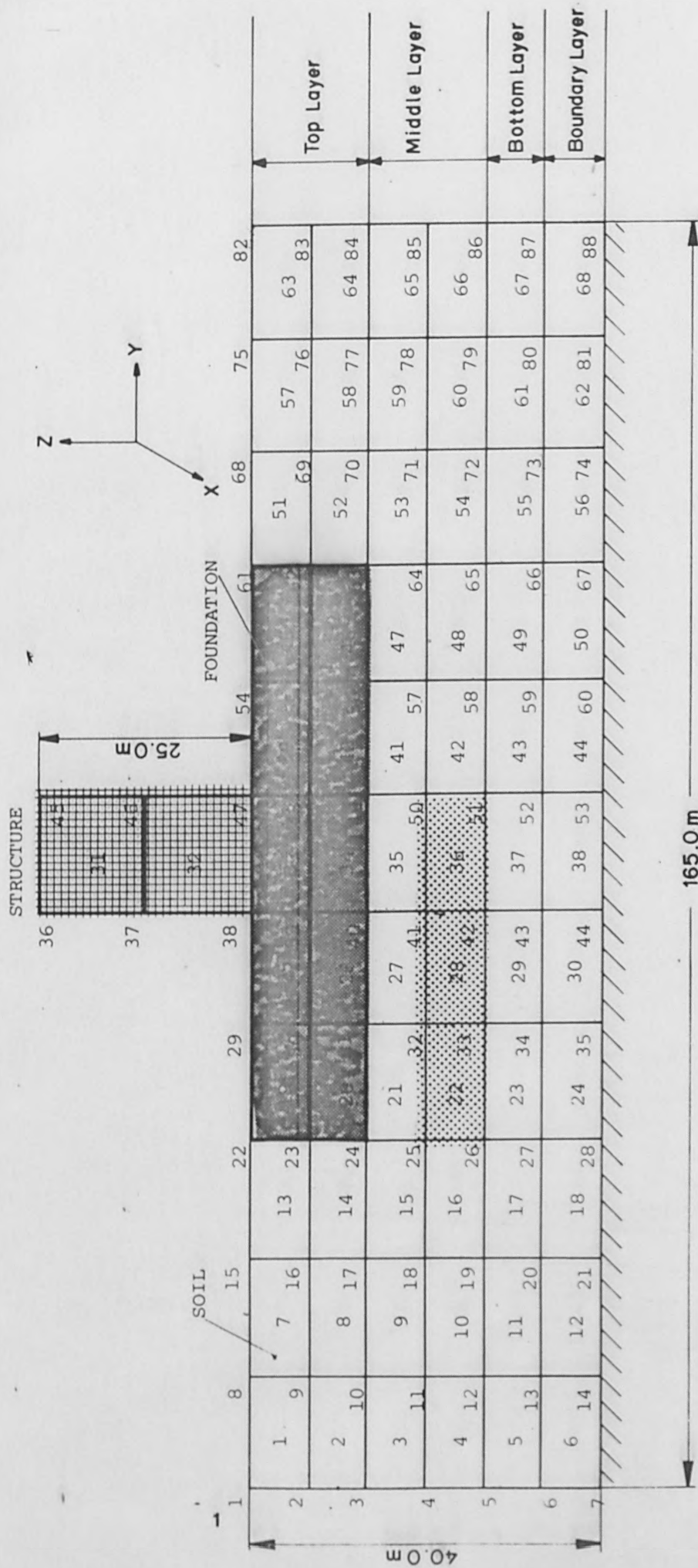
Conclusions

- 1) Necessity of correct modelling technique for soil and structure system
- 2) Awareness of the problem of wave reflections from the finite element boundary which contribute to false or unuseable results in response analysis. Necessary and adequate measures are required to counteract these effects.
- 3) Choice of suitable integration scheme and time step, so as to allow the solution not to "drift away". In nonlinear analysis, no integration scheme is unconditionally stable.
- 4) Behaviour of soil is nonlinear in general, and its loss of strength and strain hardening during the strong motion earthquake is considered essential in predicting dynamic responses of super-structure.
- 5) Minimum duration of 10.0 sec. of the time-history input must be provided in order to obtain peak structural responses whose fundamental frequency lies within the frequency band width of 2-6 HZ
- 6) Peak acceleration response at the top layer of the horizontal response spectra is suppressed by 16 % compared to the free field response spectra
- 7) Substantial deamplification of response in the lower frequency range
- 8) Considering the interaction , the peak response under the basemat is suppressed by 2.3%.

The conclusions drawn here are subject to a single study made for this thesis. These may be modified for earthquake inputs having different frequency contents, duration, and peak accelerations. The soil properties, the structure, as well as the depth of embedment would influence the results, and different conclusions would be possible. However, the study has covered a wide enough range of parameters such as artificially generated earthquake input containing a wide range of frequencies up to 30 HZ, a number of soil layers with different soil properties, dominant modes of vibration of the superstructure, the flexibility of the basemat and embedment. Although no generalisation could be made based on a single study such as reported here, but it can be concluded that under similar site conditions, and structural configuration, the response quantities as found in this investigation will not be much different, elsewhere.



TIME HISTORY ACCELERATION



After 0.3 Sec

Model For Soil Structure Interaction Study

Fig. 12.2 A

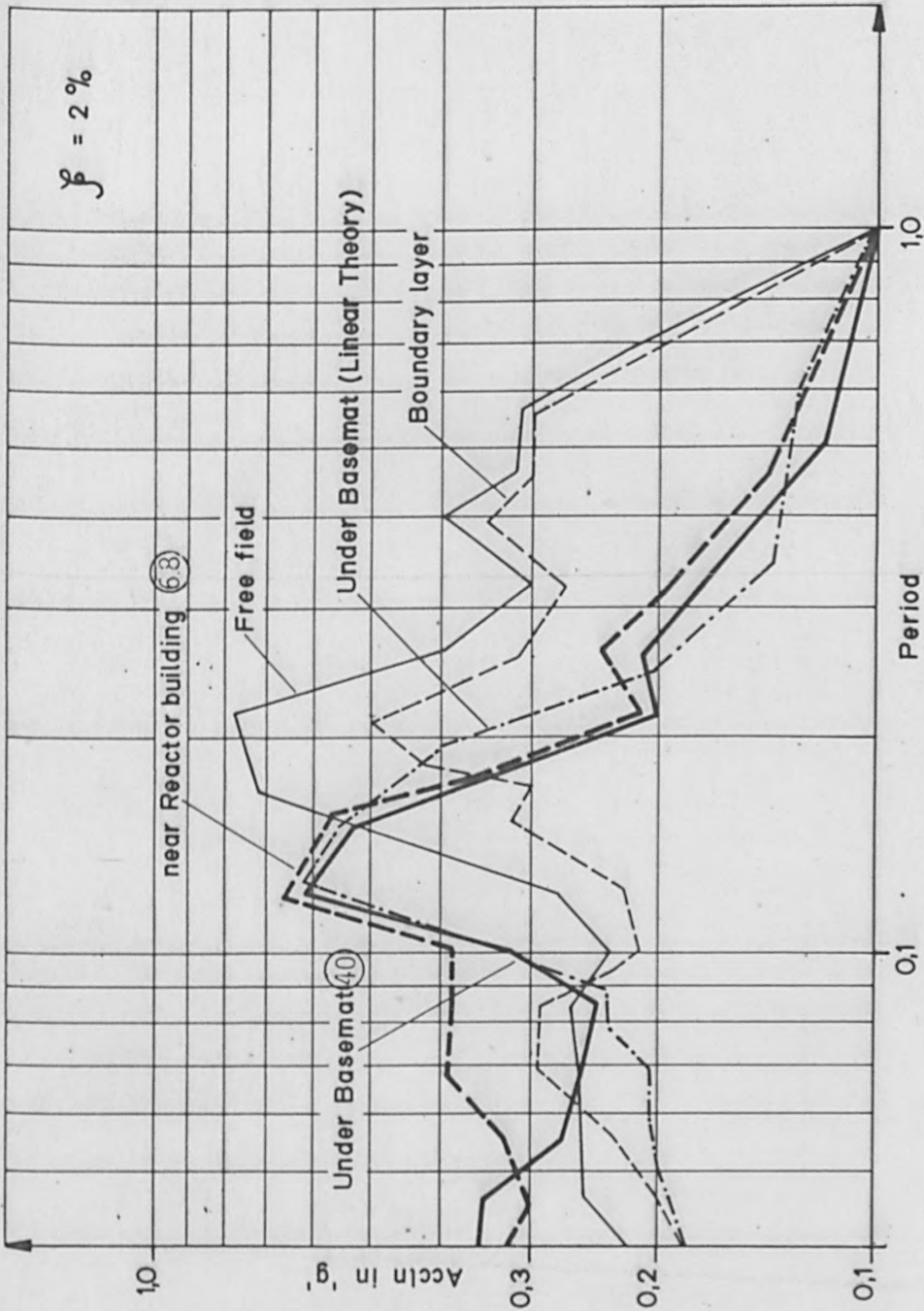


Fig. 12-3 Interaction Response spectra

TABLE 12.1

TIME HISTORY
Displacement (NP 40)

Time s	Horizontal Displacement m	Vertical Displacement m
0.01	0.17 x 10 ⁻⁵	0.13 x 10 ⁻⁷
0.02	0.12 x 10 ⁻⁴	0.13 x 10 ⁻⁶
0.03	0.36 x 10 ⁻⁴	0.48 x 10 ⁻⁶
0.04	0.67 x 10 ⁻⁴	0.81 x 10 ⁻⁶
0.05	0.98 x 10 ⁻⁴	0.513 x 10 ⁻⁶
0.06	0.122 x 10 ⁻³	-0.68 x 10 ⁻⁶
0.07	0.137 x 10 ⁻³	-0.265 x 10 ⁻⁵
0.08	0.135 x 10 ⁻³	-0.526 x 10 ⁻⁵
0.09	0.128 x 10 ⁻³	-0.86 x 10 ⁻⁵
0.10	0.102 x 10 ⁻³	-0.129 x 10 ⁻⁴
0.11	0.634 x 10 ⁻⁴	-0.182 x 10 ⁻⁴
0.12	0.11 x 10 ⁻⁴	-0.23 x 10 ⁻⁴
0.13	-0.52 x 10 ⁻⁴	-0.286 x 10 ⁻⁴
0.14	-0.125 x 10 ⁻³	-0.318 x 10 ⁻⁴
0.15	-0.206 x 10 ⁻³	-0.33 x 10 ⁻⁴
0.16	-0.296 x 10 ⁻³	-0.24 x 10 ⁻⁴
0.17	-0.398 x 10 ⁻³	-0.24 x 10 ⁻⁴
0.18	-0.51 x 10 ⁻³	-0.16 x 10 ⁻⁴
0.19	-0.63 x 10 ⁻³	-0.41 x 10 ⁻⁵
0.20	-0.77 x 10 ⁻³	0.105 x 10 ⁻⁴
0.21	-0.907 x 10 ⁻³	0.286 x 10 ⁻⁴
0.22	-0.102 x 10 ⁻²	0.506 x 10 ⁻⁴
0.23	-0.11 x 10 ⁻²	0.76 x 10 ⁻⁴
0.24	-0.120 x 10 ⁻²	0.108 x 10 ⁻³
0.25	-0.125 x 10 ⁻²	0.142 x 10 ⁻³
0.26	-0.128 x 10 ⁻²	0.182 x 10 ⁻³
0.27	-0.129 x 10 ⁻²	0.223 x 10 ⁻³
0.28	-0.128 x 10 ⁻²	0.265 x 10 ⁻³
0.29	-0.126 x 10 ⁻²	0.306 x 10 ⁻³
0.30	-0.124 x 10 ⁻²	0.343 x 10 ⁻³

TIME HISTORY
VERTICAL DISPLACEMENT
OF BASEMAT

CORRESPONDS TO TABLE 12.1

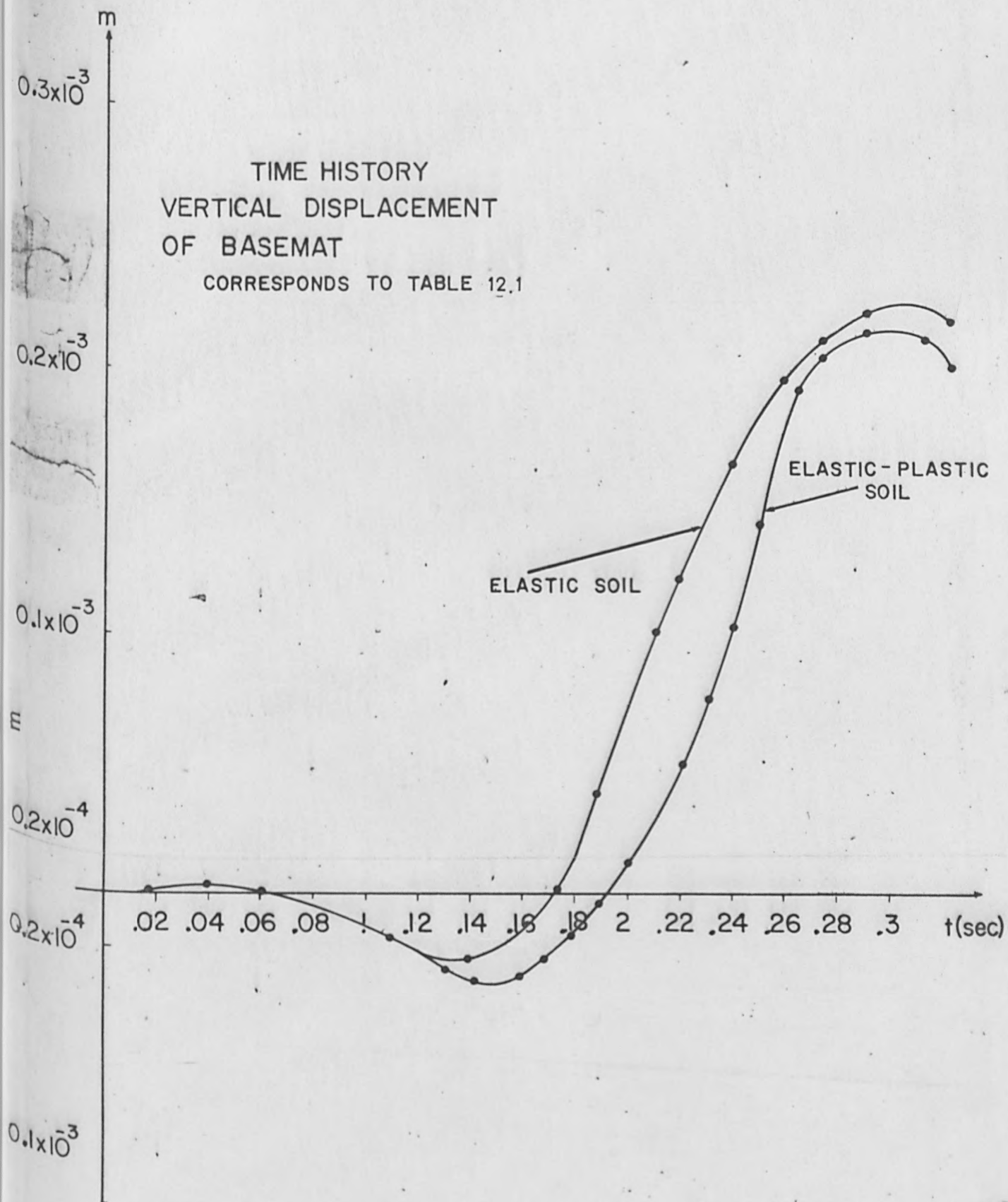


Fig. 12.4

TIME HISTORY
HORIZONTAL DISPLACEMENT
OF BASEMAT

CORRESPONDS TO TABLE 12.1

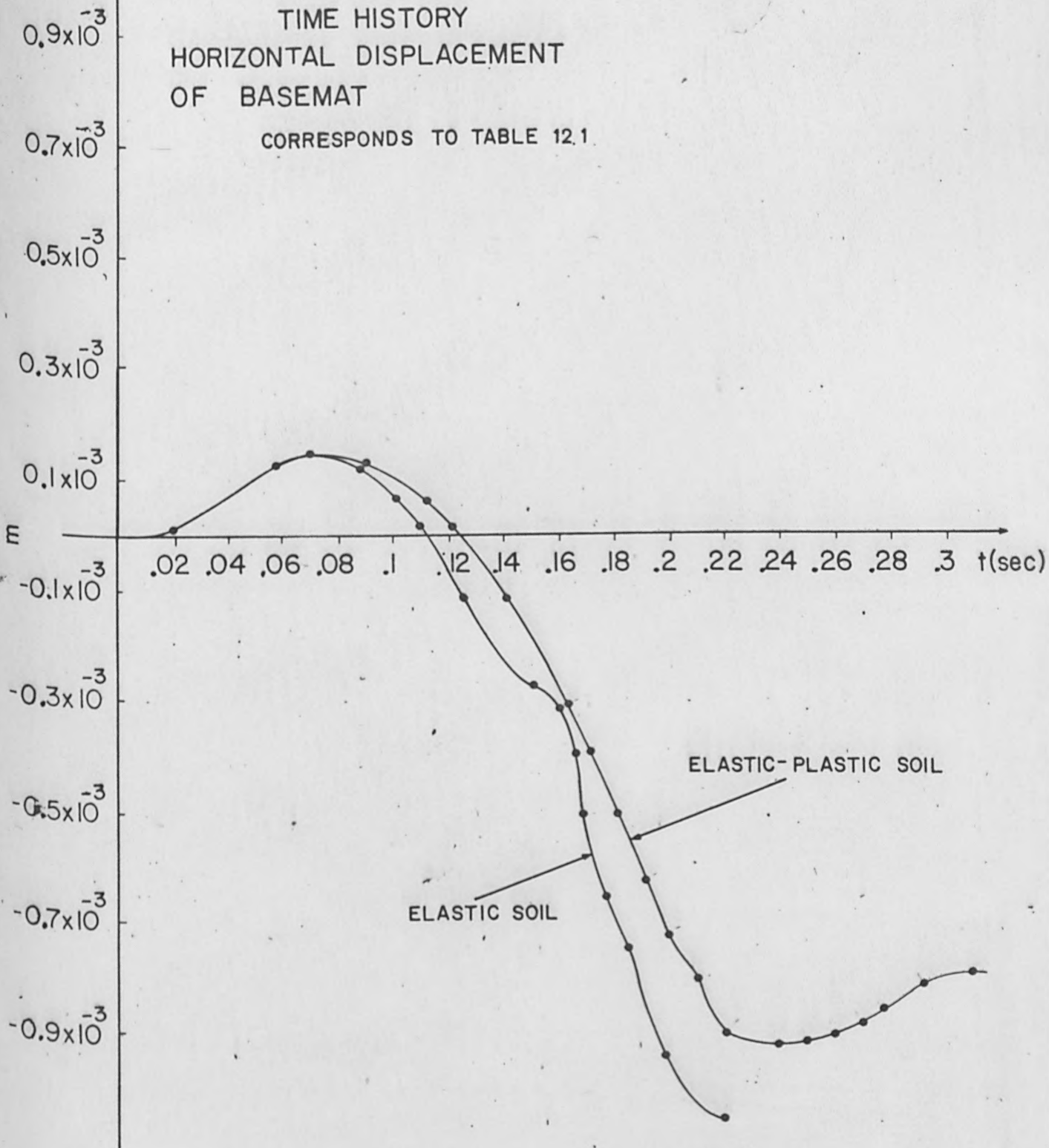


Fig. 12.5

TIME HISTORY
 VERTICAL STRESS - FREE FIELD
 SAME LEVEL AS FOUNDATION
 CORRESPONDS TO TABLE 12.2

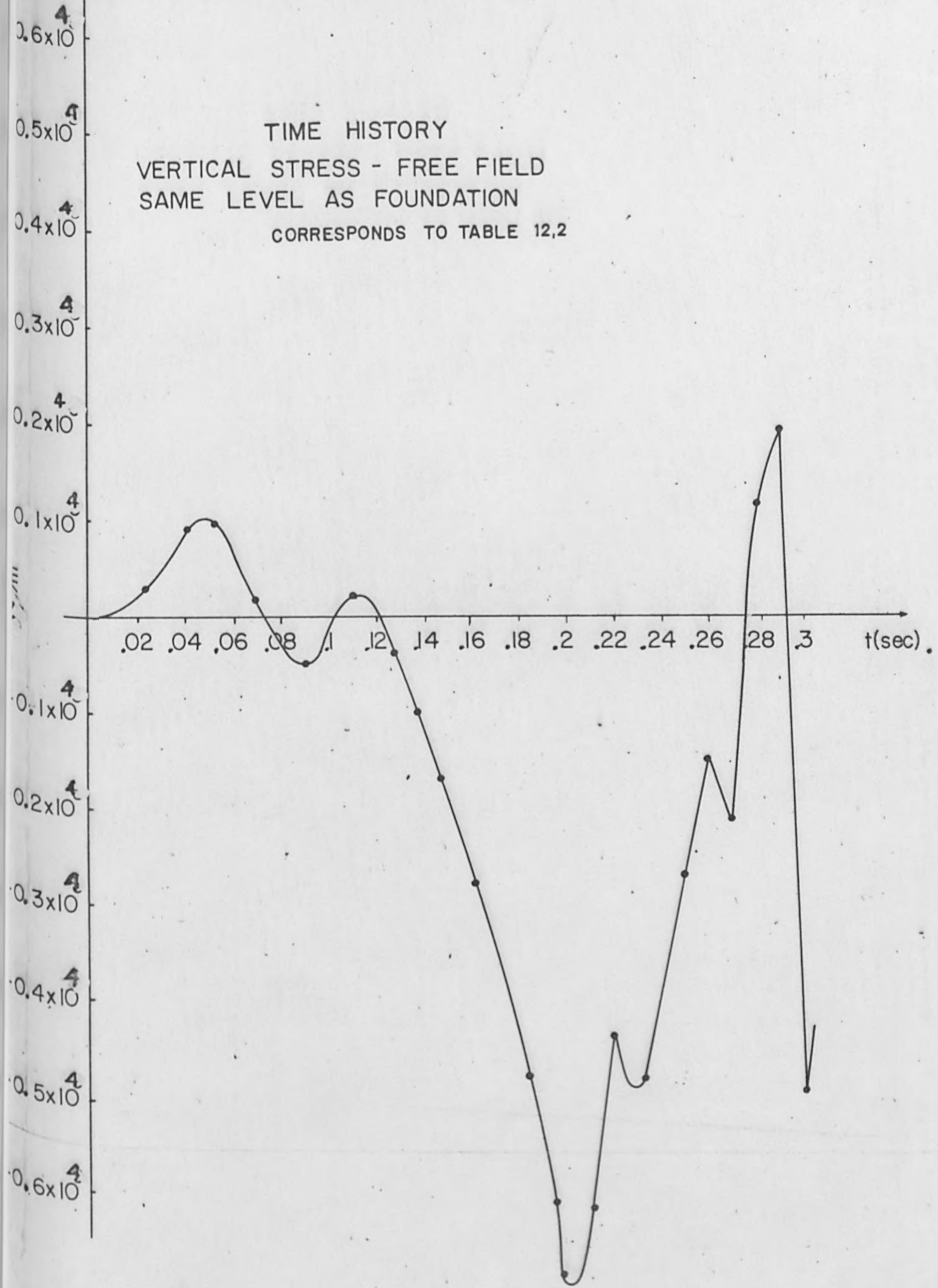


Fig. 12.6

TABLE 12.2

TIME HISTORY

VERTICAL STRESS - FREE FIELD - SAME LEVEL AS FOUNDATION

Element 34

Time sec	Vertical stress N/m ²
0.01	-0.1539 x 10 ⁴
0.02	0.374 x 10 ⁴
0.03	0.494 x 10 ⁴
0.04	0.958 x 10 ⁴
0.05	0.103 x 10 ⁵
0.06	0.717 x 10 ⁴
0.07	0.185 x 10 ⁴
0.08	-0.337 x 10 ⁴
0.09	-0.550 x 10 ⁴
0.10	-0.286 x 10 ⁴
0.11	-0.262 x 10 ⁴
0.12	0.103 x 10 ⁴
0.13	-0.232 x 10 ⁴
0.14	-0.823 x 10 ⁴
0.15	-0.166 x 10 ⁴
0.16	-0.273 x 10 ⁴
0.17	-0.330 x 10 ⁴
0.18	-0.479 x 10 ⁴
0.19	-0.540 x 10 ⁴
0.20	-0.707 x 10 ⁴
0.21	-0.673 x 10 ⁴
0.22	-0.429 x 10 ⁴
0.23	-0.494 x 10 ⁴
0.24	-0.376 x 10 ⁴
0.25	-0.267 x 10 ⁴
0.26	-0.156 x 10 ⁴
0.27	-0.215 x 10 ³
0.28	0.177 x 10 ⁴
0.29	0.294 x 10 ⁴
0.30	-0.500 x 10 ⁴

TIME HISTORY
VERTICAL VELOCITY - FREE FIELD
SAME LEVEL AS FOUNDATION
CORRESPONDS TO TABLE 12.3

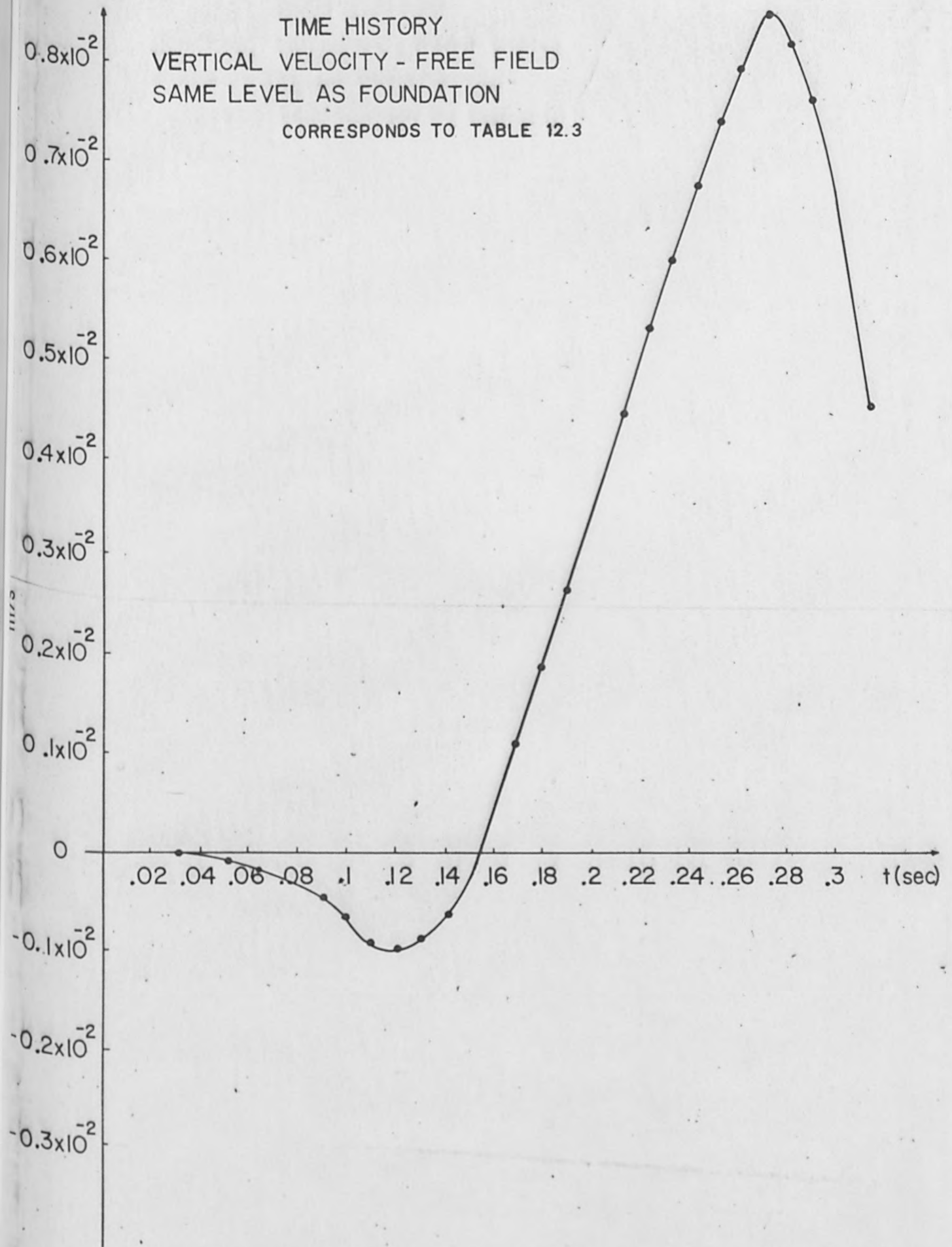


Fig. 12.7

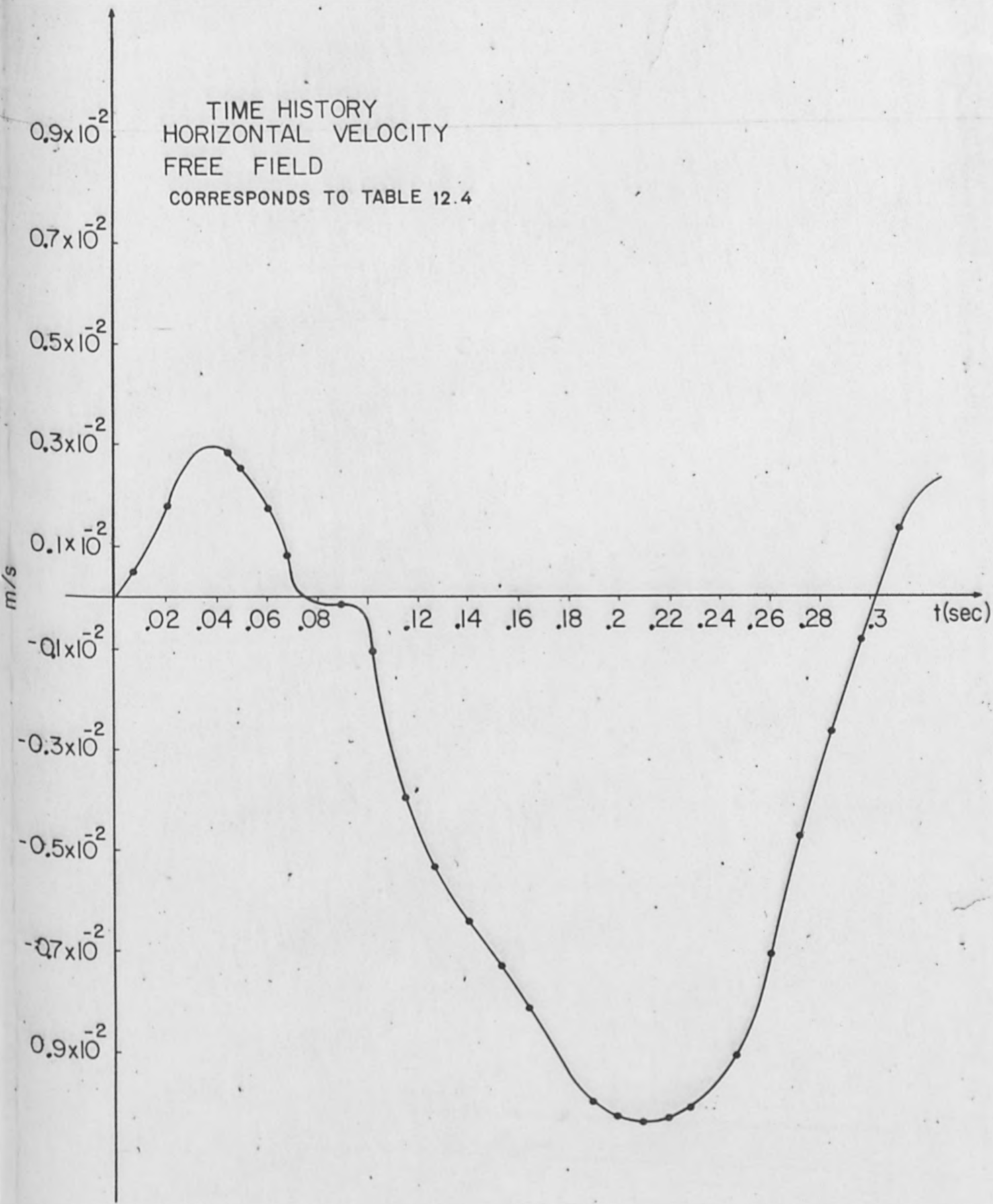
TABLE 12.3

TIME HISTORY

VERTICAL VELOCITY - FREE FIELD - SAME LEVEL AS
FOUNDATION (NP 40)

Time s	Vertical velocity m/s
0.01	0.201×10^{-5}
0.02	0.137×10^{-5}
0.03	-0.286×10^{-4}
0.04	-0.580×10^{-4}
0.05	-0.166×10^{-3}
0.06	-0.214×10^{-3}
0.07	-0.294×10^{-3}
0.08	-0.457×10^{-3}
0.09	-0.723×10^{-3}
0.10	-0.973×10^{-3}
0.11	-0.109×10^{-2}
0.12	-0.890×10^{-3}
0.13	-0.646×10^{-3}
0.14	-0.195×10^{-3}
0.15	0.261×10^{-3}
0.16	0.700×10^{-3}
0.17	0.119×10^{-2}
0.18	0.183×10^{-2}
0.19	0.264×10^{-2}
0.20	0.357×10^{-2}
0.21	0.448×10^{-2}
0.22	0.533×10^{-2}
0.23	0.609×10^{-2}
0.24	0.679×10^{-2}
0.25	0.740×10^{-2}
0.26	0.786×10^{-2}
0.27	0.800×10^{-2}
0.28	0.776×10^{-2}
0.29	0.712×10^{-2}
0.30	0.617×10^{-2}

TIME HISTORY
HORIZONTAL VELOCITY
FREE FIELD
CORRESPONDS TO TABLE 12.4



TIME HISTORY
SHEAR STRESS FREE FIELD
CORRESPONDS TO TABLE 12.4

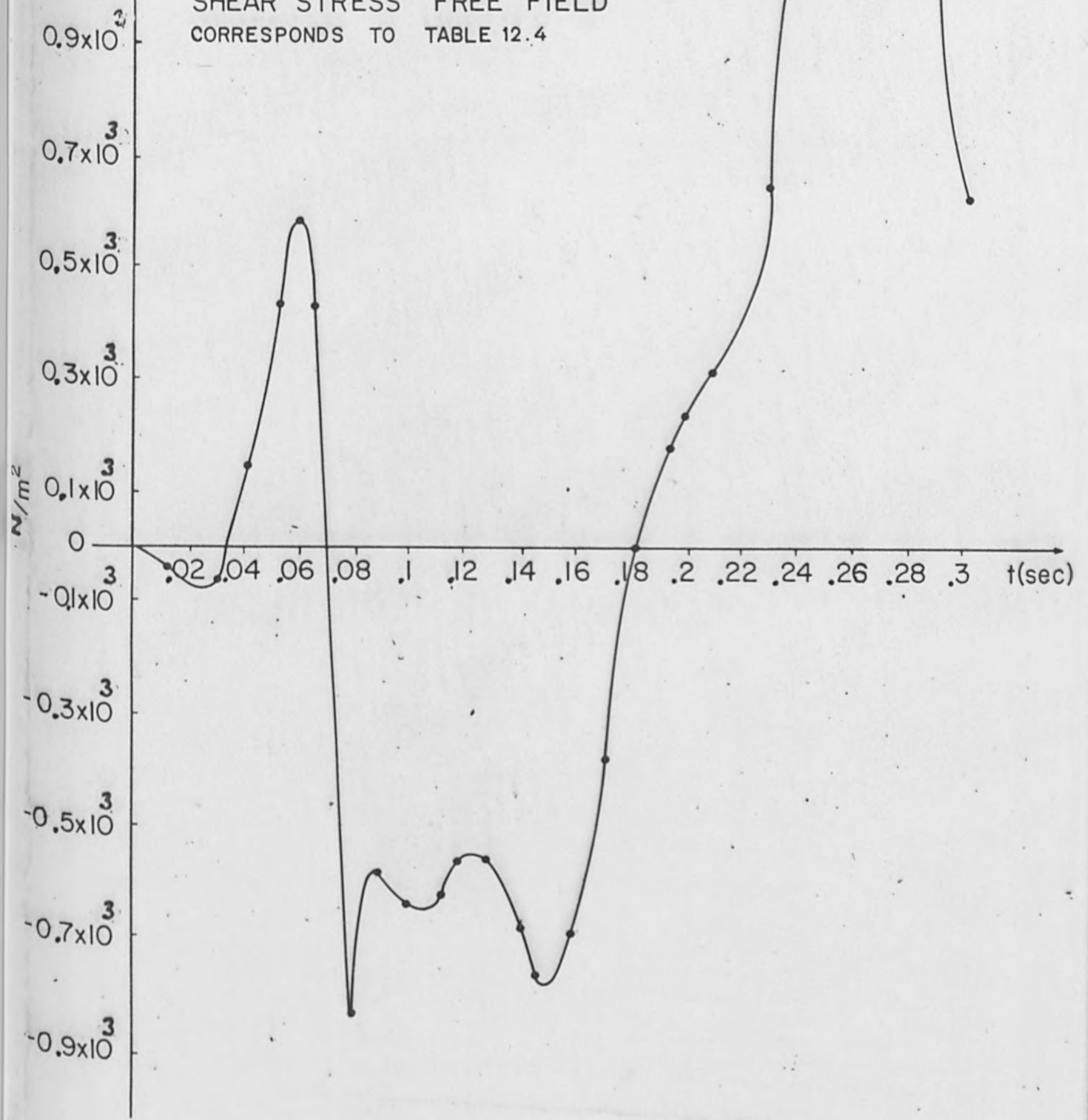


Fig. 12.9
126

TABLE 12.4

TIME HISTORY
SHEAR STRESS - HORIZONTAL VELOCITY FREE FIELD
(Same level as foundation, nodal point 70, element 52)

Time	y horizontal velocity	shear stress σ_{yz} N/m ²
0.01	0.546×10^{-3}	-0.147×10^2
0.02	0.179×10^{-2}	-0.750×10^2
0.03	0.278×10^{-2}	-0.580×10^2
0.04	0.296×10^{-2}	0.146×10^3
0.05	0.252×10^{-2}	0.438×10^3
0.06	0.176×10^{-2}	0.590×10^3
0.07	0.830×10^{-3}	0.426×10^3
0.08	-0.235×10^{-3}	-0.836×10^3
0.09	-0.145×10^{-2}	-0.531×10^3
0.10	-0.280×10^{-2}	-0.637×10^3
0.11	-0.419×10^{-2}	-0.637×10^3
0.12	-0.546×10^{-2}	-0.564×10^3
0.13	-0.650×10^{-2}	-0.568×10^3
0.14	-0.738×10^{-2}	-0.683×10^3
0.15	-0.831×10^{-2}	-0.781×10^3
0.16	-0.949×10^{-2}	-0.689×10^3
0.17	-0.108×10^{-1}	-0.376×10^3
0.18	-0.121×10^{-1}	-0.766×10^1
0.19	-0.129×10^{-1}	-0.230×10^3
0.20	-0.130×10^{-1}	0.303×10^3
0.21	-0.124×10^{-1}	0.308×10^3
0.22	-0.111×10^{-1}	0.394×10^3
0.23	-0.927×10^{-2}	0.655×10^3
0.24	-0.702×10^{-2}	0.100×10^4
0.25	-0.473×10^{-2}	0.127×10^4
0.26	-0.266×10^{-2}	0.136×10^4
0.27	-0.945×10^{-3}	0.132×10^4
0.28	0.422×10^{-3}	0.121×10^4
0.29	0.142×10^{-2}	0.102×10^4
0.30	0.194×10^{-2}	0.627×10^3

TIME HISTORY
HORIZONTAL VELOCITY UNDER BASEMAT

CORRESPONDS TO TABLE 12.5

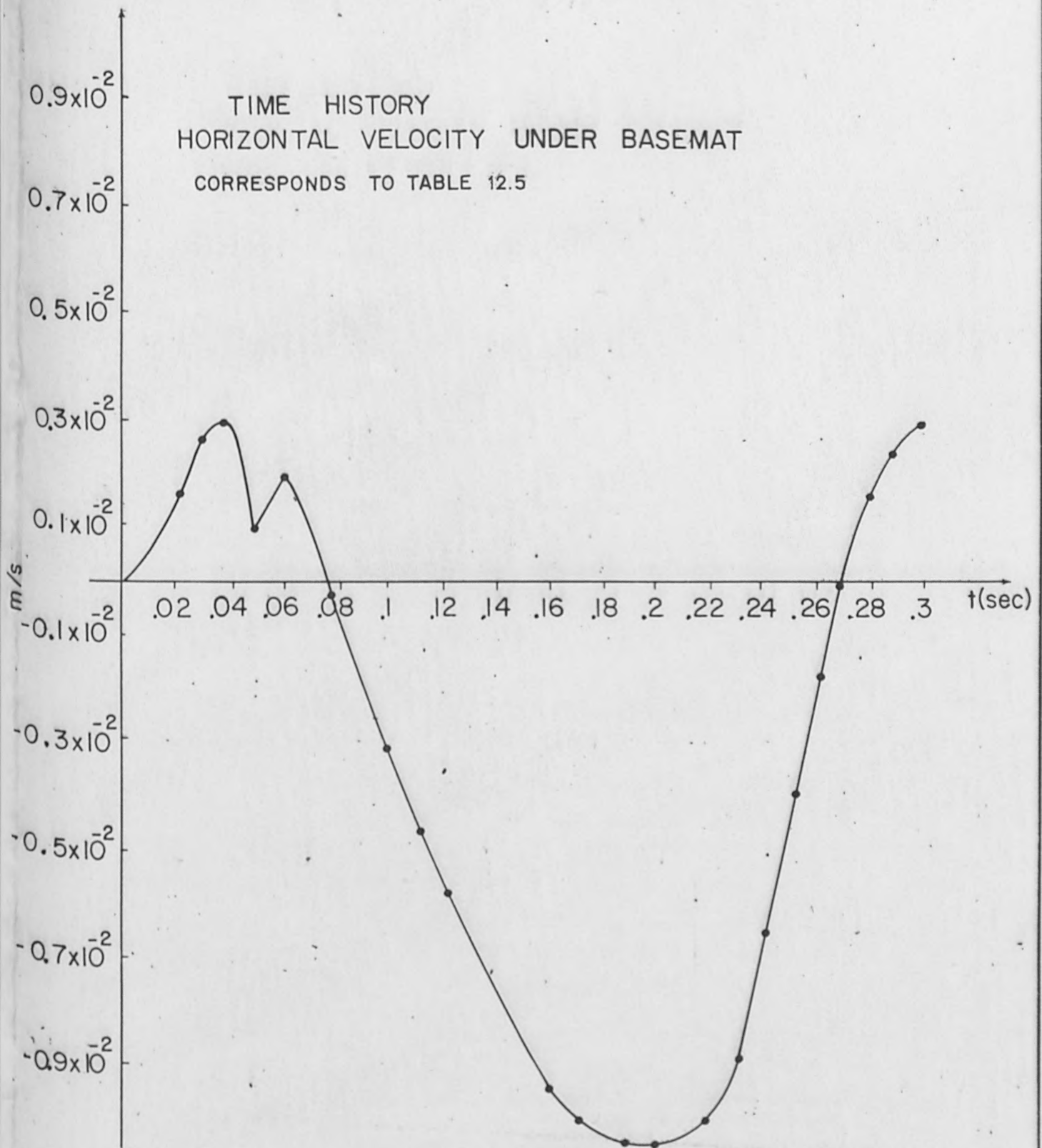


Fig. 12.10

TABLE 12.5

TIME HISTORY

ELEMENT 21 NODAL POINT 24 SAME LEVEL AS FOUNDATION

Time s	y velocity m/s horizontal	z' velocity m/s vertical	shear stress σ_{zy} N./m ²
0.01	0.519×10^{-3}	0.395×10^{-5}	-0.86500
0.02	0.175×10^{-2}	0.237×10^{-4}	0.5204×10^{-3}
0.03	0.2845×10^{-2}	0.426×10^{-4}	0.521×10^{-4}
0.04	0.3197×10^{-2}	0.1011×10^{-4}	0.167×10^{-4}
0.05	0.105×10^{-2}	-0.787×10^{-6}	0.307×10^{-4}
0.07	0.203×10^{-2}	-0.161×10^{-3}	0.389×10^{-4}
0.08	-0.450×10^{-2}	-0.295×10^{-3}	0.343×10^{-4}
0.09	-0.185×10^{-3}	-0.383×10^{-3}	0.250×10^{-4}
0.10	-0.325×10^{-2}	-0.484×10^{-3}	0.122×10^{-4}
0.11	-0.461×10^{-2}	-0.553×10^{-3}	-0.698×10^{-3}
0.12	-0.582×10^{-2}	-0.540×10^{-3}	-0.300×10^{-3}
0.13	-0.684×10^{-2}	-0.419×10^{-3}	-0.557×10^{-3}
0.14	-0.770×10^{-2}	-0.202×10^{-3}	-0.828×10^{-3}
0.15	-0.854×10^{-2}	0.839×10^{-4}	-0.109×10^{-5}
0.16	-0.955×10^{-2}	0.411×10^{-3}	-0.133×10^{-5}
0.17	-0.108×10^{-1}	0.693×10^{-3}	-0.153×10^{-5}
0.18	-0.1209×10^{-1}	0.101×10^{-2}	-0.172×10^{-5}
0.19	-0.1305×10^{-1}	0.133×10^{-2}	-0.190×10^{-5}
0.20	-0.133×10^{-1}	0.163×10^{-2}	-0.205×10^{-5}
0.21	-0.127×10^{-1}	0.200×10^{-2}	-0.205×10^{-5}
0.22	-0.113×10^{-1}	0.238×10^{-2}	-0.209×10^{-5}
0.23	-0.913×10^{-2}	0.289×10^{-2}	-0.1900×10^{-5}
0.24	-0.652×10^{-2}	0.324×10^{-2}	-0.154×10^{-5}
0.25	-0.392×10^{-2}	0.375×10^{-2}	-0.105×10^{-5}
0.26	-0.171×10^{-2}	0.410×10^{-2}	-0.305×10^{-3}
0.27	0.1086×10^{-3}	0.4169×10^{-2}	0.304×10^{-3}
0.28	0.149×10^{-2}	0.422×10^{-2}	0.6716×10^{-3}
0.29	0.232×10^{-2}	0.392×10^{-2}	0.1817×10^{-4}
0.30	0.278×10^{-2}	0.346×10^{-2}	0.254×10^{-4}

TIME HISTORY
 VELOCITY VERTICAL UNDER BASEMAT
 CORRESPONDS TO TABLE 12,5

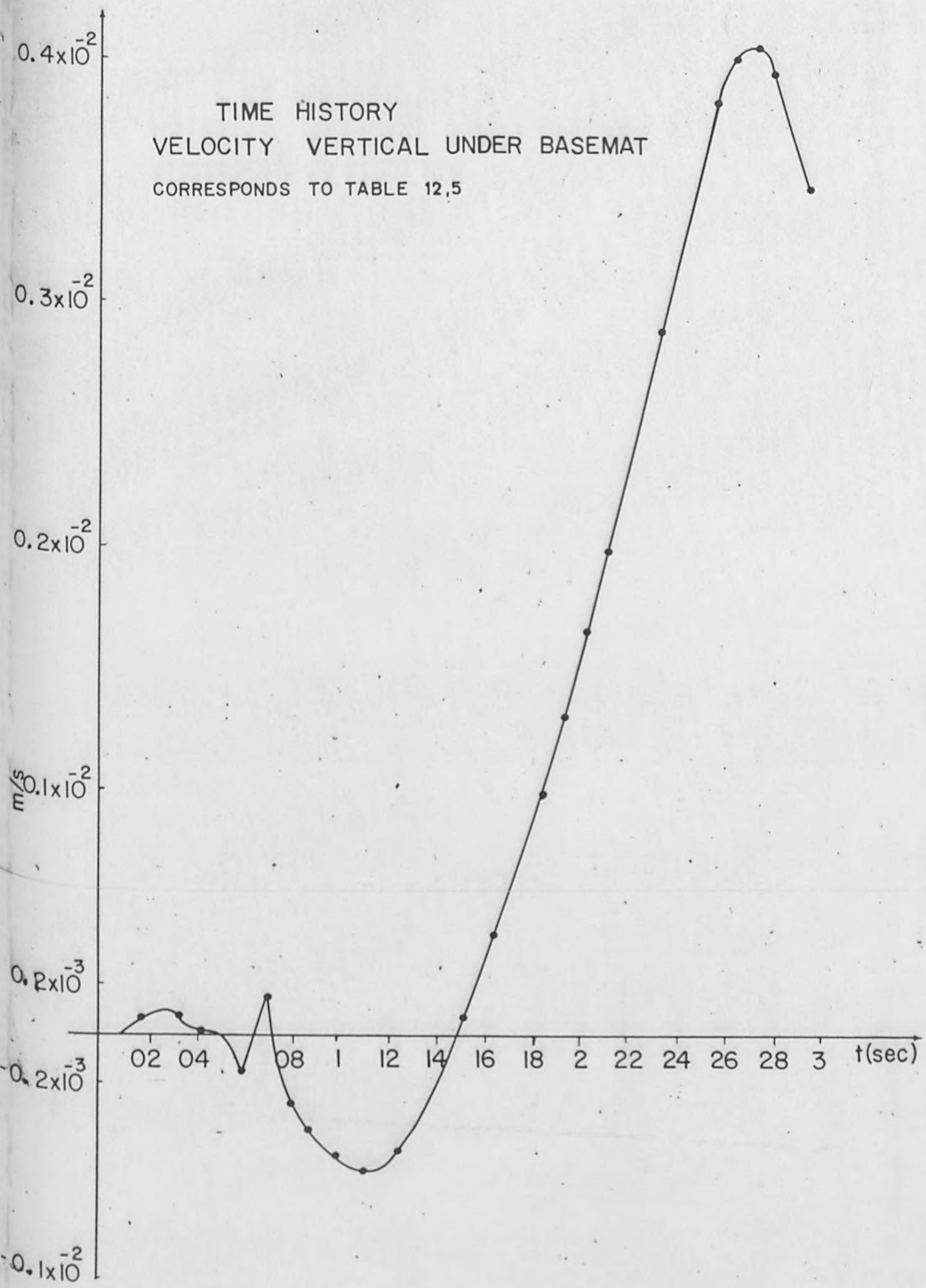


Fig. 12.11

TIME HISTORY
SHEAR STRESS UNDER BASEMAT
CORRESPONDS TO TABLE 12,5

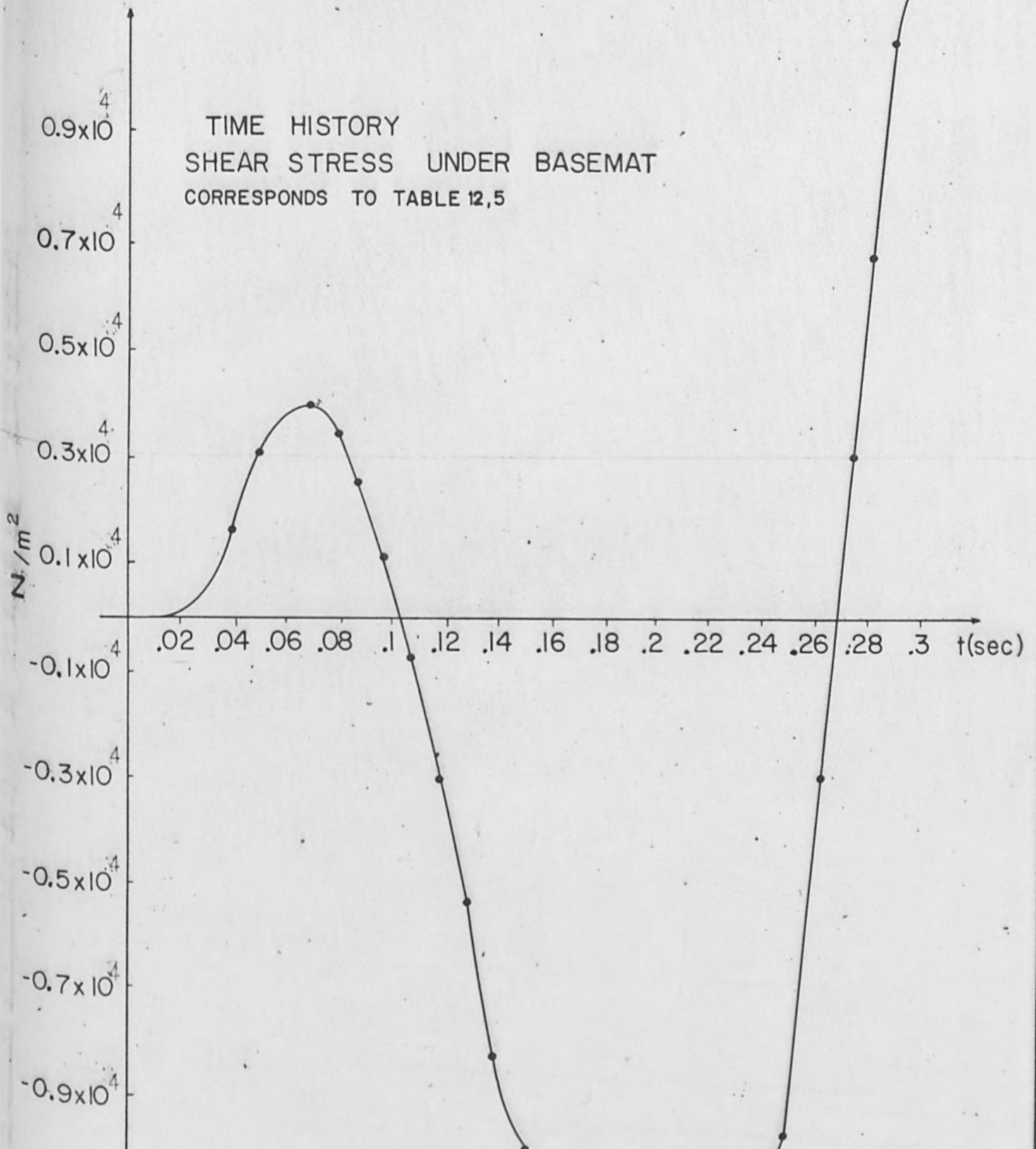


Fig. 12.12
130 A

TIME HISTORY (EXTENDED)

VERTICAL STRESS UNDER BASEMAT
RESPONSE VALUES ARE NOT TABULATED

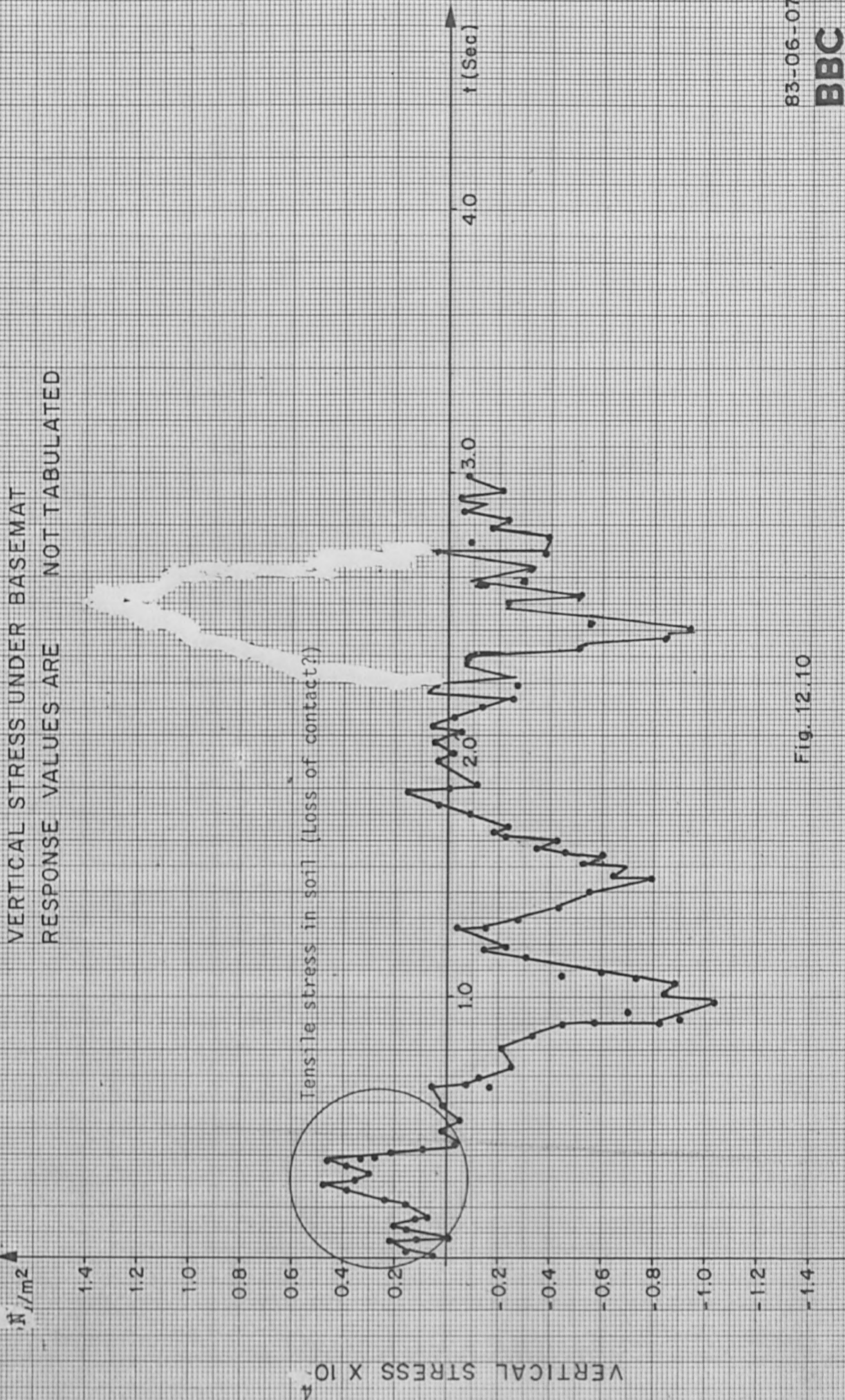


Fig. 12.10

83-06-07

BBC
BROWN BOVERI

TIME HISTORY (EXTENDED)

HORIZONTAL VELOCITY OF BASEMAT

PARTLY CORRESPONDS TO TABLE 12.5

RESPONSE VALUES BEYOND 0.3 Sec.

ARE NOT TABULATED

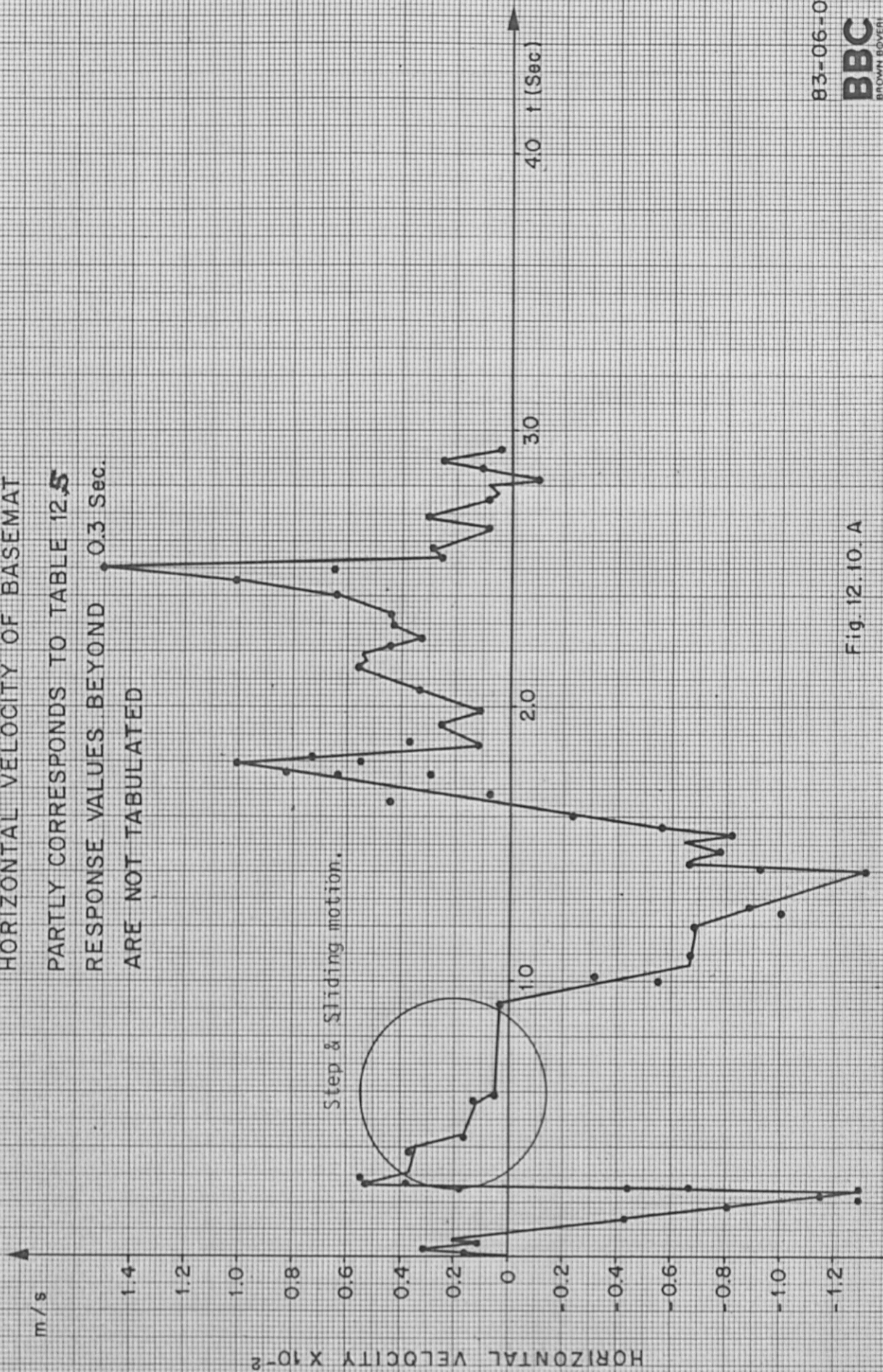


Fig 12.10.A

TIME HISTORY (EXTENDED)

VERTICAL VELOCITY OF BASEMAT

PARTLY CORRESPONDS TO TABLE 12.5
RESPONSE VALUES BEYOND 0.3 Sec.
ARE NOT TABULATED

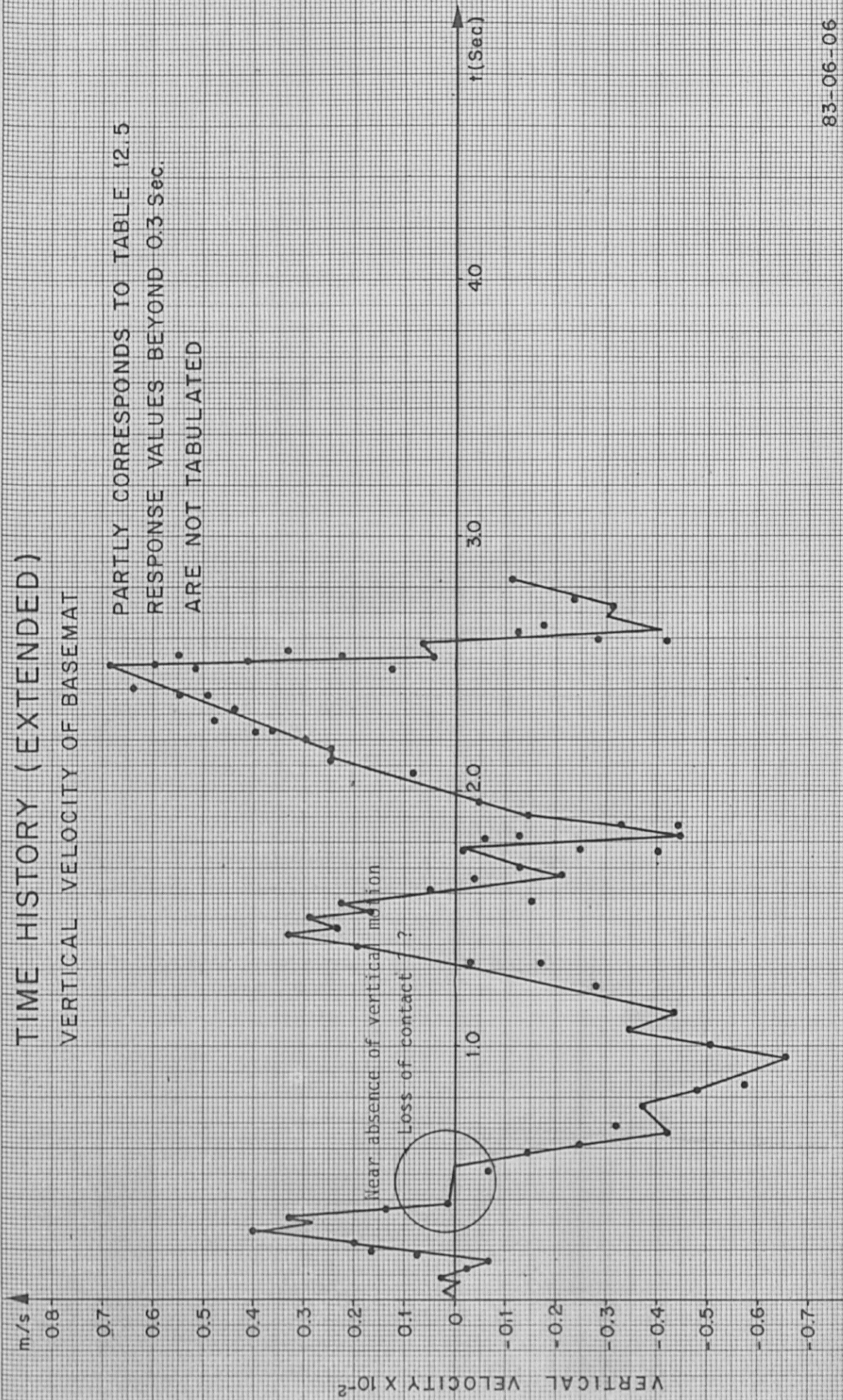
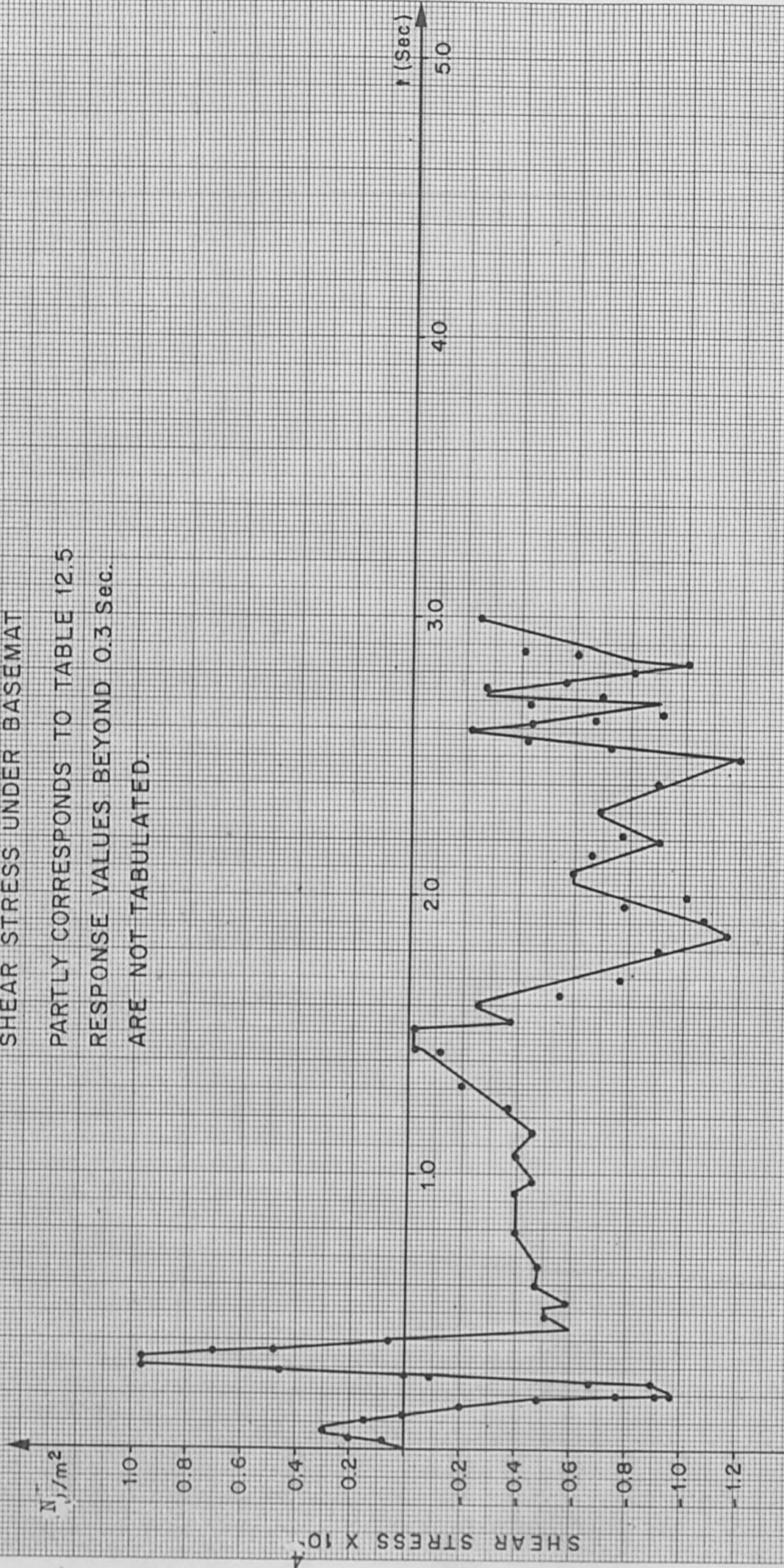


Fig. 12.11 A

TIME HISTORY (EXTENDED)

SHEAR STRESS UNDER BASEMAT

PARTLY CORRESPONDS TO TABLE 12.5
 RESPONSE VALUES BEYOND 0.3 Sec.
 ARE NOT TABULATED.



83-06-07

BBC
 BROWN BOYER

Fig. 12.12 A

Appendix A

Failure behaviour of soil.

A.1 Failure Behavior of the Soil and Yield Surface

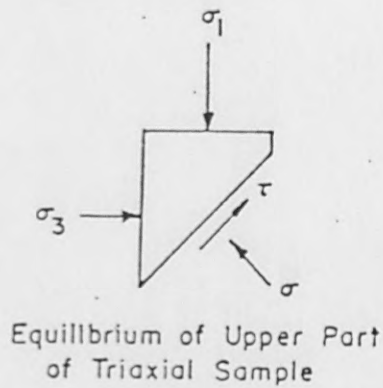
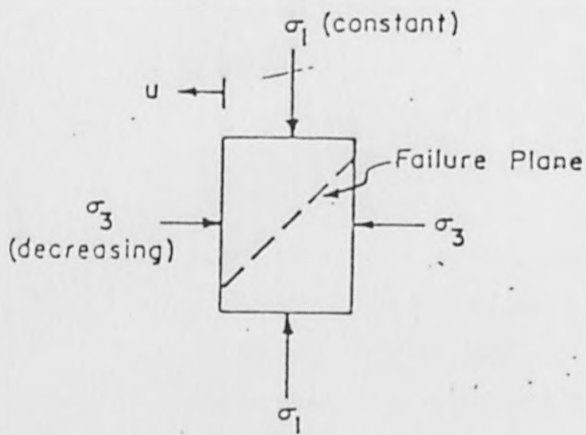
Since yielding has such a major influence on soil behavior under the basemat and since it is more difficult to understand than purely elastic behavior, some investigation of the failure mechanisms in the soil is desirable. A simplified example of the stress conditions that could lead to ground failure is illustrated in Figure A.1. The elastic stresses on typical crown and springline elements are shown.

The axial stress is σ_1 , while the lateral confining pressure is σ_3 . If σ_1 increases and σ_3 decreases, at some point σ_3 becomes so large that the failure strength of the material is exceeded.

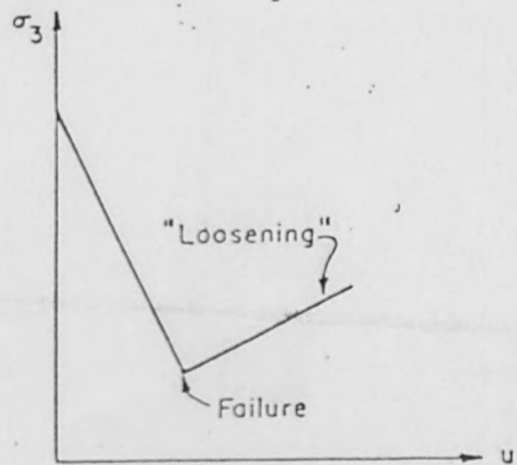
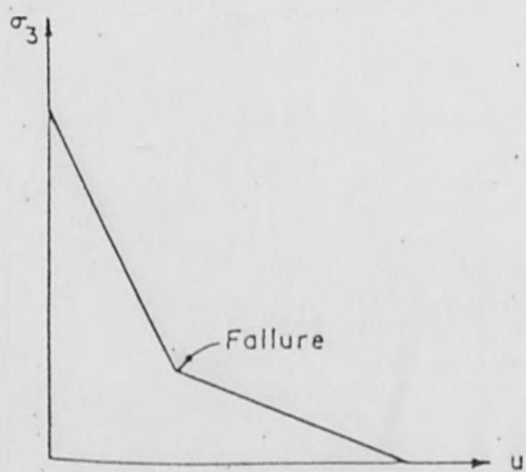
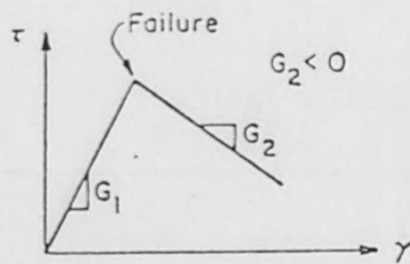
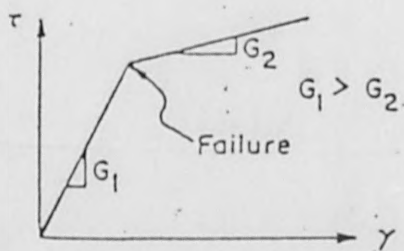
After failure occurs in the ground mass, it becomes difficult to qualitatively predict the changes in σ_1 and σ_3 . The overall stress distributions in the yielded ground mass are largely dependent upon its post-failure constitutive behavior.

If the material is strain hardening (Figure A.1b), it can continue to sustain an additional stress differential after failure. A further reduction in the lateral stress will be balanced by an increase in shear resistance along the failure plane. However, in this post-failure range large shear strains are required to mobilize this additional shear resistance. As a result, the lateral displacement, u , of the "triaxial sample" will be much greater for a given decrement of lateral stress after failure has occurred than before. The lateral stress can, however, eventually be reduced to zero without causing instability.

In strain softening material, on the other hand, the shear stresses in the material will reach a peak at failure and then decrease with additional shear strains (Figure A.1c). A reduction in the applied lateral stresses cannot now be counteracted by increased shear resistance along the failure plane even after very large strains have occurred; in fact, additional



a) CONCEPTUAL TRIAXIAL EXPERIMENT



b) STRAIN HARDENING

FIG A1

c) STRAIN SOFTENING

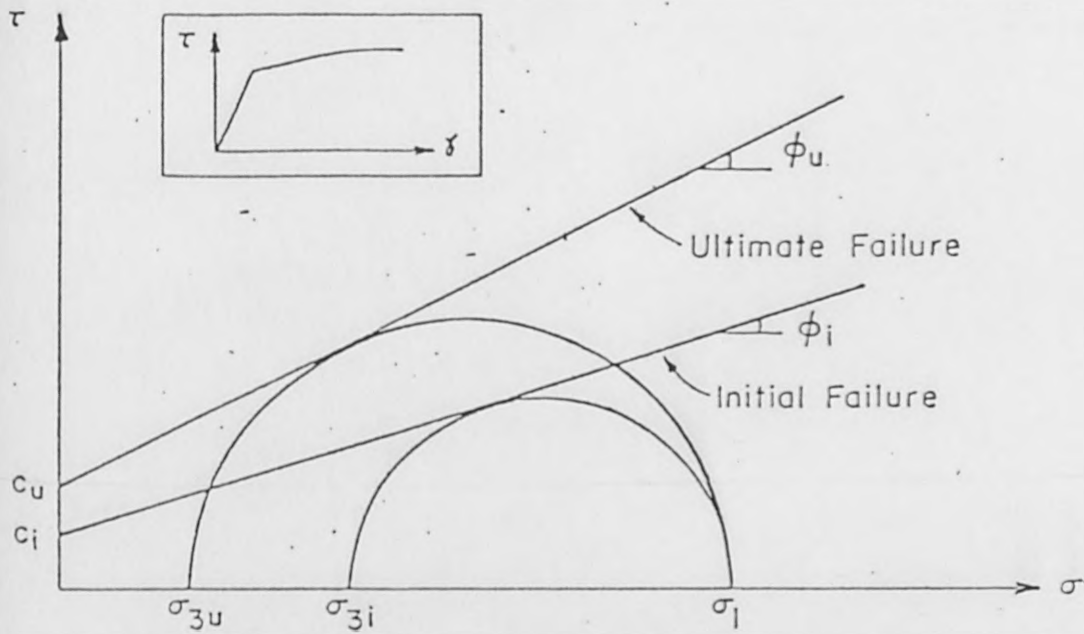
POST-FAILURE BEHAVIOR, OF SOIL (According to Swarz, Ref 33)

post-failure shear strains result in a decrease in the shear resistance along the failure plane. Therefore, the applied stress differential must be reduced by increasing the lateral stress (if the axial stress is held constant) in order to compensate for this reduction in shear strength. This increase in the lateral stress results in the upward sloping segment of the stress-displacement curve (Figure A.1c).

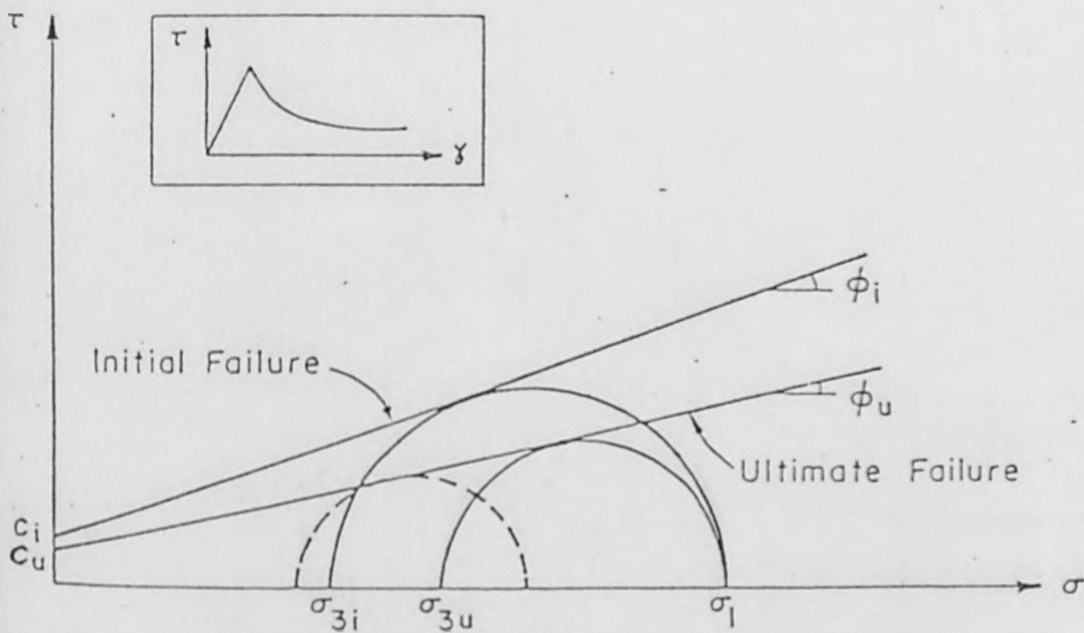
A.2 The difference between strain hardening and strain softening behavior can be viewed in another way if the ground material is assumed to follow a Mohr-Coulomb failure criterion, as illustrated in Figure A.2. The quantities ϕ_i and c_i are the initial friction angle and cohesion of the ground, while ϕ_u and c_u are the corresponding ultimate strength parameters. In a strain hardening material (Figure A.2a), these ultimate strength properties are larger than the initial values; therefore, the Mohr's circle at initial failure must expand to reach the ultimate condition. The principal stresses, σ_1 and σ_3 , can be adjusted in an infinite number of ways to satisfy this ultimate failure criterion. However, if it is again assumed that σ_1 (the axial stress in our conceptual triaxial experiment) remains constant, it is clear that σ_3 (the lateral stress) can be reduced in the ultimate condition.

The analogous case for a strain softening material is shown in Figure A.2b. Here, the ultimate strength parameters are less than the initial values; now the Mohr's circle for initial failure must shrink to the ultimate condition. If σ_1 is again assumed to remain unchanged, σ_3 must be increased in the ultimate state.

The conceptual reasoning outlined in this section can still aid in the qualitative assessment of different types of behavior, even if the stresses in the yielded soil mass are not precisely known.



a) STRAIN HARDENING



b) STRAIN SOFTENING

FIG. A2

POST-FAILURE BEHAVIOR, MOHR-COULOMB FAILURE CRITERION

A.3 An elastic-perfectly plastic constitutive model for the ground behavior was used in all of the analyses. Yielding is governed by the Drucker-Prager yield criterion for three-dimensional stress states:

$$F_{DP}(\sigma_1, \sigma_2, \sigma_3) = J_2^{1/2} - \alpha J_1 - k = 0 \quad (A.3.1)$$

in which J_1 = first invariant of the deviatoric stress tensor
 $= \sigma_1 + \sigma_2 + \sigma_3$ (A.3.2)

J_2 = second invariant of the deviatoric stress tensor

$$J_2 = 1/6 [(\sigma_1 - \sigma_2)^2 + (\sigma_1 - \sigma_3)^2 + (\sigma_2 - \sigma_3)^2]$$

α, k = yield parameters

$\sigma_1, \sigma_2, \sigma_3$ = principal stresses

The Drucker-Prager yield criterion can be thought of as the three-dimensional generalization of the two dimensional Mohr-Coulomb yield function. The yield parameters α and k can be related to the more familiar Mohr-Coulomb strength parameters c and ϕ in certain special cases. For example, for c and ϕ determined from conventional triaxial compression tests¹ ($\sigma_1 = \sigma_{axial}, \sigma_2 = \sigma_3 = \sigma_{axial}$), the values of α and k are given by Swarz (33)

¹ Triaxial extension tests ($\sigma_1 = \sigma_2 = \sigma_{confining}, \sigma_3 = \sigma_{axial}$) generally give values for c and ϕ different from those in the triaxial compression test; the relation between α and ϕ and between k and c for the extension test can be shown to equal:

$$\alpha = 2\sin\phi/\sqrt{3} (3+\sin\phi) \quad (A.3.4)$$

$$k = (6c)\cos\phi/\sqrt{3} (3+\sin\phi) \quad (A.3.5)$$

c, ϕ from triaxial extension tests.

The values for α and k should be the same for both types of tests if the tested material really does follow the Drucker-Prager yield law.

$$\alpha = 2\sin\phi/\sqrt{3} (3-\sin\phi) \quad (\text{A.3.6})$$

$$k = (6c)\cos\phi/\sqrt{3} (3-\sin\phi) \quad (\text{A.3.7})$$

The values of α and k calculated from these equations, using the values for ϕ and c given in Table A.1, are summarized in Table A.2. For purely cohesive or $\phi = 0$ strength properties, the Drucker-Prager yield criterion in Eq. A.3.1) is equivalent to the Von Mises yield function:

$$F_{VM}(\sigma_1, \sigma_2, \sigma_3) = J_2 - \sigma_0^2/3 = 0 \quad (\text{A.3.8})$$

in which σ_0 = yield stress in simple compression = $2c$. The associated flow rule is used to calculate the plastic strain increment in all cases.

Table A.1.			Table A.2	
Case	Mohr-Coulomb Yield Parameters		Drucker-Prager Yield Parameters	
	ϕ	c	α	k
1	35	0.1 psi	0.273	0.0168 psi
2A	0	16.7	0	2.77
2B	25	0.1	0.189	0.175
4A	16.1	8.68	0.118	1.53
4B	19.1	10.4	0.141	1.84
4C	16.1	40.9	0.118	7.20
4D	30	17.4	0.231	3.00
4E	40.9	26.0	0.322	4.19

Drucker-Prager Yield Parameters for the Finite Element Analysis

A.4 Yield Surface:

It is quite generally postulated as an experimental fact that yielding can occur only if the stresses σ satisfy the general yield criterion [15]

$$F(\sigma, \kappa) = 0 \quad (\text{A.4.1})$$

where κ is a 'hardening' parameter. This yield condition can be visualized as a surface in n-dimensional space of stress with the position of the surface dependent on the instantaneous value of the parameter κ (Figure A.4.1).

Flow Rule. (Normality Principle). Von Mises first suggested the basic constitutive relation defining the plastic strain increments in relation to the yield surface. At the present time, the following hypothesis appears to be generally accepted: If $d\epsilon_p$ denotes the increment of plastic strain, then

$$d\epsilon_p = \lambda \frac{\partial F}{\partial \sigma} \quad (\text{A.4.2})$$

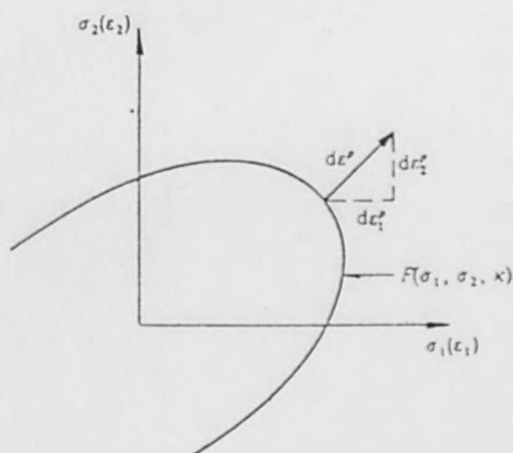


Figure A.4.1 Yield surface and normality criterion in two-dimensional stress space

or for any component n

$$d\epsilon_{n,p} = \lambda \frac{\partial F}{\partial \sigma}$$

In this, λ is a proportionality constant, as yet undetermined. The rule is known as the normality principle because relation (A.4.2) can be interpreted as requiring the normality of the plastic strain increment 'vector' to the yield surface in the space of n stress dimensions.

A reduction of the restriction of the above rule can be obtained by specifying a plastic potential

$$Q = Q(\sigma, \kappa) \quad (\text{A.4.3})$$

and

$$d\epsilon_p = \frac{\partial Q}{\partial \sigma} \quad (\text{A.4.4})$$

The particular case $Q = F$ is known as associated plasticity. When this relation is not satisfied the plasticity is non-associated. In what follows, the more general form will be considered.

Total stress-strain relations. During an infinitesimal increment of stress, changes of stress are assumed to be divisible into elastic and plastic parts. Thus

$$d\epsilon = d\epsilon_e + d\epsilon_p \quad (\text{A.4.5})$$

The elastic strain increments are related to stress increments by a symmetric matrix of constants C . Incorporating the plastic relation, we can write

$$d\epsilon = C^{-1} d\sigma + \frac{\partial Q}{\partial \sigma} \lambda \quad (\text{A.4.6})$$

When plastic yield is occurring, the stresses are on the yield surface given by Eq. (A.4.1). Differentiating this, we can write therefore

$$dF = \frac{\partial F}{\partial \sigma_1} d\sigma_1 + \frac{\partial F}{\partial \sigma_2} d\sigma_2 + \dots + \frac{\partial F}{\partial \kappa} d\kappa = 0 \quad (\text{A.4.7})$$

or

$$\left\{ \frac{\partial F}{\partial \sigma} \right\}^T d\sigma - A\lambda = 0$$

in which we make the substitution

$$A = - \frac{\partial F}{\partial \kappa} d\kappa \frac{1}{\lambda} \quad (\text{A.4.8})$$

Equations (A.4.6) and (A.4.7) can be written in a single symmetric matrix form as suggested by Zienkiewicz [15]:

$$\begin{bmatrix} d\epsilon \\ 0 \end{bmatrix} = \begin{bmatrix} C^{-1} & \frac{\partial Q}{\partial \sigma} \\ \left(\frac{\partial F}{\partial \sigma}\right)^T & -A \end{bmatrix} \begin{bmatrix} d\sigma \\ \lambda \end{bmatrix} \quad (\text{A.4.9})$$

The indeterminate constant λ can be eliminated (taking care not to multiply or divide by A which may be zero in general). This results in an explicit expansion which determines the stress changes in terms of imposed strain changes with [15]

$$d\sigma = C_{ep}^* d\epsilon \quad (\text{A.4.10})$$

$$C_{ep}^* = C - C \left\{ \frac{\partial Q}{\partial \sigma} \right\} \left\{ \frac{\partial F}{\partial \sigma} \right\}^T C [A + \left\{ \frac{\partial F}{\partial \sigma} \right\}^T C \left\{ \frac{\partial Q}{\partial \sigma} \right\}]^{-1} \quad (\text{A.4.11})$$

The elasto-plastic matrix C_{ep}^* takes the place of the elasticity matrix C_T in incremental analysis.

This matrix is symmetric only when the plasticity is associated. The non-associated material will present special difficulties if tangent modulus procedures other than the modified Newton-Raphson method are used.

The matrix is defined for ideal plasticity when $A = 0$.

Significance of the parameter 'A'. For ideal plasticity with no hardening, A is simply zero. If hardening is considered, attention must be given to the nature of the parameter (or parameters) κ on which the shifts of the yield surface depend.

With a 'work hardening' material κ is taken to be represented by the amount of plastic work done during plastic deformation. Thus,

$$d\kappa = \sigma_1 d\varepsilon_1^p + \sigma_2 d\varepsilon_2^p + \dots = \sigma^T d\varepsilon_p \quad (\text{A.4.12})$$

Substituting the flow rule equation, we have simply

$$d\kappa = \lambda \sigma^T \frac{\partial Q}{\partial \sigma} \quad (\text{A.4.13})$$

By Eq. (A.4.8) we now see that λ disappears and we can write

$$A = - \frac{\partial F}{\partial \kappa} \sigma^T \frac{\partial Q}{\partial \sigma} \quad (\text{A.4.14})$$

a strictly determinate form if explicit relationship between F and κ is known.

A.5 Non-linear constitutive problems in solid mechanics ;

Returning to the basic problem of solid mechanics formulations in terms of displacement, we note that the equilibrium equations state that (Table 4.1B)

$$f + \left(\int_V B_L^T C B_L^0 dv \right) u = 0 \quad (\text{A.5.1})$$

This derivation, based on the virtual work (and not energy) principles, is valid for any material behaviour. If now, for instance, we assume a non-linear elastic behaviour

$$\sigma = \sigma(\varepsilon) \quad (\text{A.5.2})$$

then, relation (A.5.1) defines completely the form given as

$$P(a) + f = 0 \quad (\text{A.5.3})$$

and any of the techniques of solution discussed in section 7 can be used. As relationship (A.5.2) is unique, i.e. for any

given strain a unique stress is given, $P(a)$ is also uniquely defined.

We note that the tangential matrix t_K is given by

$$\begin{aligned} {}^t_K &= \frac{dP}{du} = \int_v B_L^T \frac{d{}^t\sigma}{d{}^t\varepsilon} \frac{d{}^t\varepsilon}{d{}^tu} {}^0 dv \\ &= \int_v B_L^T {}^t_C B_L {}^0 dv \end{aligned}$$

where

$${}^t_C = d\sigma/d\varepsilon \quad (A.5.4)$$

is known as the tangential elasticity matrix.

Appendix B

Proposed experimental study.

B.1 INTRODUCTION

A proposal for the experimental study is made to understand the fundamental nature of dynamic structure-soil interaction problem. This can be realised by performing an experiment with the aid of a model of single degree of freedom structure attached to a shaker table either directly or through a layer of rubber material and assumed to represent the ground layer. Unlike most experiments of this type, the shaker table is excited in such a way, that the specified free field motion would be reproduced on the rubber surface regardless of the thickness of the layer, if the structure were absent.

This will essentially permit us to assess the effect of the structure soil interaction when a structure is placed on ground layers with identical free field surface motion but of different thickness. An experiment of this nature has been carried out in Japan under the grant of N. Science foundation but details of experimental studies are not adequately available.

B.2 ESSENTIAL FEATURES OF EXPERIMENT

The essential feature of the proposed experiment is to excite the shaker table in such a way in the absence of the structure, the horizontal motion of the surface of the rubberlayer at the point where the footing is to be clamped or glued would be identical to the specified signal regardless of the thickness of the rubber layer, including when thickness $d = 0$. This can be accomplished with the aid of analogue tape recorder, recording the motion of the table corresponding to the specified surface motion before the structure is glued. This record then can be played back to excite the table through a servo-control system after the structure is glued to the rubber, and among other quantities, the acceleration of the M_s could be measured and recorded. Different values of natural frequencies f_s of the structure can be achieved by changing the height L of mass M_s . A mechanical viscous damping can be added to the structure to provide a reasonable amount of damping (approximately 2%).

B.3 ANALYTICAL MODEL

The analytical model employed in this study is a widely accepted model for the layer in terms of equivalent translational mass and rotational moment of inertia, with corresponding linear viscous damping as shown in fig (B.3.1). Referring to fig (3.2) and (3.3) for rotations, the equation of motion can be written as follows.

$$M_r \ddot{U}_1 + M_s \ddot{U}_1 + C_{rt} \dot{U}_1 + K_{rt} U_1 + M_s \ddot{U}_2 = f_1 \quad (\text{B } 3.1)$$

$$M_s \ddot{U}_1 + M_s \ddot{U}_2 + C_s \dot{U}_2 + \frac{12EI}{L^3} U_2 - \frac{6EJ}{L^2} \theta_1 - \frac{6EJ}{L^2} \theta_2 = 0 \quad (\text{B } 3.2)$$

$$J_r \ddot{\theta}_1 + C_{ro} \dot{\theta}_1 + K_{ro} \theta_1 + \frac{4EJ}{L} \theta_1 + \frac{2EJ}{L} \theta_2 = 0 \quad (\text{B } 3.3)$$

$$\frac{2EJ}{L} \theta_1 + J_s \ddot{\theta}_2 + \frac{4EJ}{L} \theta_2 = 0 \quad (\text{B } 3.4)$$

Whereby it is noted that M_r and J_r represent the combined effect of mass and moment of inertia of the footing and the "ground layer" (rubber layer) respectively.

The above equations of motion can be written in the equilibrium form i.e. stiffness x displacement = force.

Contrary to the usual matrix form the modified equations of motions in the force displacement form will be enable us to compute the parameters such as J_r , M_r and C_{rt} from the measured values of the K_{rt} and K_{ro} the transtational and rotational stiffness of the rubber layer respectively.

Let us now regroup the equations of motions and write in the force-displacement form.

$$\alpha_{11} = M_r \frac{d^2}{dt^2} () + M_s \frac{d^2}{dt^2} () + C_{rt} \frac{d}{dt} () + K_{rt} ()$$

$$\alpha_{22} = m_s \frac{d^2}{dt^2} () + C_s \frac{d}{dt} () + \frac{12EJ}{L^3} ()$$

$$\alpha_{33} = J_r \frac{d^2}{dt^2} () + C_{ro} \frac{d}{dt} () + K_{ro} () + \frac{4EJ}{L} ()$$

$$\alpha_{44} = J_s \frac{d^2}{dt^2} (\) + \frac{4EJ}{L} (\)$$

$$\alpha_{12} = M_s \frac{d^2}{dt^2} (\) = \alpha_{21}$$

$$\alpha_{23} = -\frac{6EJ}{L^2} (\)$$

$$\alpha_{24} = -\frac{6EJ}{L^2} (\)$$

$$\alpha_{34} = \frac{2EJ}{L} (\)$$

Therefore writing in the matrix form

$$\begin{bmatrix} \alpha_{11} & \alpha_{12} & 0 & 0 \\ \alpha_{21} & \alpha_{22} & \alpha_{23} & \alpha_{24} \\ 0 & 0 & \alpha_{33} & \alpha_{34} \\ 0 & 0 & 0 & \alpha_{44} \end{bmatrix} \begin{bmatrix} U_1 \\ U_2 \\ \theta_1 \\ \theta_2 \end{bmatrix} = \begin{bmatrix} f_1 \\ 0 \\ 0 \\ 0 \end{bmatrix} \quad (\text{B 3.5})$$

Where $f_1 = (K_{rt} + C_{rt} \frac{d}{dt}) U_0$

The equation (B.3.5) is the familiar matrix form of static equilibrium equation. As mentioned before J_r and M_r can be computed from K_{rt} and K_{ro} . However a value can be chosen for C_{rt} the translational damping of the rubber layer. It is proposed that a value of C_{rt} may be so chosen, so that the theoretical and experimental frequency response agree closely.

B.4 THEORETICAL ANALYSIS OF THE FREQUENCY RESPONSE

The equations (1-4) can be rewritten in the familiar matrix form of equations of motions as follows

$$[M] \{\ddot{U}\} + [C] \{\dot{U}\} + [K] \{U\} = \{Q\} \quad (\text{B 4.1})$$

Where Q is externally applied time varying force such that $Q \rightarrow Q(t)$.
 Now $[C]$ is considered as structural damping matrix. Equation B 4.1 can also be written.

$$[M] \{U\} + [K] \{U\} + ig [K] \{U\} = Q(t)$$

By using Laplace transform technique, and defining the impedance function $[Z(s)]$

$$[Z(s)] = s^2 [M] + (1 + ig) [K] \quad (B 4.2)$$

we obtain the transform of response [27]

$$\begin{aligned} \{U(s)\} &= [Z(s)]^{-1} \{Q(s)\} \\ &= \frac{1}{|Z(s)|} [C(s)] \{Q(s)\} \end{aligned} \quad (B 4.3)$$

Where $|Z(s)|$ is the determinant of the impedance matrix and $[C(s)]$ is the adjoint of $[Z(s)]$. The elements of the impedance matrix are complex number and elements of $\{C(i\Omega_j)\}$ are also complex ($S = i\Omega$). The steady state response can be written as follows:

$$\{U(t)\} = \sum_{j=1}^n \frac{Q_{0j}}{|Z(i\Omega_j)|} \{C(i\Omega_j)\} e^{i(\Omega_j t - \psi_j)} \quad (B 4.4)$$

In the presence of damping, the vibration components of the natural frequencies will disappear, on the other hand those components having frequencies of the impressed force will persist.

The complex frequency response $H(\Omega)$ of the system can be obtained by taking Fourier transform of the steady state response

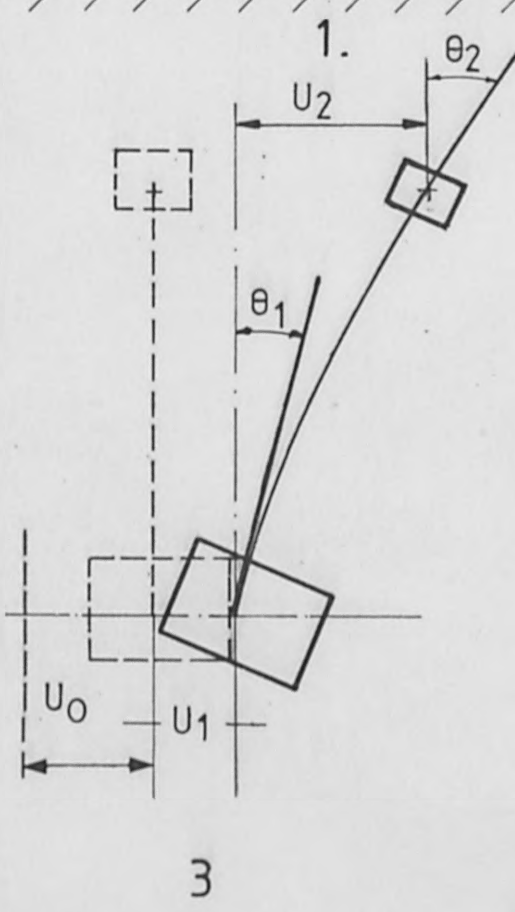
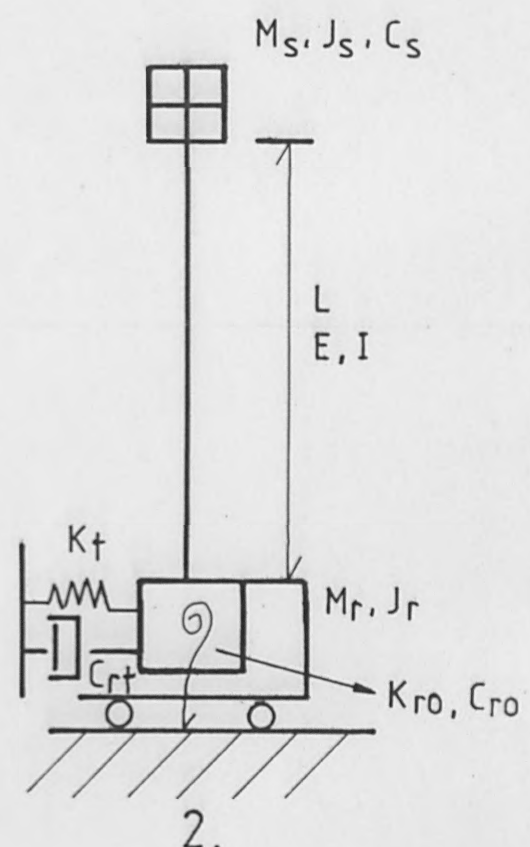
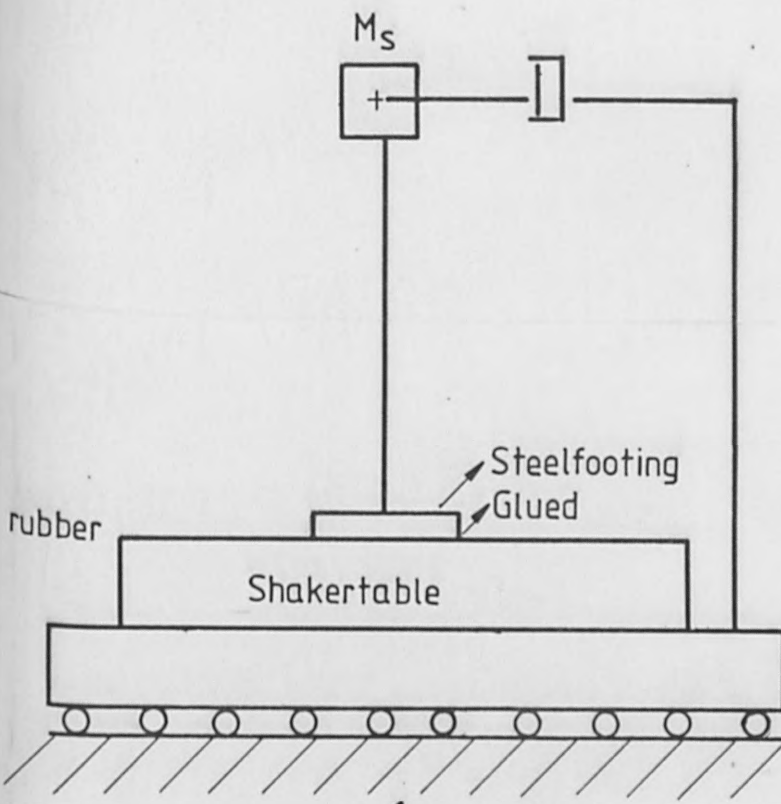
$$U(t) = H(\Omega) e^{i\Omega t} \quad (B 4.5)$$

$$\text{or } H(\Omega) = \frac{U(t)}{e^{i\Omega t}}$$

./.

The relationship between the structural response (translational acceleration (M_s)) and the table excitation in the frequency domain is indicated in the block diagram (Fig. B.4).

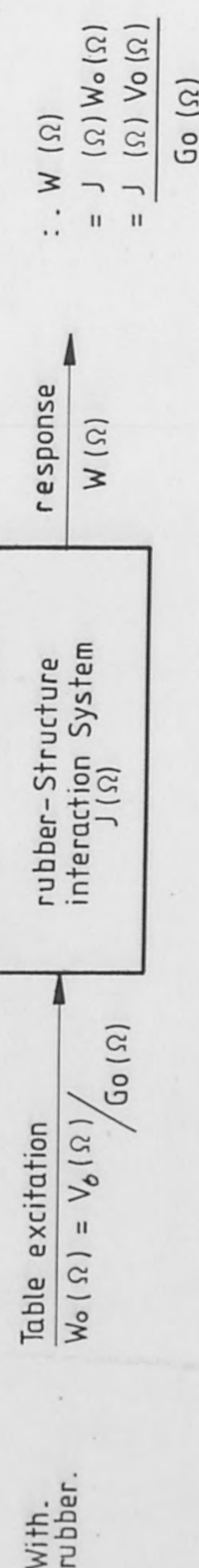
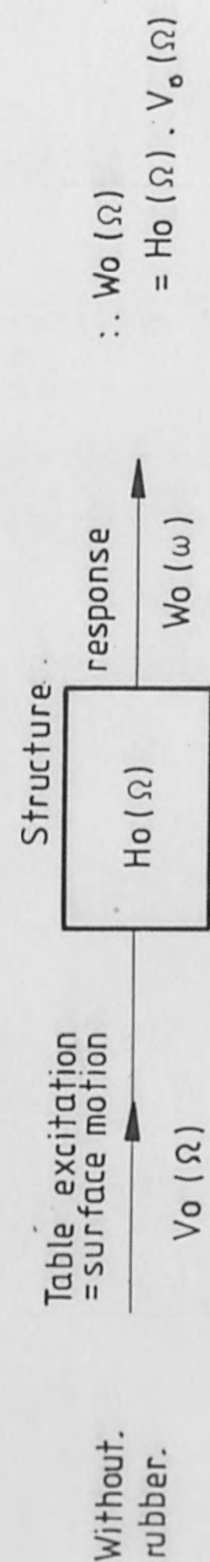
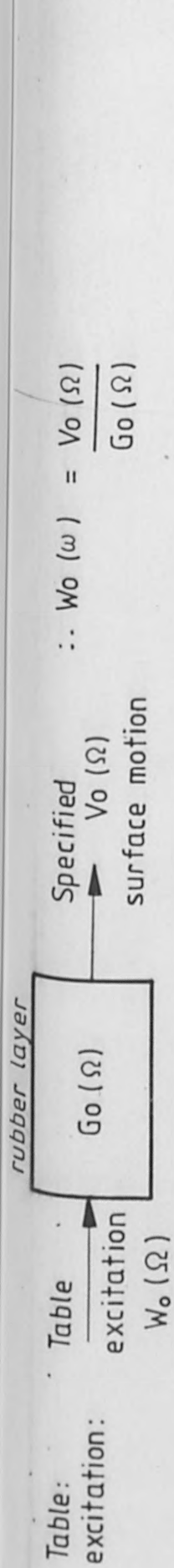
Where $U_0(\Omega)$, $V_0(\Omega)$, $W_0(\Omega)$ and $W(\Omega)$ are Fourier transform of signals as indicated, and $G_0(\Omega)$, $H_0(\Omega)$ and $I(\Omega)$ are frequency response functions of assumedly linear system. The interaction ratio $I(\Omega)$ as defined in Fig. (B.4) is the ratio between the response amplitudes with and without interaction.



M = mass
 J = Moment of Inertia
 K = Spring constant
 C = Damping

 Subscripts
 S = Structure
 r = rubber
 o = rotation
 t = translation

Fig. B. 3



Interaction ratio

$$= \frac{I(\Omega)}{J(\Omega)} = \frac{W(\Omega) / W_o(\Omega)}{J(\Omega)}$$

$$= \frac{H_o(\Omega) G_o(\Omega)}{J(\Omega)}$$

Fig. B.4.

Appendix_C

Comparison between the Elastic Half Space and F E
method of the dynamic response of footings to vertical
loading.

Introduction

The objective of this section is to describe the dynamic behaviour of footings, by means of well established method of dynamic analysis due to Bycroft [42], Lysmer [44], and Richart [43]. This investigation is limited to the case of circular footing resting on a plane soil surface and excited by a vertical time dependent force in the axis of symmetry.

To arrive at a model that can be analysed mathematically it is assumed that the subsoil can be considered as a perfectly elastic, isotropic and homogeneous half space and that only normal stresses are transferred at the interface between footing and soil. Half-space models have been used by several investigators, notably E. Reissner(56). Who developed a method for finding the steady-state surface displacements of an elastic half space for any given surface pressure distribution with axial symmetry.

The elastic half-space model differs from most classical dynamic systems, because its dimensions are infinite. This Geometrical peculiarity causes an apparent loss of energy by wave propagation in to half space. It can be shown, that the effect of energy loss is comparable to that of the dashpot of a simple damped oscillator [44]. This observation has led to the adoption of a simplified spring-dashpot-analog for practical calculation. Finally a simple example is chosen, and the analytical results are then compared with the Finite element solution of the same problem.

C.1 Steady state motion

Before we focus our attention to the elastic half-space model, we may study a larger class of dynamic system. It consists of a linear system S , excited by a periodic vertical force $P(t)$. The system may or may not exhibit viscous damping and it may be finite or infinite dimension.

The force $P = P_0 e^{i\omega t}$ is assumed to act at a point o , such that the displacement of the point o is vertical at all times.

In the case of steady state motion it is known that all forces and displacements are harmonic with circular frequency ω and proportional to the amplitude p_0 of the exciting force. The displacement can be written in the form

$$\delta = \frac{P_0}{k} F e^{i\omega t}. \quad (C.1.1)$$

The quantity k is referred to as "spring constant" and is usually equal to the static spring constant of the system S.

The time-independent complex function $F = F_1 + i F_2$ is generally a function of the frequency ω and the properties of the systems F is also referred as displacement function by some authors. If k is a static spring constant then $F = F_1 = 1$, for $\omega = 0$.

We now consider a mass less system as shown in Fig (C.1), and write down the equation of motion for system S in fig. (C.1)

$$C \dot{\delta} + K \delta = P_0 e^{i\omega t} \quad (C.1.2)$$

C and K are real. Substituting eqn (C.1.1) into (C.1.2),

$$i \omega C F + K F = k \quad (C.1.3)$$

By means of separation of Variable we obtain the following pair of equation.

$$- \omega F_2 C + F_1 K = k \quad (C.1.4)$$

$$\omega F_1 C + F_2 K = 0$$

which have the solution

$$K = \frac{F_1}{F_1^2 + F_2^2} k \quad (C.1.5)$$

$$C = \frac{-F_2/\omega}{F_1^2 + F_2^2} k$$

With respect to F_1 and F_2

$$F_1 = \frac{k K}{K^2 + \omega^2 C^2} \quad (C.1.6)$$

$$F_2 = \frac{-\omega k C}{K^2 + \omega^2 C^2}$$

Next, we consider a dynamic system $s+m$ as shown in fig (C.1.) This system is formed by supplementing the system S by a rigid mass m at point o. Let the system be excited by a harmonic force

$$Q = Q_0 e^{i\omega t} \quad (C.1.7)$$

acting on the mass m . We define the displacement function of this system by \bar{F} , where

$$\bar{F} = \bar{F}_1 + i\bar{F}_2$$

the displacement of the mass m is δ and is equal to

$$\delta = \frac{Q_0}{k} \bar{F} e^{i\omega t} \quad (C.1.8)$$

By introducing the reaction P acting on m at point 0, the equation of motion for the mass m is as follows

$$m \ddot{\delta} = (Q_0 - P_0) e^{i\omega t} \quad (C.1.9)$$

Differentiating eqn (C.1.1) and (C.1.8)

$$\text{gives } m \ddot{\delta} = -\frac{m \omega^2}{k} F. P_0 e^{i\omega t} \quad (C.1.10)$$

$$\text{and } m \ddot{\delta} = -\frac{m \omega^2}{k} \bar{F} Q_0 e^{i\omega t} \quad (C.1.11)$$

using eqn (C.1.9) yields

$$P_0 = \frac{Q_0}{1 - \frac{m\omega^2}{k} F} \quad (C.1.12)$$

and

$$\bar{F} = \frac{F}{1 - \frac{m\omega^2}{k} F} \quad (C.1.13)$$

Substituting (C.1.13) in (C.1.8) we obtain the displacement of point o in s+m system.

$$\delta = \frac{Q_0}{k} \frac{F e^{i\omega t}}{1 - \frac{m\omega^2}{k} F} \quad (C.1.14)$$

The response magnification factor: $M = |\bar{F}| =$

$$= \sqrt{\frac{F_1^2 + F_2^2}{\left[1 - \frac{m\omega^2}{k} F_1\right]^2 + \left[\frac{m\omega^2}{k} F_2\right]^2}} \quad (C.1.15)$$

C.2 Elastic Half-space with uniform periodic loading

In the previous section we treated a very general concept of a linear system, and obtained an expression for displacement of s+m system in terms of displacement function F which is frequency dependent. We will use this basic analytical technique, in another field of interest known as elastic half-space. In the present problem shown in Fig. (C.2) we focus our attention on a perfectly elastic half space with the mass density ρ and the elastic constant G and μ . The half space is excited by a vertical, uniform surface loading $P = P_0 e^{i\omega t}$ per unit area, and the displacement δ of the free surface is to be evaluated. Because no horizontal displacement occur we can assume a column of unit-area, and this column will be have like a rod with zero lateral displacement- and its elastic modulus is therefore

$$E_p = \frac{G}{s^2} \quad (C.2.1)$$

$$\text{in which } s^2 = \frac{1-2\mu}{2(1-\mu)}$$

The velocity of P wave propagating along the rod is

$$v_p = \sqrt{\frac{E_p}{\rho}} = \frac{1}{s} \sqrt{\frac{G}{\rho}} = \frac{v_s}{s} \quad (\text{C.2.2})$$

v_s = the velocity of shear wave. As the "rod" is infinitely long, no reflection will occur. The displacements of the rod is therefore

$$w = A e^{i\omega t (t - z/v_p)} \quad (\text{C.2.3})$$

which is an expression for a sinusoidal wave with amplitude A propagating down-wards with a constant velocity v_p .

The tensile stress on a horizontal plane is

$$\begin{aligned} \sigma(z) &= E_p \frac{\partial w}{\partial z} \\ &= -i A E_p \frac{\omega}{v_p} e^{i\omega(t - z/v_p)} \end{aligned} \quad (\text{C.2.4})$$

On the surface $z = 0$, and the stress boundary condition yields:

$$\sigma(0) = -P_0 e^{i\omega t} = -i A E_p \frac{\omega}{v_p} e^{i\omega t} \quad (\text{C.2.5})$$

which implies

$$A = \frac{-i P_0}{\omega \sqrt{\rho} E_p} = \frac{i s P_0}{\omega \sqrt{\rho G}} \quad (\text{C.2.6})$$

Hence the displacement δ at the surface is

$$\delta = \frac{-i s P_0 e^{i\omega t}}{\omega \sqrt{\rho G}} \quad (\text{C.2.7})$$

This is the steady state solution of the differential equation of motion

$$\sqrt{\frac{\rho G}{s}} \dot{\delta} = P_0 e^{i\omega t}$$

If we are only concerned with the vertical displacement, we can use the above analogy for the uniformly loaded half-space.

The above analogy between energy dissipation caused by wave propagation and that resulting from viscous damping is of considerable interest, because it allows the study of the behaviour of an infinite system by considering a simple finite system.

C.3 Rigid circular footing

We will consider an idealised half-space model for the footing-soil system. This model is shown in fig. (C.3.1), and consists of a circular rigid footing of mass m resting on a homogeneous, isotropic and perfectly elastic half space with physical constants G , M , ρ . For a simple damped oscillator $m = 0$.

If the Poisson's ratio is given then F can at the most, depend on the parameters ω , r_0 , G and ρ . The only dimensionless ratio that can be formed by these is the frequency ratio

$$a_0 = \omega r_0 \sqrt{\frac{P}{G}} = \frac{r_0}{v_s} \cdot \omega \quad (C.3.1)$$

and because F is dimensionless, it is seen to be a function of M and a_0 only.

The expression for the displacement of the massless footing is according to eqn (C.1.1).

$$\delta = \frac{P_0}{k} F(a_0, \mu) e^{i\omega t} \quad (C.3.2)$$

where the static spring constant

$$k = \frac{4 G r_0}{(1-\mu)} \quad (C.3.3)$$

The analytical solution and determination of function F involves the solution of the wave equation for an elastic solid with a mixed boundary condition, namely a zero stress condition on the free surface of a half space, and uniform displacement condition under footing. This difficult-mathematical problem has not yet been solved exactly, but J. Lysmer [44] has evaluated an approximate solution for a special case of Poisson's ratio equal to $1/3$. The solution is shown with dotted curve in fig (C.4.1), which can actually be used for all values of Poisson's ratio because the variation of F with M is insignificant for practical calculation. Bycroft [42], and most other authors use a slightly different displacement function $f = f_1 + i f_2$ which is related to F through the simple relationship $f = -1/4 (1-\mu) F$. This function depends markedly on Poisson's ratio. Which makes the use of the function f more inconvenient.

C.4 Equation of motion of footing-soil system

The equation of motion (C.1.2) was extended by Lysmer [44], and gave the following equation of the footing-soil system.

$$m \ddot{\delta} + c_1 \frac{k r_0}{v_s} \dot{\delta} + k_1 k \delta = Q_0 e^{i\omega t} \quad (C.4.1)$$

The equation has a steady state solution of the form

$$\delta = \left(\frac{Q_0}{k}\right) \bar{F} e^{i\omega t} \quad (C.4.2)$$

which on substitution in (C.4.1) yields

$$\bar{F} = \frac{1}{(k_1 - B a_0^2) + i c_1 a_0} \quad (C.4.3)$$

$$\text{where } k_1 = \frac{F_1}{F_1^2 + F_2^2}, \quad c_1 = \frac{-F_2/a_0}{F_1^2 + F_2^2}$$

where the mass ratio B is defined by

$$B = \frac{m}{k} \left(\frac{v_s}{r_0}\right)^2 = \frac{1-\mu}{4} \frac{m}{\rho r_0^3} \quad (C.4.4)$$

The response magnification factor M of (C.1.15) is consequently

$$M = |\bar{F}| = \sqrt{\frac{1}{(k_1 - Ba_0^2)^2 + (c_1 a_0)^2}} \quad (C.4.5)$$

As it has been already pointed out that F is practically independent of Poisson ratio ν . Lysmer has shown that the variation of F with M is also relatively small. The steady state spectra due to Lysmer is given in Fig (C.4.2).

$$\text{Hence } \delta = \frac{Q_0}{k} M \cos(\omega t + \phi) \quad (C.4.6)$$

$$\text{the phase shift } \phi = \tan^{-1} \frac{-c_1 a_0}{k_1 - Ba_0^2} \quad (C.4.7)$$

which is the complete steady state solution for the elastic half-space.

The velocity and acceleration responses are:

$$\dot{\delta} = -\frac{Q_0}{k} M \omega \sin(\omega t + \phi) \quad (C.4.8)$$

$$\ddot{\delta} = -\frac{Q_0}{k} M \omega^2 \cos(\omega t + \phi) \quad (C.4.9)$$

C.5 Numerical Example

A numerical example is considered in this section. This example represents the elastic half space problem

The footing-soil system defined by the physical constants:

$$\begin{aligned} r_0 &= 1,50 \text{ m} \\ G &= 1,72 \cdot 10^7 \text{ N/m}^2 \\ m &= 2,195 \cdot 10^5 \text{ kg} \\ \rho &= 2062 \text{ kg/m}^3 \\ M &= 1/3 \end{aligned}$$

The velocity of the wave in the half space

$$v_s = \sqrt{\frac{G}{\rho}} = \frac{1,72 \cdot 10^7}{2062} = 91,33 \text{ m/s.}$$

Mass ratio:

$$B = \frac{1 - \mu}{4} \cdot \frac{m}{\rho r_0^3}$$

$$= \frac{1 - 1/3}{4} \cdot \frac{2,195 \cdot 10^5}{2062 \cdot 1,5^3} = 5,283 \sim 5$$

The natural frequency (damped)

$$\omega_d = \frac{v_s}{r_0} \sqrt{\frac{B - 0,18}{B}} \quad (\text{given by Lysmer using simplified analog [44] }).$$

$$\omega_d = \frac{91,33}{1,5} \cdot \frac{5 - 0,18}{5} = 26,25 \text{ sec}^{-1}$$

$$\text{Corresponding period } \frac{2\pi}{\omega_d} = 0,24 \text{ sec.}$$

Assuming now that the system is excited by a constant force of $1 \cdot 10^6$ N for a period of 1 sec. We find the static and time-varying response of footing-soil system

$$\delta_{\text{static}} = \frac{Q_0}{k} = \frac{1 \cdot 10^6}{k}$$

$$\text{where } k = \text{static spring constant} = \frac{4G \cdot r_0}{1 - \mu}$$

$$= \frac{4 \cdot 1,72 \cdot 10^7 \cdot 1,5}{1 - 0,33} = 1,54 \cdot 10^8 \text{ N/m}$$

$$\text{Therefore } \delta_{\text{static}} = \frac{1 \cdot 10^6}{1,54 \cdot 10^8} = 0,65 \text{ Cm.}$$

C.5.1 Dynamic response

In this section our aim is to compare the dynamic response due to a steady sinusoidal load $P(t) = P_0 \sin \omega t$ where $P_0 = 1.0 \times 10^6$ N and $\omega = 27.6/\text{sec}$, acting on a footing soil system in terms of elastic half space model and equivalent finite element model of the system. Now theoretically if we include damping effect, it is extremely doubtful that we will have a common basis to compare the results of the elastic half space model and finite element representation of the elastic half space. The reasons are as follows:

- 1) Damping term used in elastic half space model is frequency dependent (factors C1 and K1 in fig. C 4.3.)
- 2) Response magnification factor is a function of factors C1 and K1,
- 3) Finite element model of the elastic half space is arbitrary. Although the model is large enough, it does not truly represent the elastic half space.
- 4) The damping matrix is proportional to mass matrix and stiffness coefficient matrix, and therefore, the effect of damping in the response evaluation does not have a common basis with the halfspace theory.

However from fig. C4.2 with $a_0 = 0,45$ and $B = 5.0$ we obtained the value of M.

Equation C.4.6. and C4.9 were used to find the Steady State time history responses in fig. 5.1. and 5.2.

For the finite element model of the elastic half space in fig. 6.1. we used proportional damping

$$\tilde{C} = \alpha \tilde{K} + \beta \tilde{M}$$

Following values are obtained from the free vibration analysis of the soil model.

Mode	Frequency C/S	Participation factor	Modal damping
1	2.15	- 9.08	0.084
3	2.27	1.01	0.051
5	3.10	3.07	0.071

The frequencies and modal damping values are used to evaluate the damping constants α and β .

We used Newmark's step by step method for about 1.0 seconds duration with a time step $t = 0.01$ sec. The time history responses thus obtained in the elastic half space and finite element analysis were used to plot the response spectrum curves in fig. 6.2 and 6.3 to show the comparison between the two different approaches. It will be observed that there is a small difference in peak response on the frequency scale of the response spectrum curve, and the peak responses are not exactly the same. The differences thus appeared between the two methods, are not significant and can be considered within the acceptable limits. It should be pointed out that non reflecting boundary condition was used to prevent reflection from the bottom nodes using subroutine VELCOR in conjunction with main program NONSAP.

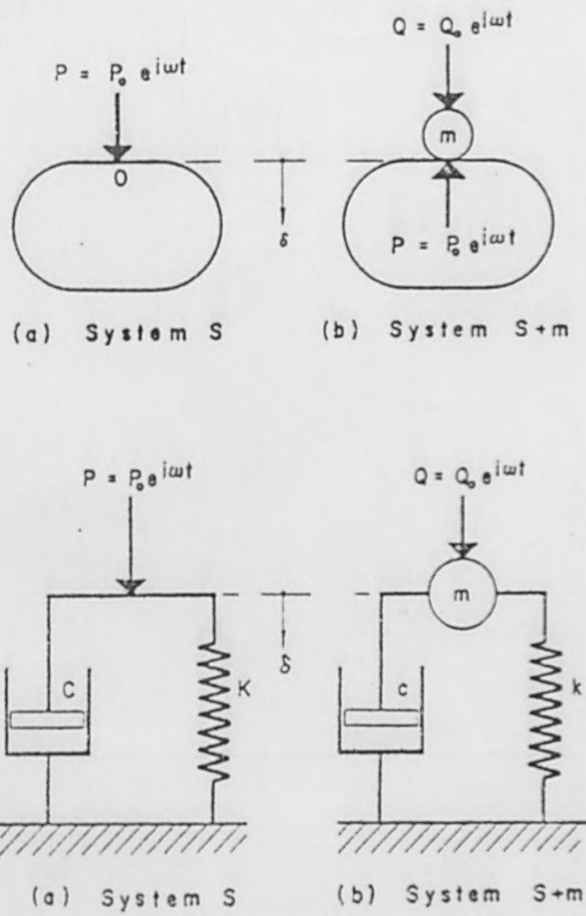


Fig. C.1: Simple damped oscillators

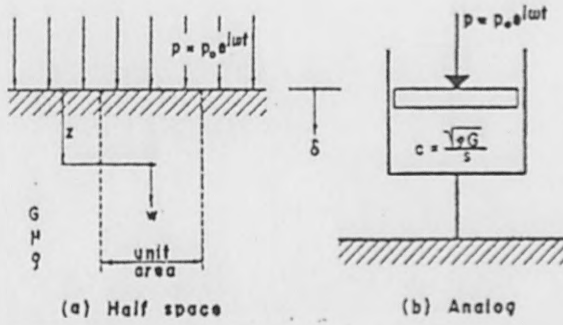


Fig. C.2: Uniformly loaded half space and its analog

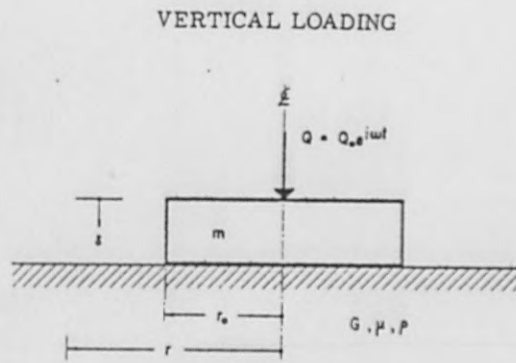


Fig. C.3.1: Footing-soil system

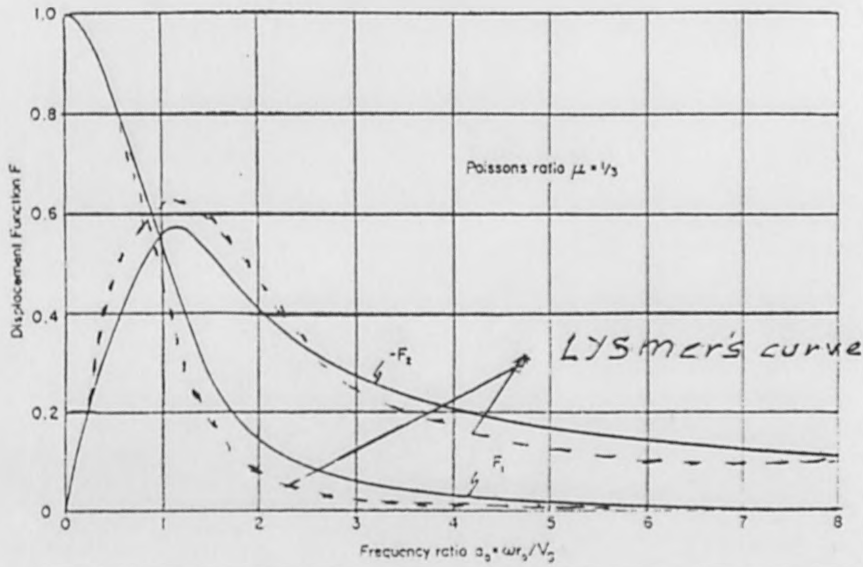


Fig. C.4.1: Displacement function for rigid circular footing on elastic half space (3)

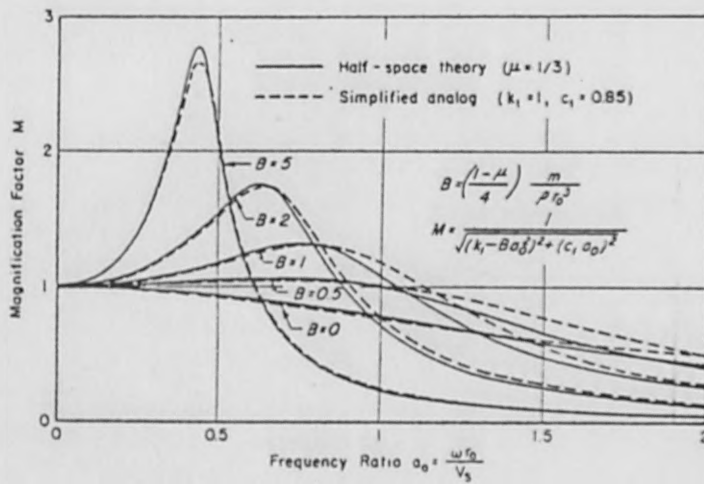


Fig. C.4.2: Steady state spectra

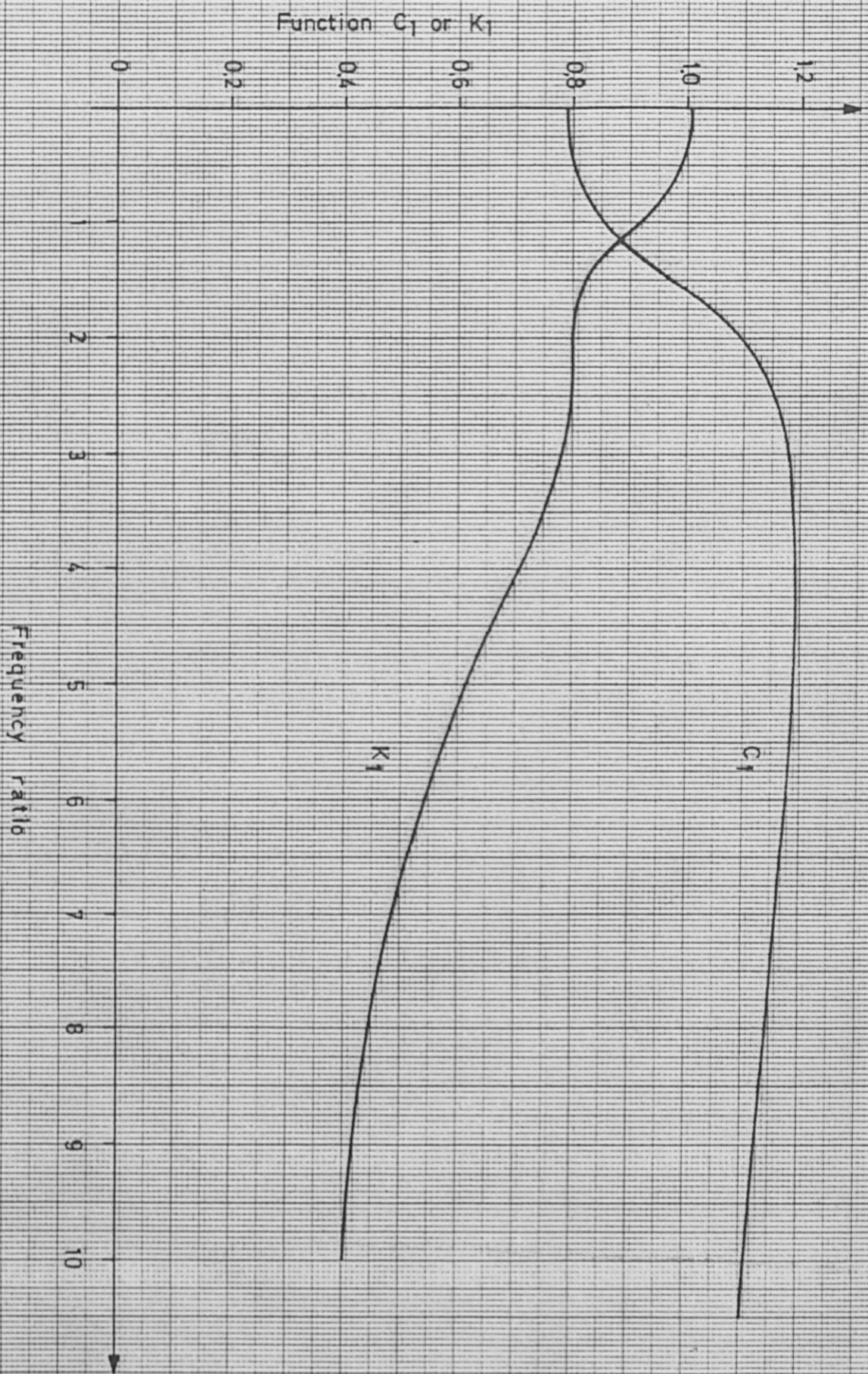
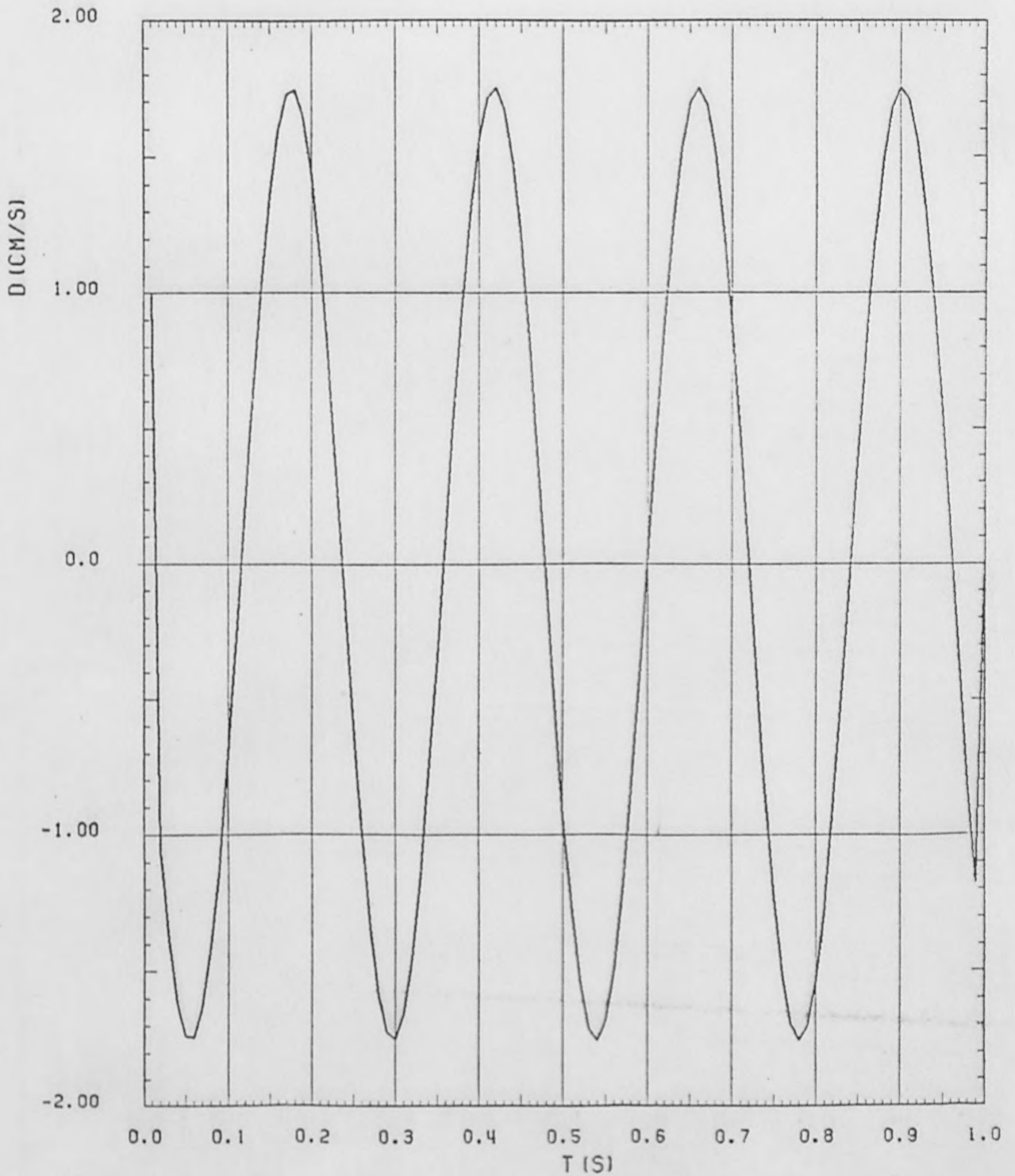
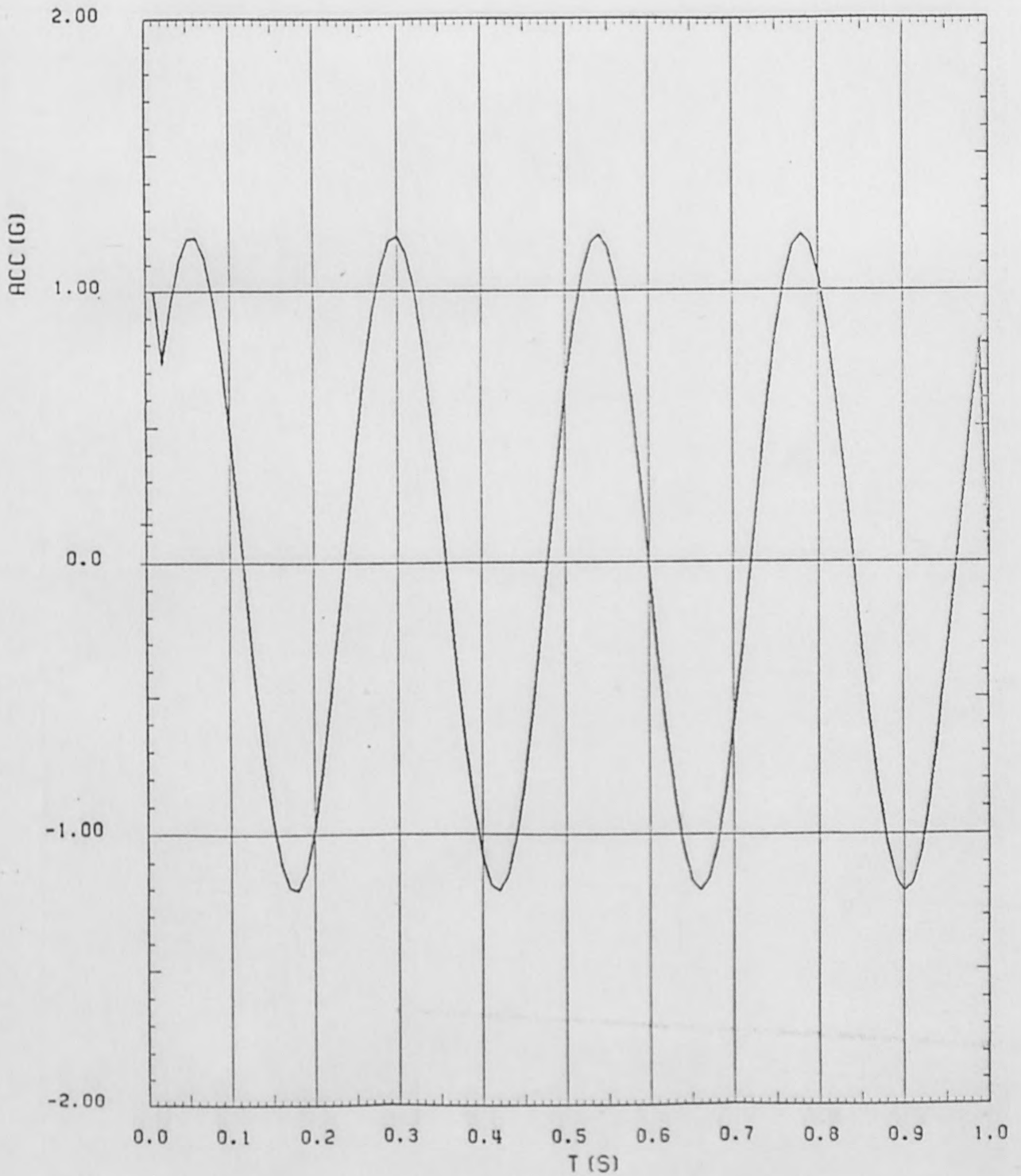


FIG. 14.3



DISPLACEMENT-TIME HISTORY (ELASTIC HALF-SPACE)

FIG.5.1



ACCELERATION-TIME HISTORY (ELASTIC HALF-SPACE)

FIG. 5.2

ACC. RESPONSE SPECTRA OF F E MODEL OF ELASTIC HALF SPACE.

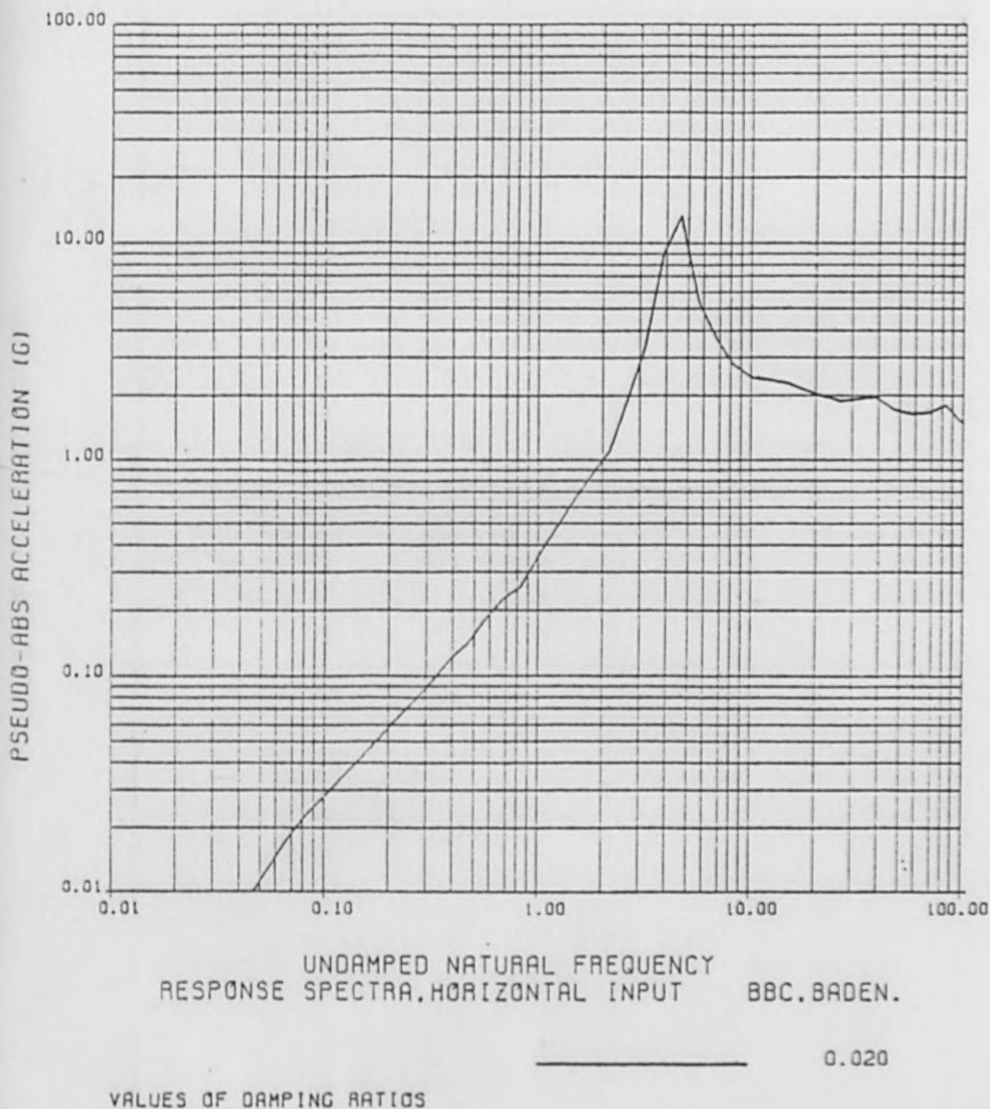


FIG. 6.2

172

JOB IIRSO25M
 DATE 81-07-07
 TIME 14.59.37

ACC. RESPONSE OF ELASTIC HALF SPACE MODEL.

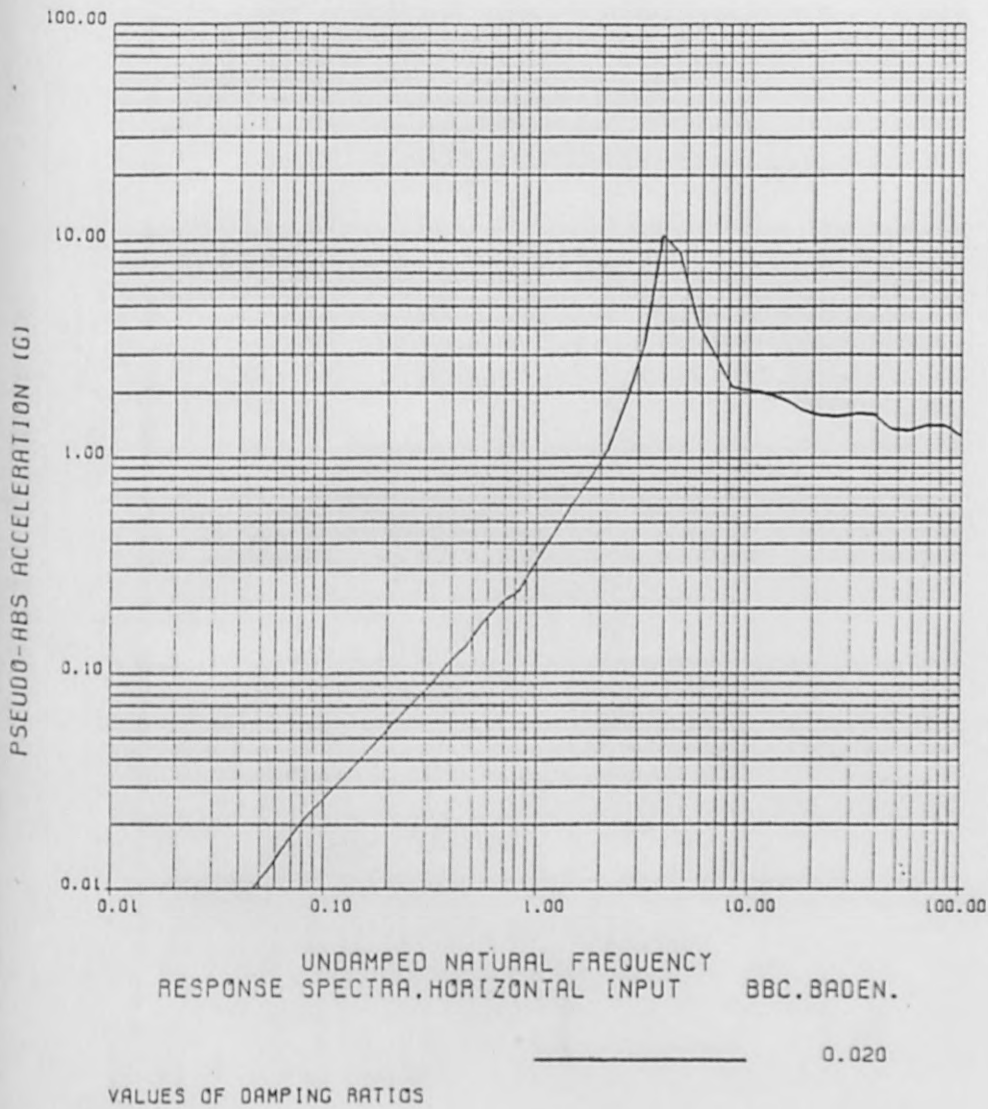


FIG. 6.3

Number of nodal points = 162

Velocity of shear wave = 91.33 m/s

Shear modulus = $1.72 \times 10^7 \text{ N/m}^2$

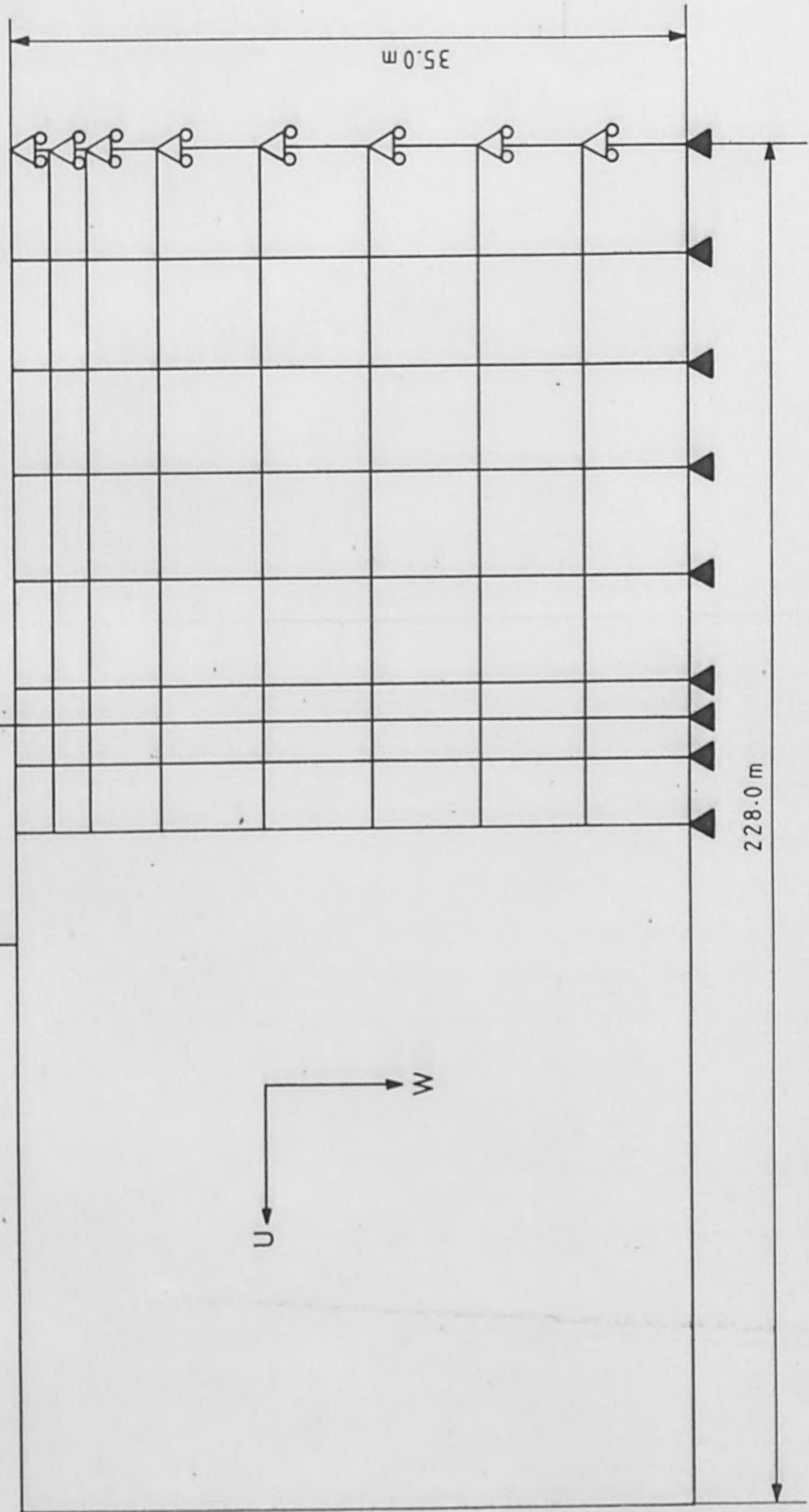
Mass density = 2062 kg/m³

Excitation frequency = 4.39 c/s

Radius of Baseemat $r_0 = 1.5 \text{ m}$ Poisson's ratio = 0.33

Data used in Elastic half space and FE model

$$|P_0 e^{i\omega t}$$



FINITE MODELS FOR FOOTING ON HALF SPACE

FIG.(6.1)

REFERENCES

- (1) Housner, G.W. "Behavior of structures during earthquake", J. of Eng. Mech. Div. Proc. ASCE, Vol. 85, No. EM4, October 1959.
- (2) Werner, S.D. "A study of earthquake motions for seismic design" AJA R-6914-925, Asbabian-Jacobsen Assoc. AEC Contract No. AT(49-5)-3012, June 1970.
- (3) Parmelee, R.A. et al. "Seismic response of structure-foundation systems", J. of the Eng. Mech. Div. Proc. ASCE, Vol. 94, No. EM6, December 1968.
- (4) Isenberg, J. "Analytical modelling of rock structure interaction", Asbabian Associates, Vol. 4, pp. 978-886, 1966.
- (5) Scavuzzo et al. "Lateral structure foundation interaction of nuclear power plants with large base masses", Technical Report No. 3, Univ. of Toledo, The Research Foundation, DEC Contract No. AT-(40-1)-3822, September, 1969.
- (6) Chu, S., Agarwal, and Singh. "Finite element treatment of soil-structure interaction problem for nuclear power plant under seismic excitation", Second Int. SMIRT Conference, Berlin, Germany, 10-14 September 1973.
- (7) Turner, M.J., Dill, E.H., Martin, H.C., Melosh, R.J. "Large deflection analysis of complex structures subjected to heating and external load", J. Aerospace Sci. 27, 97-106, 1960.
- (8) Popov, P., Chow, Y.C. See Reference 28.

- (9) Fulton, R., "Numerical analysis of shells of revolution", Paper presented at the IUTAM Symp. High Speed Comput. Elastic Struct., Liege, Belgium, Aug. 29 - Sept. 6, 1970
- (10) Pugh, C.E. et al. "Currently recommended constitutive equations for inelastic design analysis of FFTF components", Report No. TM-3602, Oak Ridge National Laboratory, Tennessee, 1972.
- (11) Stricklin, J.A. "Geometrically nonlinear static and dynamic analysis of shells of revolution". Proc. Symp. IUTAM Univ. of Liege 1970.
- (12) Oden, J.T. Finite Elements of Nonlinear Continua, McGraw Hill, 1972.
- (13) Fillipa, CA. and Sharifi, P. "Computer implementation of nonlinear finite element analysis", Proc. Symp. ASME, November 1973, Detroit.
- (14) Martin, H.C. and Carey, C.F. Introduction to Finite Element Analysis, McGraw Hill, 1973.
- (15) Zienkiewicz, F.C. Finite Element Methods in Engineering Science, McGraw Hill, London, 1971.
- (16) Argyris, J.H. et al. "Nonlinear oscillations using finite element techniques", Computer Methods in Applied Mechanics and Engineering, Vol. 2, pp. 203-250, 1973.
- (17) Bathe, K.J. and Wilson, E.L. "Finite element formulation for large displacement and large strain analysis", SESM Report No. 73-14, Dept. of Civil Engineering, Univ. of California, Berkeley, September 1973.

- (18) Bathe, K.J.,
Ramm, E.,
Wilson, E.L. "Finite element formulation for large displacement and large strain analysis", SESM Report 73-19, Dept. of Civil Engineering, Univ. of California, Berkeley, 1973.
- (19) Bathe, K.J.,
Wilson, E.,
Iding, R. "NONSAP - A structural analysis program for static and dynamic response of non-linear systems", Univ. of California, Berkeley, 1974.
- (20) Malvern, L.E. Introduction to Mechanics of Continuous Medium, Prentice Hall, Inc. 1969.
- (21) Clough, R.W. Notes from lectures on "Finite element in continuous mechanics", Univ. of California, Berkeley, 1974.
- (22) Weeks, G. "Temporal operations for nonlinear structural dynamics problems" Journal of Eng. Mech. Div., Proc. ASCE, October 1972.
- (23) McNamara, J.F. and
Marcal, P. "Incremental stiffness method for finite element analysis of the non-linear dynamic problem", Numerical and Computer Methods in Structural Mechanics, Academic Press, Inc., New York, 1973.
- (24) Dahlquist, G.,
Björk, A. Numerical Methods, Prentice Hall, Englewood Cliffs, NJ, 1974.
- (25) General Electric Provisional Safety Analysis of Nuclear Power Plants Report. General Electric Corporation, San Jose, California, U.S.A., Vol. 3A, 1970.
- (26) Woodward Lundgren
Associates "Structural Analysis Report of PSAR 3A/A-A3 G.E. Nuclear Power Plant", San Francisco, California, 1970.

- (27) Hurty, Dynamics of Structure
Rubenstein
- (28) Klein, S. and "The linear elastic dynamic analysis
Sylvester, R. of shells of revolution by matrix
displacement method", Air Force Flight
Dynamics Lab., TR-66-80, pp. 299-329,
1966.
- (29) Marcal, P.V. "Finite element analysis of combined
problems of non-linear material and
geometric behavior", Proc. ASME Joint
Computer Conf. Comput. Approach Appl.
Mech., Chicago, 1969.
- (30) Popov, P. See Reference 28.
Chow, Y.C.
- (31) Belytschko, T. "Comparative evaluation of numerical
methods for dynamic analysis", Int.
Seminar on Extreme Load Conditions
and Limit Analysis Procedures,
Bundesanstalt für Materialprüfung,
Berlin (West), 8-11 Sept. 1975.
- (32) Kolsky Stress Waves in Solids, Dover Publica-
tions.
- (33) Swarz, W. Ph.D. Thesis, Department of Civil
Engineering, MIT, 1979.

- [34] Scavuzzo R.J. "Foundation-Structure interaction in the analysis of wave motions". Bull of the Seismological Society of America Vol 57, No4, PP 735-746.
- [35] Chlapetta, R. "Effect of soil-structure Interaction on the Response of Reactor Structures to Seismic Ground motion, IIT Research Institute, AEC Contract AT (40-1) 3822, July 1. 1969.
- [36] Th. von Karman "on the Propagation of Plastic deformation of solid" NDRC Report No A29. OSRD No 365.1942.
- [37] G.I. Taylor "The Plastic wave in a wire Extended by an impact Load". The Scientific papers of G.I. Taylor". Edited by G.K. Bachelor University Press Cambridge, UK 1958.
- [38] Kh. A. Rakhmatulin "On propagation of the unloading wave" (in Russian). Prikladnya Matematika i mehanika vol. 9, 1945 (English translation is available, at Barkar's Lib. MIT).
- [39] Clifton, R.J. & Bodner, s.R. "In Analysis of Longitudinal Elastic-Plastic Pulse Propagation" Journal of Applied Mechanics, Paper No 65-WA/APM - 29. July 27, 1965
- [40] Kachanov, L.M. "Foundation of the Theory of Plasticity" (Russian). Leningrad University 1971 (English translation is available at M.IT Cambridge, USA
- [41] Mukherjee S.N. "Elasto-Plastic Stress wave propagation in finite bar BROWN-BOVERI Internal report no. TN 027 1977.

References:

- (42) Bycroft, G.N. "Forced Vibration of a Rigid Circular Plate on a Semi-Infinite Elastic Space or Elastic Stratum". Philosophical Transactions. Royal Society of London, Vol.248 1956. PP. 327-368.
- (43) Richart, F.E.Jr. "Foundation Vibration" Journal of Soil Mechanics and Foundation Division ASCE Vol. 86 No. SM 4 Proc. Paper 2564 August 1960 P.P. 1-34.
- (44) Lysmer, J. "Vertical Motion of Rigid Footings" Contract Report No. 3-115. The University of Michigan Ann Arbor Mich. for the U.S Army Engr. Waterways Experiment Stn. Vicksburg June. 1965 Contract No. DA-22-078-ENG-340.
- (45) Cole, J. and Huth, J. "Stresses Produced in a Half-plane by Moving Loads, Journal of Applied Mechanics, Dec. 1958, /433
- (46) Newmark, N.M. "A Method of Computation for Structural Dynamics", Journal of the Engineering Mechanics Division, ASCE, 1959, PP. 67-94
- (47) Houbolt, J.C. "A Recurrence Matrix Solution for the Dynamic Response of Elastic Aircraft", Journal of Aeronautical Sciences, No. 17, 1950, PP. 540-550.
- (48) Weeks, G., "Temporal Operators for Nonlinear Structural Dynamic Problems", ASCE Proceedings, Journal of the Engineering Mechanics Division, 1972, PP. 1087-1104.

- (49) Lysmer, et al (1974) "LUSH A Computer Program for Complex Response Analysis of Soil-Structure Systems". Report No. EERC 74-4 University of California, Berkeley
- (50) Kausel and Roesset, "Soil-Structure Interaction Problems for Nuclear Containment Structures". ASCE Power Division Speciality Conference, Denver Colorado 1974.
- (51) Huang et al, "A simplified three Dimension Soil Structure Interaction Study". Second ASCE Speciality Conference on Structural Design of Nuclear Plant Facilities, New Orleans, Dec. 1975.
- (52) Tzung and Lee, "A New Transmitting Boundary Representaion for three Domain Analysis of Soil Structure Interaction Problems". SMIRT Conference Div.K (a), Paris, France, Aug. 1981
- (53) Mukherjee, S. "Non Linear Analysis of embeded Structure Under Transient Load". ADINA Conference M.I.T., Cambridge USA, 1977
- (54) Mukherjee, S. "Three Dimensional Structure to Structure Interaction Analysis". 6th International Seminar on Computational Aspect of Finite Element Method". Paris, France, Aug. 1981.
- (55) Trifunac, M. "Method for Prediction of Strong Earthquake Ground Motion". Final Technical Report, Oct. 1976 - Sept. 1977, US Nuclear Regulatory Commission.
- (56) Reissner, E., "Stationäre, axialsymmetrische durch eine schüttelnde Masse erregte Schwingungen eines homogenen elastischen Halbraumes", Ingenieur-Archiv, Vol. 7, December, 1936, pp. 381-396.

- (57) Kunar and Rodriguez-Ovejero 'A model with non reflecting boundaries for use in explicit soil structure interaction analysis'. Earthquake engineering and structural dynamics Vol 8 pp 361 - 374. 1980.